ISBN 90-9019050-3

谨以此论文集献给辛勤培育我成长的父母亲

Low-Molecular Weight Caldesmon in Glioma Neovascularization

Laag-moleculair caldesmon in de vaatnieuwvorming van gliomen

Proefschrift

ter verkrijging van de graad van doctor
aan de Erasmus Universiteit Rotterdam
op gezag van de Rector Magnificus

Prof.dr. S.W.J. Lamberts
en volgens het besluit van het College voor Promoties

De openbare verdediging zal plaatsvinden op
woensdag 16 februari 2005 om 11:45 uur

door
Ping-Pin Zheng

geboren te Ningbo, Zhejiang, China (PRC)

Promotiecommissie

Promotor: Prof.dr. J.W. Oosterhuis

Overige leden:

Prof.dr. P.A.E. Sillevis Smitt

Prof.dr. C.I. de Zeeuw

Prof.dr. C.J.J. Avezaat

Co-promotor: Dr. J.M. Kros

CONTENTS

Chapter 1

1.1 General introduction

Gliomas are defined as tumors that display histological, immunohistochemical and ultrastructural evidence of glial differentiation [1]. Gliomas are the most common primary brain tumors and are particularly highly vascularized and, therefore, serve as an excellent model to elucidate the process of tumor neovascularization. Vasculogenesis, a process of the *in situ* differentiation of primitive endothelial progenitors (known as angioblasts) into endothelial cells that aggregate into a primary capillary plexus, is predominantly responsible for the development of the vascular system during embryogenesis, but may also occur in post-natal neovascularization [2-4]. Another form of neovascularization, i.e., sprouting angiogenesis, characterized by the formation of new blood vessels by a process of sprouting from preexisting vessels, occurs both during development and in postnatal life [3, 5, 6]. This pattern of neovascularization, localized at the abluminal site of the vessels, is initiated by proteolytic degradation of the basement membrane, after which endothelial cells migrate into the extracellular matrix (ECM) and proliferate [7]. Non-sprouting angiogenesis, also called intussusceptive angiogenesis [7, 8], is an alternative mode of sprouting angiogenesis characterized by the protrusion of opposing microvascular walls (luminal site of the vessel wall) into the capillary lumen creating a contact zone between endothelial cells [7].

Neovascularization is a complex process regulated by multiple stimulatory and inhibitory factors modulating the migration and/or proliferation of microvascular cells resulting in the formation of neovasculature from preexisting vessels. It involves well-coordinated steps including production and release of angiogenic factors, proteolytic degradation of extracellular matrix (ECM) components to allow the formation of capillary sprouts, proliferation and directional migration of microvascular cells, finally leading to the composition of new vessels [9]. Neovascularization and tumor cell invasion are pathophysiological processes playing a pivotal role in glioma development and growth from the earliest phase [10]. Neovascularization and tumor invasion both can be considered as processes implying invasiveness in which cells are activated. Neovascularization is particularly important in the growth and progression of malignant gliomas and proliferation and hyperplasia of the cellular components of blood vessels are used as indicators of the degree of malignancy of a glial tumor [11]. A high degree of neoplastic neovascularization has been shown to correlate with poor survival in patients with glioma [12-15]. It seems that soon after the initiation of a glial tumor its malignancy largely depends on its angiogenic potential. Therefore, in addition to parameters derived from the neoplastic glial cells themselves, the high level of neovascularization offers a target for surveillance of glioma. Hence, the application of anti-angiogenic therapy would offer a potential impact on the proliferation of gliomas.

1.2 Pathological endothelialisation in glioma neovascularization

Capillaries of the normal brain consist of a continuous endothelium in which cells are joined by well developed and complex tight junctions; there are no fenestrae, and there are very few plasmalemmal vesicles [16]. It is generally accepted that the maintenance of the blood brain barrier (BBB) is the result of the presence of the tight endothelial junctions, the lack of transcytotic vesicles, the complete basement membrane, and the tight junctions present among the astrocytic foot processes [17]. In glioma, an exceptionally high degree of vascularization is seen. The microvessels in gliomas characteristically have lost their normal BBB properties and leak fluid into the neuropilema. The vasculature in gliomas is highly disordered, with numerous vascular shunts, irregular vascular diameters, wide inter-endothelial junctions, large numbers of fenestrated and transendothelial channels, and discontinuous or absent basement membranes [18, 19]. Cerebral edema is the consequence of the disfunction of this vasculature. Ultrastructural investigations of glioma blood vessels have revealed the opening of intermicrovessel endothelial cell tight junctions [20-22]. The tight junctions are formed by a group of molecules that comprise the proteins occludin, claudins and junctional adhesion molecules.

It has been noticed that the proteins forming the tight junctions in glioma microvasculature are down-regulated [23-25]. Basically, these proteins are the morphological correlates for the BBB. Loss of tight junction proteins appears to be a central event in the opening of the BBB in gliomas.

1.3 Angiogenic mechanisms and sources of glioma vessels

Glioma vessels may develop from various sources and undergo various phases of (abortive) development in which multiple mechanisms are involved. The initial phase consists of *de novo* vessel formation (vasculogenesis) through single endothelial cells (ECs) or endothelial precursor/progenitor cells (EPCs) [26], or non-canalized endothelial cell chains (NCECCs) [27] either shed from vessel walls or mobilized from bone marrow [28]. In the early phase, sprouting occurs either from the newly formed vessels or from host vessels, in a process called angiogenesis [20, 29]. Also, tumor cells may take over host vessels (cooption) [27], or form perivascular cuffs around host vessels [30]. After the initial/early phase, additional vascular growth and development of complex vascular beds, including their continuous remodeling and adaptation, occurs predominantly by intussusceptive vascular growth (IVG) [7]. An important characteristic of IVG is that it is achieved by an exceedingly low rate of EC proliferation [7]. The advantage of the biological mechanism of IVG over that of sprouting is that blood vessels are generated more rapidly in an energetically and metabolically more advantageous manner, as extensive cell proliferation, basement membrane degradation, and invasion of the surrounding tissue are not required [7].

1.4 Angiogenic and anti-angiogenic factors

It is well accepted that solid tumors must create a vascular system for nutrient delivery and waste removal in order to grow appreciably. The cascade of events in this process of blood vessel formation involves a complex interplay between tumor cells, endothelial cells, and their surrounding basement membranes in which enzymatic degradation of surrounding ground substance and subsequent endothelial cell migration, proliferation, and tube formation, occurs. It is likely that a host of growth factors is responsible for mediating these key events. In recent years much progress in the understanding of tumor angiogenesis has been made by the revelation of the function of some growth factors and their receptors acting on both tumor cells and endothelial cells in a paracrine/autocrine manner [31-33]. The variety of growth factors can be divided into three classes [34]. The first class consists of factors specifically acting on endothelial cells, e.g., the vascular Endothelial Growth Factor (VEGF) family [35] and the angiopoietins [36]. The second class encompasses direct-acting factors which activate a broad range of target cells besides endothelial cells, e.g., several cytokines, chemokines and angiogenic enzymes [37]. The third class consists of indirect-acting factors with an effect on angiogenesis resulting from the release of substances from macrophages, endothelial or tumor cells, e.g., tumor necrosis factor-alpha (TNF-α) and transforming growth factor-beta (TGF-β). There is evidence that a number of growth factors exhibit angiogenic activity in the adult central nervous system (CNS) in both reactive and neoplastic states. Various angiogenic stimulating factors have been identified in gliomas and other tumors, including VEGF [38], platelet-derived growth factor (PDGF) [39-42], basic fibroblast growth factor (bFGF) [43-46], TGF-beta [47, 48], and epidermal growth factor (EGF) [49]. These growth factors may influence glioma neovascularization by directly stimulating endothelial cell proliferation, by mediating the expression of key proteases on endothelial cells necessary for neovascularization, or by regulating the expression of VEGF, and of each other. Tumor neovascularization is believed to be mediated by these soluble factors released from tumor cells. The molecular mechanisms that drive the formation of new blood vessels in response to tumor growth has revealed a great deal of complexity, at the heart of which are competing pro- and anti-angiogenic influences. The angiogenic factors may be useful markers of glioma surveillance.

Angiogenesis appears to be a balance between angiogenic and anti-angiogenic factors. Some endogenous inhibitors of angiogenesis are known, e.g., angiostatin [50, 51], endostatin [52], antithrombin [53], prolactin [54], thrombospondin [55], troponin [56], IFN-α [57], IFN-γ [58], pigment epithelium-derived factor (PEDF) [59], CXCL10 (IP-10) [60], platelet factor 4 [61], interleukin-12 [62], interleukin 4 [63], vascular endothelial growth inhibitor (VEGI) [64], tissue inhibitor of metalloproteinases (TIMP) [65], plasminogen activator inhibitor 1 (PAI1) [66], retinoic acid [67],

angiopoietin-2 (Ang-2) [68], 2-methoxyoestradiol [69]. Anti-angiogenic factors can act directly or indirectly on endothelial cells [70].

1.5 Potential roles of actin-binding proteins in neovascularization

Despite the increasing number of growth factors and receptors that are being focused on, only little attention has been drawn to the essential role of the actin regulatory proteins taking part in the process of tumor neovascularization. In fact, actin polymerization and remodeling is involved in many cellular functions that include motility, migration, cell division and endocytosis [71]. All of the actin-binding proteins are regulated by a complex network of bi-directional outside-in and inside-out signaling cascades that lead to the proper organization and dynamics of the actin filaments [71]. Cytotoskeletal dynamics is of prime importance in the physiology of endothelial cells engaged in an angiogenic or vasculogenic program [72]. Actin filament remodeling is a critical element of cell motility [73]. Besides cell motility, actin binding proteins and actin remodelling play crucial roles in several responses, including cell differentiation, secretion, and cell shape changes [74-77]. In the endothelium, cytoskeletal organization is regulated by adhesive interactions with neighboring cells or the extracellular matrix (ECM) and allows endothelial permeability and vessel wall integrity [72, 78] [79]. The endothelial cell cytoskeleton is particularly exposed to remodelling[72].

1.6 Podosomes-mediated adhesion supposed to be present in activated EC

Podosomes are highly dynamic, actin-rich adhesion structures that are usually found in motile cells and that control the activity of matrix metalloproteases [80]. In cell types in which podosomes are found an association with migratory behavior has been shown [80]. Podosomes are thought to contribute to tissue invasion and matrix remodeling. Actin-binding proteins play an important role in podosome turnover [80]. Podosomes were first thought to represent cellular feet [81]. Ultrastructural analysis by transmission electron microscopy showed that podosomes are in fact peculiar glove finger invaginations found at the ventral membrane of the cell and directed towards the center, perpendicularly from the substratum [82]. Although podosomes share major structural components with stable focal contacts, yet they are distinct in size, morphology, organization and turnover [80]. Immunofluorescence showed that they are composed of a core of actin filaments and actin-associated proteins surrounded by a ring of vinculin, talin and paxillin [80]. Such actin-based attachment structures are constitutively found in monocyte-derived cells, including osteoclasts, macrophages, leukocytes and immature dendritic cells, where they are believed to play a role in bone absorption, migration, diapedesis, and motility [80]. Podosomes are also found in certain transformed fibroblasts [81], carcinoma cells [84, 85] and have recently been discovered in various other cell types [80] including endothelial cells in which podosomes were induced by Cdc42 in vitro [72]. ECs are usually resting cells, but may be triggered to swiftly projecting sprouts in a well-coordinated and intentional manner [79]. Capillary cells (ECs) are able to switch between different states including growth, apoptosis, differentiation, motility through adhesive interactions with ECM by modulating their cell shapes and cytoskeletal structures [86]. Podosomes seem to be dedicated to facilitate specific physiological processes such as angiogenesis, vascular permeability, transcytosis, or the process of extravasation of blood leukocytes. Podosomes may manifest themselves in neoplastic neovascularization with inevitable consequences for the functions of ECs. At this point, it is not yet known whether podosomes are transient F-actin structures occurring in a given step or process, or alternatively, that they are constitutively found in pathological states [72].

1.7 Current clinical views and prospects of anti-angiogenesis

Continued advances in understanding the mechanism of the angiogenic process at the biochemical- and molecular level may provide further diagnostic and therapeutic benefits in a variety of diseases. Progress in this area have lead to the discovery of many proangiogenic factors as well as their inhibitors, and anti-angiogenic factors. The off-spin of research in angiogenesis has already reached the stage of clinical trials [87]. Current strategies of inhibition of tumor angiogenesis [37, 70] imply the inhibition of pro-angiogenic factors. The application of natural anti-angiogenic substances like angiostatin or endostatin lead to the inactivation of endothelial cells and the inhibition of molecules

which support invasiveness of new blood vessels in surrounding tissue. Several anti-angiogenic drugs are already being used in clinical trials of gliomas [88]. The promising results obtained with antiangiogenic treatment in animal studies have raised high hopes for applications to brain tumor patients. Neovascularization involves multiple processes mediated by a wide of range of angiogenic inducers, including growth factors, chemokines, angiogenic enzymes, endothelial specific receptors, and adhesion molecules. There is probably no single strategy that will be successful all by itself in eradicating solid tumors like gliomas. Therefore, more efficient therapeutic methods, including specific anti-angiogenic drugs, targeted drug delivery systems, and the combination of anti-angiogenic agents with immunotherapy, chemotherapy or radiotherapy should be explored to render positive results in the future. In addition, as the understanding of the regulatory mechanisms underlying neovascularization improves, we should be in a better position to elaborate novel treatment strategies taking into account the presence of different EC phenotypes such as individual ECs/EPCs, sprouting and non-sprouting patterns. With the development of tumor model assessment systems, the clinical use of anti-angiogenic tumor therapy methods may be achieved.

1.8 Advantages of anti-angiogenic therapy as compared to agents directed against tumor cells

Neovascularization is a prerequisite for progressive growth of most tumors and their metastases. Therefore, inhibition of neovascularization could be one of the most promising strategies that may lead to the development of anticancer therapy.
Anti-angiogenic therapy targetting activated endothelial cells offers several advantages over therapies directed against tumor cells. ECs form a genetically stable, diploid and homogenous target, while spontaneous mutations and drug resistance rarely occur in these cells. In contrast, tumor cells are genetically unstable, rapidly mutating, and able to develop multidrug resistance [89]. The turnover of tumor ECs may be 50 times higher than that of endothelium in normal quiescent tissues, and activated blood vessels express specific markers. Because anti-angiogenic therapy should be targetted at activated ECs, its target should be easily accessible by systemic adminstration of the drugs [34]. Based on the specific localization of at least a large part of the ECs, the cells lining the tumor blood vessel wall present a more attractive site-specific target for anti-angiogenic drugs than tumor cells do, as they are more easily accessible from the blood stream [90]. Considering the high dependency of tumor growth and survival on an efficient blood supply, inhibition of neovascularization appears to be an attractive target for tumor therapy [91].

1.9 Applying proteomics: informative tools for searching tumor-associated markers

The term “tumor marker” is used for the biochemical measurement of a substance (e.g, protein, RNA, DNA, amino acids or metabolites) that is associated with the presence of a particular tumor [92]. The term “Proteomics” has been defined as *the global analysis of gene expression by a particular cell, organism or tissue type at a given time or under a specific set of environmental conditions using a combination of techniques to identify, quantitate or characterize proteins* [93]. An important target of the application of proteomics to cancer research is to obtain insight in the differences in protein expression between neoplastic and non-neoplastic conditions at the level of single cells or tissue types. The elucidation of differentially or uniquely expressed proteins or protein isoforms will provide clues as to the normal function of these proteins and will be crucial for the selection of cell or tissue type-specific biomarkers for clinical utilities.

The molecular analysis of tissues at all three levels, i.e., genomic, transcriptomic and proteomic levels, is referred to as “operomics” [99]. Investigations at the genomic and transcriptomic level in tumors have yielded a large variety of genetic changes or markers which result in the disruption or the blocking of the normal production or action of functional proteins. However, the DNA sequence by itself does not reveal the possible post-translational modifications of the encoding proteins, which are essential for function and activity [94, 95]. Quantitation of mRNA does not provide information about the amount of active protein in a cell neither [96, 97]. Moreover, mRNAs potentially may be translationally repressed [98]. Therefore, a candidate tumor marker should preferably be sought at the functional (protein) level. Of course, information derived from the different compartments encompassed in operomics would offer complementary information. Not

surprisingly, the focus of researchers is changing gradually from genomic aberrations to the post-genomic events in the normal and abnormal situation. In tumors or tumor vasculature/endothelial cells, changes in the rate of protein synthesis, altered post-translational modifications, inter-compartmental transports, and alterations in the degradation of proteins, are encountered. Besides tracing tumor and/or tumor EC lineage-specific proteins, the identification of alterations in intracellular protein processing may yield relevant information as to therapeutic susceptibilities as well. Investigations at the protein level is well on the way, not only to characterize the different types of tumors, but perhaps more importantly, defining new therapeutic or anti-angiogenic targets crucial for treatment options. Therefore, proteomics has the potential to identify novel targets for therapy and novel markers for (early) diagnosis [99].

Numerous traditional and advanced techniques as listed in the flowchart were and/or are being applied for fractionation and identification/detection of tumor markers. Proteomics is a rapidly developing area of research and it is expected that it will lay a powerful foundation for the analysis of the entire set of proteins expressed by normal or transformed cells and tissues. It will become crucial for the identification of disease-specific targets as well as differentially displayed proteins, identifying specific parameters of disease and neoplasia in particular. The nascent field of proteomics and its diagnostic potential for primary brain tumors has been summarized in a review (*Zheng et al. Proteomics in primary brain tumors. Front Biosci. 2003 Jan 01;8:d451-63.)*

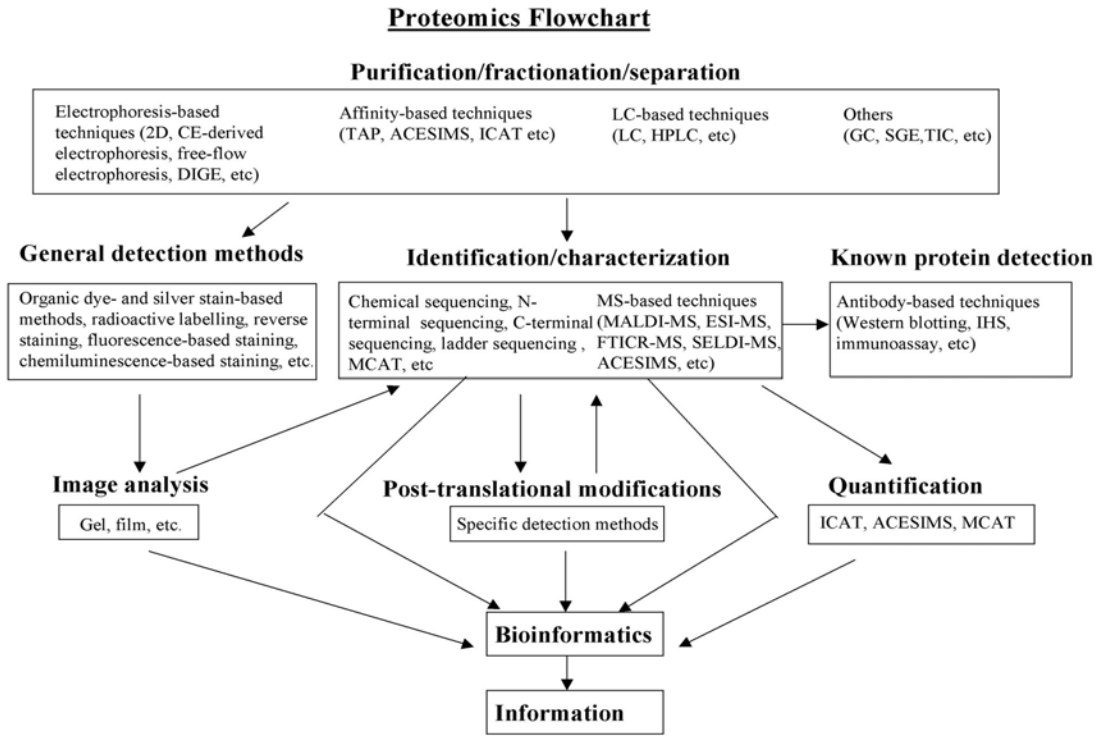

Flowchart illustrating the working procedures in proteomics

Abbreviations used:

2D, two dimensional electrophoresis; CE, capillary electrophoresis; DIGE, difference gel electrophoresis;

TAP, tandem affinity purification; ACESIMS, affinity capture-release electrospray ionization mass spectrometry; LC; liquid chromatography; HPLC; high performance liquid chromatography; GC; gas chromatography; SGE, slab gel electrophoresis; TLC, thin-layer chromatography; MCAT, mass coded abundance tagging; MALDI-MS, matrix-assisted laser desorption/ionization mass spectrometry; ESI-MS, electrosprayionization mass spectrometry; FTICR-MS, Fourier-transform ion cyclotron resonance mass spectrometry; SELDI-MS, surface enhanced laser desorption; ICAT, isotope-cold affinity tags; HIS; immunohistochemical staining.

1.10 Design and outline of this thesis

1.10.1 Screening of differentially expressed proteins by gliomas for the identification of potential glioma markers

So far, no reliable marker has yet been been identified for use in the diagnosis and surveillance of patients with gliomas [100]. An ideal tumor marker should be readily obtained and quantified. Genetic tumor markers usually require actual tumor tissue samples from surgical interventions. For gliomas, such samples must be taken from a craniotomy or brain biopsy, making its usefulness in patient surveillance both cumbersome and difficult. Tumor or disease markers can reside in any body fluid or cavity (e.g. serum, CSF, urine, bile, cysts of tumors, etc.). A glial tumor marker derived from serum or CSF would be easy to collect, quantify, and also be more practical for clinical application. The abundance of protein present in serum has a potential masking effect on the presence of a target protein. A major advantage of searching for disease-related proteins in CSF over serum is the lower protein concentration in the former.

In Chapter 2 of this thesis the screening and identification of tumor-related proteins by proteomic-based techniques in CSF is described. Low molecular weight caldesmon (*l*-CaD) was one of the proteins selectively identified in the CSF of glioma patients in this study. There were no data for this protein related to gliomas in the literature so far. The results of our immunohistochemical explorations confirmed that this protein is uniquely localized in vessels, while no expression in glial cells or glial tumor cells was present. In the hyperplastic or proliferated glioma vessels a much stronger expression of *l*-CaD was found as compared to normal brain vessels. This study raised questions for a subsequent investigation: does the stronger expression of *l*-CaD in glioma vasculature indeed indicate an up-regulation of the protein? What kind of mechanisms are involved in the regulation of the altered expression of the *l*-CaD?

1.10.2 Quantification of l-CaD and investigation of the putative regulation mechanisms for the altered expression of l-CaD in glioma tissue samples versus normal controls

Based on the data mentioned in Chapter 2, in Chapter 3 the results of subsequent investigations are revealed. The up-regulation of *l*-CaD was confirmed by immunoblotting experiments in which glioma tissue samples were compared to normal cerebral tissue samples. Three mechanisms are putatively involved in the regulation of altered protein expression. Firstly, there could be regulation at the transcriptional level. Secondly, the expression level could simply result from posttranslational modifications of the protein product. Finally, there could be a regulatory mechanism at both protein and the transcriptional level. Since the human caldesmon gene (*CALD1*) is typically a single gene with multiple alternatively spliced exons or exon sets corresponding to various splice variants, altered expression of the splice variants was postulated as the most plausible mechanism of the altered protein expression levels. This hypothesis was verified by experiments at the mRNA level. The results showed that there is differential expression of the *l*-CaD splice variants in glioma vasculature versus normal brain vessels. The expression of caldesmon protein isoforms, encoded by splice variants, potentially may be used as specific targets for anti-angiogenic therapy.

1.10.3 Tracking the uniquely expressed l-CaD isoforms in glioma vasculature

Based on the results mentioned in Chapter 3, the unique expression of Hela *l*-CaD in glioma vasculature was hypothesized and its expression was tracked by using specific antibody to the Hela-*l* CaD. The results shown in Chapter 4 indicate that Hela *l*-CaD is uniquely expressed in glioma vasculature, while it is absent from the normal cerebral blood vessels. Hela *l*-CaD appears to be preferentially expressed in early phases of glioma neovascularization, such as individual ECs/EPCs and sprouting angiogenesis. It was also found that morphological features, focal adhesion and F-actin structures of Hela *l*-CaD-positive endothelial cells overlap with those of motile cells, suggestive of these Hela *l*-CaD-positive endothelial cells becoming capable of migrating, serving the process of ubiquitous neovascularization.

1.10.4 The expression of the Hela l-CaD in tumor vessels of non-glial tumors

To determine whether the findings in glioma vessels can be generalized to other tumor and tissue types, a variety of cancers and normal tissues were examined for the expression of the Hela *l*-CaD. In Chapter 5 the findings of investigating 150 tumor samples including cancers of breast, stomac, colon, kidney, prostate, ovary and endometrium. The highest percentages of Hela *l*-CaD-positive endothelial cells and bloodvessels were traced in breast cancer, gastric adenocarcinoma and renal cell carcinoma. Cancers of the ovary, prostate and endometrium contained relatively low percentages of these Hela *l*-CaD endothelial cells and vessels. Cancers of thyroid, lung, liver, colon and breast were intermediate regarding the expression. Just like in the gliomas, Hela *l*-CaD expression was predominantly found in individual ECs/EPCs, NCECCs and sprouting/branching microvessels. There was low or absent expression of the protein in vessels showing IVG or fibrosis. No immunoreactivity of the protein was observed in co-opted vessels within the tumors or in normal vessels of the control samples. The Hela *l*-CaD$^+$ ECs often show alterations in cell shape, such as cell enlargement or elongated protrusions, multinucleation, or an epithelioid phenotype, all different from the morphology of quiescent endothelial cells.

1.10.5 Testing l-CaD as a serum marker for glioma

Since *l*-CaD is detectable in CSF samples from glioma patients, it was hypothesized that the protein may also be present in sera from glioma patients. Therefore, a large cohort of sera samples from glioma patients, other non-glial CNS tumor patients, patients with
neurological diseases but no tumors, and a group of 30 healthy individuals, was examined by enzyme-linked immunosorbent assay (ELISA) and combination of immunoprecipitation and immunoblotting. In Chapter 6 the results of this investigation are presented. The median level of *l*-CaD level in the serum of patients with gliomas is significantly higher as compared to that of the control groups. At this point, although this result is remarkable, the value of the serum *l*-CaD level in an individual patient for making the diagnosis, or to be used for monitoring disease following therapy, remains to be tested in prospective studies.

1.11 References

1. Kleihues P, Louis DN, Scheithauer BW*, et al.* The WHO classification of tumors of the nervous system. *J Neuropathol Exp Neurol* 2002;61:215-225; discussion 226-219.

2. Reyes M, Dudek A, Jahagirdar B, Koodie L, Marker PH,Verfaillie CM. Origin of endothelial progenitors in human postnatal bone marrow. *J Clin Invest* 2002;109:337-346.

3. Peichev M, Naiyer AJ, Pereira D*, et al.* Expression of VEGFR-2 and AC133 by circulating human CD34(+) cells identifies a population of functional endothelial precursors. *Blood* 2000;95:952-958.

4. Masuda H, Asahara T. Post-natal endothelial progenitor cells for neovascularization in tissue regeneration. *Cardiovasc Res* 2003;58:390-398.

5. Watt SM, Gschmeissner SE,Bates PA. PECAM-1: its expression and function as a cell adhesion molecule on hemopoietic and endothelial cells. *Leuk Lymphoma* 1995;17:229-244.

6. Reyes M, Lund T, Lenvik T, Aguiar D, Koodie L,Verfaillie CM. Purification and ex vivo expansion of postnatal human marrow mesodermal progenitor cells. *Blood* 2001;98:2615-2625.

7. Djonov V, Baum O,Burri PH. Vascular remodeling by intussusceptive angiogenesis. *Cell Tissue Res* 2003;314:107-117.

8. Burri PH, Djonov V. Intussusceptive angiogenesis--the alternative to capillary sprouting. *Mol Aspects Med* 2002;23:1-27.

9. Senger DR. Molecular framework for angiogenesis: a complex web of interactions between extravasated plasma proteins and endothelial cell proteins induced by angiogenic cytokines. *Am J Pathol* 1996;149:1-7.

10. Bello L, Giussani C, Carrabba G, Pluderi M, Costa F,Bikfalvi A. Angiogenesis and invasion in gliomas. *Cancer Treat Res* 2004;117:263-284.

11. Puduvalli VK. Inhibition of angiogenesis as a therapeutic strategy against brain tumors. *Cancer Treat Res* 2004;117:307-336.

12. Chaudhry IH, O'Donovan DG, Brenchley PE, Reid H,Roberts IS. Vascular endothelial growth factor expression correlates with tumour grade and vascularity in gliomas. *Histopathology* 2001;39:409-415.

13. Ke LD, Shi YX, Im SA, Chen X,Yung WK. The relevance of cell proliferation, vascular endothelial growth factor, and basic fibroblast growth factor production to angiogenesis and tumorigenicity in human glioma cell lines. *Clin Cancer Res* 2000;6:2562-2572.

14. Plate KH, Breier G, Weich HA,Risau W. Vascular endothelial growth factor is a potential tumour angiogenesis factor in human gliomas in vivo. *Nature* 1992;359:845-848.

15. Samoto K, Ikezaki K, Ono M*, et al.* Expression of vascular endothelial growth factor and its possible relation with neovascularization in human brain tumors. *Cancer Res* 1995;55:1189-1193.

16. Peters A PS, Webster H. The Fine Structure of the Nervous System. In: A Peter S, Palay, H Webster, ed. Oxford: Oxford University Press, 1991:pp 344-355

17. Roberts WG, Delaat J, Nagane M, Huang S, Cavenee WK,Palade GE. Host microvasculature influence on tumor vascular morphology and endothelial gene expression. *Am J Pathol* 1998;153:1239-1248.

18. Deane BR, Lantos PL. The vasculature of experimental brain tumours. Part 1. A sequential light and electron microscope study of angiogenesis. *J Neurol Sci* 1981;49:55-66.

19. Vick NA, Bigner DD. Microvascular abnormalities in virally-induced canine brain tumors. Structural bases for altered blood-brain barrier function. *J Neurol Sci* 1972;17:29-39.

20. Plate KH, Mennel HD. Vascular morphology and angiogenesis in glial tumors. *Exp Toxicol Pathol* 1995;47:89-94.

21. Vajkoczy P, Menger MD. Vascular microenvironment in gliomas. *J Neurooncol* 2000;50:99-108.

22. Davies DC. Blood-brain barrier breakdown in septic encephalopathy and brain tumours. *J Anat* 2002;200:639-646.

23. Liebner S, Fischmann A, Rascher G*, et al.* Claudin-1 and claudin-5 expression and tight junction morphology are altered in blood vessels of human glioblastoma multiforme. *Acta Neuropathol (Berl)* 2000;100:323-331.

24. Papadopoulos MC, Saadoun S, Woodrow CJ*, et al.* Occludin expression in microvessels of neoplastic and non-neoplastic human brain. *Neuropathol Appl Neurobiol* 2001;27:384-395.

25. Zheng PP, Sieuwerts AM, Luider TM, van der Weiden M, Sillevis-Smitt PA,Kros JM. Differential expression of splicing variants of the human caldesmon gene (CALD1) in glioma neovascularization versus normal brain microvasculature. *Am J Pathol* 2004;164:2217-2228.

26. Goldbrunner RH, Bernstein JJ, Plate KH, Vince GH, Roosen K,Tonn JC. Vascularization of human glioma spheroids implanted into rat cortex is conferred by two distinct mechanisms. *J Neurosci Res* 1999;55:486-495.

27. Holash J, Maisonpierre PC, Compton D*, et al.* Vessel cooption, regression, and growth in tumors mediated by angiopoietins and VEGF. *Science* 1999;284:1994-1998.

28. Rafii S. Circulating endothelial precursors: mystery, reality, and promise. *J Clin Invest* 2000;105:17-19.

29. Yancopoulos GD, Davis S, Gale NW, Rudge JS, Wiegand SJ,Holash J. Vascular-specific growth factors and blood vessel formation. *Nature* 2000;407:242-248.

30. Carmeliet P, Jain RK. Angiogenesis in cancer and other diseases. *Nature* 2000;407:249-257.

31. Cavallo T, Sade R, Folkman J,Cotran RS. Tumor angiogenesis. Rapid induction of endothelial mitoses demonstrated by autoradiography. *J Cell Biol* 1972;54:408-420.

32. Folkman J, Klagsbrun M. Angiogenic factors. *Science* 1987;235:442-447.

33. Folkman J, Merler E, Abernathy C,Williams G. Isolation of a tumor factor responsible or angiogenesis. *J Exp Med* 1971;133:275-288.

34. Liekens S, De Clercq E,Neyts J. Angiogenesis: regulators and clinical applications. *Biochem Pharmacol* 2001;61:253-270.

35. Veikkola T, Alitalo K. VEGFs, receptors and angiogenesis. *Semin Cancer Biol* 1999;9:211-220.

36. Davis S, Aldrich TH, Jones PF*, et al.* Isolation of angiopoietin-1, a ligand for the TIE2 receptor, by secretion-trap expression cloning. *Cell* 1996;87:1161-1169.

37. Zhang ZL, Wang JH,Liu XY. Current strategies and future directions of antiangiogenic tumor therapy. *Sheng Wu Hua Xue Yu Sheng Wu Wu Li Xue Bao (Shanghai)* 2003;35:873-880.

38. Dunn IF, Heese O,Black PM. Growth factors in glioma angiogenesis: FGFs, PDGF, EGF, and TGFs. *J Neurooncol* 2000;50:121-137.

39. Plate KH, Breier G, Farrell CL,Risau W. Platelet-derived growth factor receptor-beta is induced during tumor development and upregulated during tumor progression in endothelial cells in human gliomas. *Lab Invest* 1992;67:529-534.

40. Risau W, Drexler H, Mironov V*, et al.* Platelet-derived growth factor is angiogenic in vivo. *Growth Factors* 1992;7:261-266.

41. Hermanson M, Funa K, Hartman M*, et al.* Platelet-derived growth factor and its receptors in human glioma tissue: expression of messenger RNA and protein suggests the presence of autocrine and paracrine loops. *Cancer Res* 1992;52:3213-3219.

42. Krupinski J, Issa R, Bujny T*, et al.* A putative role for platelet-derived growth factor in angiogenesis and neuroprotection after ischemic stroke in humans. *Stroke* 1997;28:564-573.

43. Klagsbrun M, Sasse J, Sullivan R,Smith JA. Human tumor cells synthesize an endothelial cell growth factor that is structurally related to basic fibroblast growth factor. *Proc Natl Acad Sci U S A* 1986;83:2448-2452.

44. Montesano R, Vassalli JD, Baird A, Guillemin R,Orci L. Basic fibroblast growth factor induces angiogenesis in vitro. *Proc Natl Acad Sci U S A* 1986;83:7297-7301.

45. Shing Y, Folkman J, Haudenschild C, Lund D, Crum R,Klagsbrun M. Angiogenesis is stimulated by a tumor-derived endothelial cell growth factor. *J Cell Biochem* 1985;29:275-287.

46. Zagzag D, Miller DC, Sato Y, Rifkin DB,Burstein DE. Immunohistochemical localization of basic fibroblast growth factor in astrocytomas. *Cancer Res* 1990;50:7393-7398.

47. Krupinski J, Kumar P, Kumar S,Kaluza J. Increased expression of TGF-beta 1 in brain tissue after ischemic stroke in humans. *Stroke* 1996;27:852-857.

48. Stiles JD, Ostrow PT, Balos LL*, et al.* Correlation of endothelin-1 and transforming growth factor beta 1 with malignancy and vascularity in human gliomas. *J Neuropathol Exp Neurol* 1997;56:435-439.

49. Ekstrand AJ, James CD, Cavenee WK, Seliger B, Pettersson RF,Collins VP. Genes for epidermal growth factor receptor, transforming growth factor alpha, and epidermal growth factor and their expression in human gliomas in vivo. *Cancer Res* 1991;51:2164-2172.

50. O'Reilly MS, Holmgren L, Shing Y*, et al.* Angiostatin: a novel angiogenesis inhibitor that mediates the suppression of metastases by a Lewis lung carcinoma. *Cell* 1994;79:315-328.

51. Cao Y. Therapeutic potentials of angiostatin in the treatment of cancer. *Haematologica* 1999;84:643-650.

52. O'Reilly MS, Boehm T, Shing Y*, et al.* Endostatin: an endogenous inhibitor of angiogenesis and tumor growth. *Cell* 1997;88:277-285.

53. O'Reilly MS, Pirie-Shepherd S, Lane WS,Folkman J. Antiangiogenic activity of the cleaved conformation of the serpin antithrombin. *Science* 1999;285:1926-1928.

54. Struman I, Bentzien F, Lee H*, et al.* Opposing actions of intact and N-terminal fragments of the human prolactin/growth hormone family members on angiogenesis: an efficient mechanism for the regulation of angiogenesis. *Proc Natl Acad Sci U S A* 1999;96:1246-1251.

55. Iruela-Arispe ML, Dvorak HF. Angiogenesis: a dynamic balance of stimulators and inhibitors. *Thromb Haemost* 1997;78:672-677.

56. Feldman L, Rouleau C. Troponin I inhibits capillary endothelial cell proliferation by interaction with the cell's bFGF receptor. *Microvasc Res* 2002;63:41-49.

57. Dinney CP, Bielenberg DR, Perrotte P*, et al.* Inhibition of basic fibroblast growth factor expression, angiogenesis, and growth of human bladder carcinoma in mice by systemic interferon-alpha administration. *Cancer Res* 1998;58:808-814.

58. Sato N, Nariuchi H, Tsuruoka N*, et al.* Actions of TNF and IFN-gamma on angiogenesis in vitro. *J Invest Dermatol* 1990;95:85S-89S.

59. Dawson DW, Volpert OV, Gillis P*, et al.* Pigment epithelium-derived factor: a potent inhibitor of angiogenesis. *Science* 1999;285:245-248.

60. Moore BB, Keane MP, Addison CL, Arenberg DA,Strieter RM. CXC chemokine modulation of angiogenesis: the importance of balance between angiogenic and angiostatic members of the family. *J Investig Med* 1998;46:113-120.

61. Sulpice E, Contreres JO, Lacour J, Bryckaert M,Tobelem G. Platelet factor 4 disrupts the intracellular signalling cascade induced by vascular endothelial growth factor by both KDR dependent and independent mechanisms. *Eur J Biochem* 2004;271:3310-3318.

62. Sgadari C, Angiolillo AL,Tosato G. Inhibition of angiogenesis by interleukin-12 is mediated by the interferon-inducible protein 10. *Blood* 1996;87:3877-3882.

63. Volpert OV, Fong T, Koch AE*, et al.* Inhibition of angiogenesis by interleukin 4. *J Exp Med* 1998;188:1039-1046.

64. Zhai Y, Ni J, Jiang GW*, et al.* VEGI, a novel cytokine of the tumor necrosis factor family, is an angiogenesis inhibitor that suppresses the growth of colon carcinomas in vivo. *Faseb J* 1999;13:181-189.

65. Gomez DE, Alonso DF, Yoshiji H,Thorgeirsson UP. Tissue inhibitors of metalloproteinases: structure, regulation and biological functions. *Eur J Cell Biol* 1997;74:111-122.

66. Bajou K, Noel A, Gerard RD*, et al.* Absence of host plasminogen activator inhibitor 1 prevents cancer invasion and vascularization. *Nat Med* 1998;4:923-928.

67. Lingen MW, Polverini PJ,Bouck NP. Inhibition of squamous cell carcinoma angiogenesis by direct interaction of retinoic acid with endothelial cells. *Lab Invest* 1996;74:476-483.

68. Maisonpierre PC, Suri C, Jones PF*, et al.* Angiopoietin-2, a natural antagonist for Tie2 that disrupts in vivo angiogenesis. *Science* 1997;277:55-60.

69. Yue TL, Wang X, Louden CS*, et al.* 2-Methoxyestradiol, an endogenous estrogen metabolite, induces apoptosis in endothelial cells and inhibits angiogenesis: possible role for stress-activated protein kinase signaling pathway and Fas expression. *Mol Pharmacol* 1997;51:951-962.

70. Mentlein R, Held-Feindt J. Angiogenesis factors in gliomas: a new key to tumour therapy? *Naturwissenschaften* 2003;90:385-394.

71. Houle F, Rousseau S, Morrice N*, et al.* Extracellular signal-regulated kinase mediates phosphorylation of tropomyosin-1 to promote cytoskeleton remodeling in response to oxidative stress: impact on membrane blebbing. *Mol Biol Cell* 2003;14:1418-1432.

72. Moreau V, Tatin F, Varon C,Genot E. Actin can reorganize into podosomes in aortic endothelial cells, a process controlled by Cdc42 and RhoA. *Mol Cell Biol* 2003;23:6809-6822.

73. Pollard TD, Borisy GG. Cellular motility driven by assembly and disassembly of actin filaments. *Cell* 2003;112:453-465.

74. Condeelis J. Life at the leading edge: the formation of cell protrusions. *Annu Rev Cell Biol* 1993;9:411-444.

75. Arora PD, McCulloch CA. Dependence of fibroblast migration on actin severing activity of gelsolin. *J Biol Chem* 1996;271:20516-20523.

76. Hartwig JH, Kwiatkowski DJ. Actin-binding proteins. *Curr Opin Cell Biol* 1991;3:87-97.

77. Howard T, Chaponnier C, Yin H,Stossel T. Gelsolin-actin interaction and actin polymerization in human neutrophils. *J Cell Biol* 1990;110:1983-1991.

78. Zaidel-Bar R, Ballestrem C, Kam Z,Geiger B. Early molecular events in the assembly of matrix adhesions at the leading edge of migrating cells. *J Cell Sci* 2003;116:4605-4613.

79. Carmeliet P. Angiogenesis in health and disease. *Nat Med* 2003;9:653-660.

80. Linder S, Aepfelbacher M. Podosomes: adhesion hot-spots of invasive cells. *Trends Cell Biol* 2003;13:376-385.

81. Tarone G, Cirillo D, Giancotti FG, Comoglio PM,Marchisio PC. Rous sarcoma virus-transformed fibroblasts adhere primarily at discrete protrusions of the ventral membrane called podosomes. *Exp Cell Res* 1985;159:141-157.

82. Nitsch L, Gionti E, Cancedda R,Marchisio PC. The podosomes of Rous sarcoma virus transformed chondrocytes show a peculiar ultrastructural organization. *Cell Biol Int Rep* 1989;13:919-926.

83. Gavazzi I, Nermut MV,Marchisio PC. Ultrastructure and gold-immunolabelling of cell-substratum adhesions (podosomes) in RSV-transformed BHK cells. *J Cell Sci* 1989;94 (Pt 1):85-99.

84. Spinardi L, Rietdorf J, Nitsch L*, et al.* A dynamic podosome-like structure of epithelial cells. *Exp Cell Res* 2004;295:360-374.

85. Schuuring E, Verhoeven E, Litvinov S,Michalides RJ. The product of the EMS1 gene, amplified and overexpressed in human carcinomas, is homologous to a v-src substrate and is located in cell-substratum contact sites. *Mol Cell Biol* 1993;13:2891-2898.

86. Ingber DE. Mechanical signaling and the cellular response to extracellular matrix in angiogenesis and cardiovascular physiology. *Circ Res* 2002;91:877-887.

87. Folkman J, Shing Y. Angiogenesis. *J Biol Chem* 1992;267:10931-10934.

88. Jansen M, de Witt Hamer PC, Witmer AN, Troost D,van Noorden CJ. Current perspectives on antiangiogenesis strategies in the treatment of malignant gliomas. *Brain Res Brain Res Rev* 2004;45:143-163.

89. Folkman J. Addressing tumor blood vessels. *Nat Biotechnol* 1997;15:510.

90. Molema G, Meijer DK,de Leij LF. Tumor vasculature targeted therapies: getting the players organized. *Biochem Pharmacol* 1998;55:1939-1945.

91. Kerbel R, Folkman J. Clinical translation of angiogenesis inhibitors. *Nat Rev Cancer* 2002;2:727-739.

92. Sampath P, Weaver CE, Sungarian A, Cortez S, Alderson L,Stopa EG. Cerebrospinal fluid (vascular endothelial growth factor) and serologic (recoverin) tumor markers for malignant glioma. *Cancer Control* 2004;11:174-180.

93. Wilkins MR, Sanchez JC, Williams KL,Hochstrasser DF. Current challenges and future applications for protein maps and post-translational vector maps in proteome projects. *Electrophoresis* 1996;17:830-838.

94. Humphery-Smith I, Cordwell SJ,Blackstock WP. Proteome research: complementarity and limitations with respect to the RNA and DNA worlds. *Electrophoresis* 1997;18:1217-1242.

95. Simpson RJ, Dorow DS. Cancer proteomics: from signaling networks to tumor markers. *Trends Biotechnol* 2001;19:S40-48.

96. Banks RE, Dunn MJ, Hochstrasser DF*, et al.* Proteomics: new perspectives, new biomedical opportunities. *Lancet* 2000;356:1749-1756.

97. MacBeath G, Schreiber SL. Printing proteins as microarrays for high-throughput function determination. *Science* 2000;289:1760-1763.

98. Steger K. Haploid spermatids exhibit translationally repressed mRNAs. *Anat Embryol (Berl)* 2001;203:323-334.

99. Hanash SM. Operomics: molecular analysis of tissues from DNA to RNA to protein. *Clin Chem Lab Med* 2000;38:805-813.

100. Novak K. Angiogenesis inhibitors revised and revived at AACR. American Association for Cancer Research. *Nat Med* 2002;8:427.

Chapter 2

Identification of tumor-related proteins by proteomic analysis of cerebrospinal fluid from patients with primary brain tumors

J Neuropath Exp Neurol 2003 Aug; 62(8):855-862

Ping-Pin Zheng, Theo M. Luider, Rob Pieters, Cees J.J. Avezaat, Martin J. van den Bent, Peter A.E. Sillevis Smitt, Johan M. Kros

Abstract

Cerebrospinal fluid has been rediscovered in the post-genomic era as a great source of searching potential protein biomarkers for various diseases. The source allows rapid screening, low sample consumption, and accurate protein identification by proteomic technology. In the present study, we identified 2 candidate tumor-related proteins, *N-myc* oncoprotein and low molecular weight caldesmon (*l*-CaD), in cerebrospinal fluid (CSF) samples of patients with primary brain tumors by using two-dimensional polyacrylamide gel electrophoresis (2D PAGE) followed by matrix-assisted laser desorption/ionization-time of flight- mass spectrometry (MALDI-TOF-MS) analysis.
N-myc and *l*-CaD were related to tumor cell nuclei and blood vessels, respectively, in tissue sections of the tumor biopsies taken from the same patients from whom CSF was processed. *N-myc* oncoprotein and *l*-CaD have not yet been detected in CSF before. The practical value of these proteins as possible tumor markers, prognosticators or their utility in monitoring response to chemotherapy is currently subject of investigation. It is concluded that the combination of 2D PAGE and MALDI-TOF-MS is successful as an unbiased global screening tool for CSF.

Introduction

Almost all proteins normally present in cebrospinal fluid (CSF) are derived from serum. Only a few proteins, such as beta-trace protein (prostaglandin D2 synthase) and gamma-trace protein (Cystatin C), are synthesized intrathecally (1) . Protein entry into the CSF is thought to be mainly dependent on pinocytosis by the capillary endothelial cells of the brain and spinal cord that constitute the blood-brain barrier (BBB). The normal protein content of CSF is a 100-400 fold lower as compared to serum and depends upon the relative exclusion of macromolecules by the BBB (1) . Under pathological conditions one may find proteins which are usually absent from CSF . The presence of such proteins either results from disruption of the BBB or intrathecal production. An example of the latter is the increased CSF concentration of the tumor markers like LD5, beta-glucuronidase and beta-2-microglobuline in cases of leptomeningeal metastases (2, 3) . The identification of proteins in the CSF that are intrathecally secreted or shedded by the tumor or its microenvironment may reveal cellular mechanisms relevant to cancer biology. Also, it may result in the development of new tumor markers and may ultimately target new therapies. Recently, protein expression profiling has become a valuable tool in obtaining information about the state of protein circuits inside tumor cells and at the tumor-host interface (4) . Proteomic techniques are applicable to serum but also to CSF for the detection of peptides and proteins resulting from diseases, including cancer. A major advantage of the search for disease-related proteins in CSF over serum is the lower protein concentration in the former. Two-dimensional polyacrylamide gel electrophoresis (2D PAGE) is still a widely used technique to study protein expression profiles with a high resolution for the separation of complex protein mixtures (5, 6) . The identification of proteins separated by 2D PAGE has improved over the last decade due to advances in matrix-assisted laser desorption/ionization time-of-flight-mass spectrometry (MALDI-TOF-MS)(7, 8) . The combination of the two techniques has become a powerful tool in protein expression analysis in all fields of life science (9) .

Although 2D PAGE and subsequent analysis by MALDI-TOF-MS have successfully been applied for the identification of proteins in CSF (10) and in CSF of patients with neurological diseases (11) , these techniques have not yet been applied to search for brain tumor-related proteins in CSF. In the present study the CSF protein profiles of patients with primary brain tumors **(**i.e. 2 oligodendrogliomas, 3 anaplastic oligodendrogliomas, 2 anaplastic oligoastrocytomas, 2 pilocytic astrocytomas, 1 glioblastoma and 2 medulloblastomas) were compared with those of normal controls. The presence of the identified proteins was further confirmed by immunohistochemistry on tissue sections from the tumors of the patients from whom the CSF samples were obtained.

Materials and methods

CSF samples
All samples were collected at the Departments of Neuro-Oncology and Pediatrics, Erasmus MC, Rotterdam, The Netherlands. Informed consent was obtained in all cases. CSF samples from 12 patients with primary brain tumors (5 oligodendrogliomas, 2 anaplastic mixed oligoastrocytoma, 2

pilocytic astrocytoma, two medulloblastomas, 1 glioblastoma) were used for this study (Table). One of the oligodendroglioma patients had leptomeningeal metastatic spread of the tumor as demonstrated by positive cytology and MRI. The tumors were histologically typed according to the latest WHO guidelines (12) . Fourteen control samples (7 adults and 7 children) without evidence of neurological disease or systemic cancer were used. In order to exclude the possibility that proteins present in CSF of patients with brain tumors simply mirror a breakdown of the BBB (13), CSF samples from 9 multiple sclerosis (MS) patients were added. All samples were collected by lumbar puncture and transferred into a sterile container. Protein concentration and cell counts were performed routinely. The samples were stored at -80 °C until analysis.

Table. Presence of N-myc and *l*-CaD as Revealed by 2D and MALDI, and Immunohistochemistry, respectively

				2D and MALDI			
						IHC	
Case No	Sex/Age	CSF Cytology	Histological diagnosis	*N-myc*	*l-CaD*	*N-myc*	*l-CaD*
1	F/32	-	oligodendroglioma	+	-	ND	ND
2	F/55	-	oligodendroglioma	+	+	+	+
3	F/53	-	anaplastic oligodendroglioma	+	+	+	+
4	F/45	+	anaplastic oligodendroglioma	+	+	+	+
5	M/63	-	anaplastic oligodendroglioma	+	+	+	+
6	F/56	-	anaplastic mixed oligoastrocytoma	+	+	+	+
7	F/56	-	anaplastic mixed oligoastrocytoma	-	-	+	+
8	M/6	-	pilocytic astrocytoma	+	+	+	+
9	M/17	-	pilocytic astrocytoma	-	-	+	+
10	M/6	-	glioblastoma	-	+	+	+
11	F/16	-	medulloblastoma	+	-	+	+
12	M/4	-	medulloblastoma	+	-	+	+

F = female; M = male; - = negative; + = positive; IHC = immunohistochemistry; ND = not done

2D PAGE

For isoelectric focusing using immobilized pH strips, 1 ml CSF was precipitated in cold acetone (-20°C) at a final concentration of 95% (v/v). After precipitation, the samples were centrifuged at 20,800 g for 10 min at 4°C. The pellets were air dried at room temperature for 5 min and directly dissolved in 350 μl sample buffer mix (8M urea, 2% CHAPS, 0.5% IPG Buffer, 120 mM DTT, and bromophenol blue as an indicator) and then loaded on linear Immobiline DryStrips (IPG), pH 3-10 (Amersham Biosciences, Uppsala, Sweden). The IPG strips were reswollen for 12 hours at room temperature. The first dimensional separation was run for 1 h at 500V; 1h at 1,000 V and finally 8 h at 8,000 V on an IPG phor (Amersham Biosciences, Uppsala, Sweden) at 20°C. A minimum of 50,000 Vh was required before the run was ended. All focusing steps were carried out under mineral oil as recommended by the manufacturer. All chemicals were commercially obtained (Genomic Solutions, Hundington, UK or Amersham Biosciences, Uppsala, Sweden).

2-Dimensional Gel Electrophoresis

The IPG strips were transferred to equilibration buffer (0.3 M TrisBase; 0.075 M TrisHCL; 3% SDS) containing 8 mg/ml dithiothreitol for 2 min and followed by an additional 2 min in equilibration buffer containing 18.75 mg/ml iodoacetamide (Merck, Amsterdam, the Netherlands). Ten percent duracryl (10% acrylamide, 0.27% BIS) (Genomic Solutions, Hundingdon, UK) gels were casted. The second dimensional separation was vertically performed in a multiple electrophoresis system for ten gels (Genomic Solution, Hundingdon, UK) at a constant current (120mA) at 4°C. When the bromophenol blue dye front reaches within 1 cm from the bottom of the gel, the 2D PAGE was stopped.

Collodial Coomassie Brilliant Blue Staining and Silver Staining of the 2D Gels
After overnight fixation (40% methanol, 5% phosphoric acid, 55% MilliQ), gels were washed twice in MilliQ water for 10 min. Subsequently, the gels were stained in colloidal Coomassie Brilliant Blue (CBB) ((Invitrogen, Life Technologies, Breda, the Netherlands) overnight. Silver staining was performed according to Morrissey (14) . For each sample a pair of gels stained with CBB and silver were obtained.

Gel scanning and image comparison
Gels were scanned with a UMAX PowerLook II scanner (Genomic Solutions, Hundingdon, UK). Pattern-recognized analysis was performed by eyeball examination of the gels on an illuminator. Comparisons were made among the CBB and silver-stained gels of the controls, the tumor patients and between the tumor patients and the controls. The silver-stained gels generated more information than the CBB-stained gels. By overlaying the paired silver-stained and CBB-stained gels, protein spots of interest were picked from the CBB gels and subsequently analyzed by MALDI-TOF-MS.

Sample Preparation for MALDI-TOF-MS
The selected protein spots of the CBB-stained gels were further analyzed by MALDI-TOF-MS. The spots were picked manually from the CBB-stained gels with blunt pipette tips with a diameter of 2 mm. Gel plugs were washed with 100 μl MilliQ for 10 min on a Thermomixer (650 rpm, Eppendorf, Merck, Amsterdam, The Netherlands) in Nunc heat-resistant hydrophobic microtiter plates (Life Technologies, Breda, the Netherlands). Gel plugs were destained with 30% acetonitrile in 0.1 M ammonium hydrogen carbonate (Merck, Amsterdam, The Netherlands) and washed with MilliQ. The gel pieces were lyophilized by a Speedvac evaporator (Savant, Farmingdale, USA) for 30-60 min, followed by digestion with 0.4 μg (2U) trypsin (Promega Madison, WI, USA) in 4 μl 3 mM TrisHCL (pH 8.8) overnight at room temperature. Extraction of the peptide mixture from the gel plug was obtained with 7 μl (33% acetonitrile, 0.1% TFA in MilliQ). From the peptide mixture 0.5 μl was mixed on a MALDI target with 0.5 μl saturated matrix solution consisting of α-cyano-hydroxycinnamic acid (Merck, two times crystallized) resuspended in 1 ml acetonitrite.

MALDI-TOF-MS
MALDI-TOF-MS was performed on a Biflex ™ III (Bruker Daltonik, Bremen, Germany) equipped with a SCOUT 384 XY table. An anchorchip with 400 μm sample wells (Bruker Daltonik) was used to measure the peptide profiles. Data acquisition was performed on a SUN Ultra using XACQ software, Version 5.1 (Bruker Daltonik). We used close external calibration containing a standard peptide mixture of peptides (Sigma, St Louis, MO) with masses 756.9 (bradykinin), 1046.2 (angiotensin II), 1296.5 (angiotensin I), 1619.9 (bombesin), 2465.7 (ACTH). Database searching of MALDI-MS peptide masses was performed by using the MASCOT Peptide Mass Fingerprint software (www.matrixscience.com). The following general searching parameters were used: monoisotopic molecular mass, enzyme specificity trypsin, human database (NCBI database), maximal missed trypsin cleavages was set on one, peptide mass tolerance (200 ppm or lower). Significant Mowse score was at a probability of $p < 0.05$ (15) .

Immunohistochemical Staining
Immunohistochemical staining was performed by the immunoperoxidase technique following predigestion and trypsinization. Antibodies used were a mouse monoclonal antibody for *l*-CaD at a 1:40 dilution (Novacastra Laboratories Ltd, United Kingdom) and a mouse monoclonal antibody at a 1:15 dilution for *N-myc* (Novacastra Laboratories Ltd, United Kingdom). The sections were mounted to poly-L-lysin coated microslides, deparaffinized in xylene, dehydrated through graded alcohol and immersed in 70% methanol with H_2O_2 to block endogenous peroxidase. The sections were incubated with 1% (v/v) goat serum/PBS for 1 hour at room temperature, washed in phosphate-buffered saline (PBS), and incubated with the antibody in 2% (w/v) bovine serum albumin BSA/PBS overnight at 4 C°. Sections were then incubated with biotinylated goat-anti-mouse immunoglobulin (IgG) (Dako, Glostrup, Denmark) in 2% (w/v) BSA/PBS for 1 hour at room temperature followed by avidin-biotin-horseradish peroxidase complex (Dako, Glostrup, Denmark) for 30 minutes at room temperature. The final reaction products were visualized with diaminobenzidine (Novacastra Laboratories Ltd, United

Kingdom), and the sections were counterstained with hematoxylin. Between the incubation steps, sections were thoroughly washed in 0.005% (v/v) Tween 20/PBS. Negative and positive control slides were included to assess nonspecific staining.

Selection Criteria of Tumor-Related Proteins
The following criteria were applied to select a tumor-related protein: 1) The candidate spots had to be present in the CSF of the brain tumor cases, not in the control samples. 2) A candidate spot should not overlap with any other spots. 3) Identification of the candidate spots by MALDI-TOF-MS was feasible. 4) Immunohistochemical detection of the proteins in the tissue sections of the brain tumors of the same patients was required.

Results

Protein expression profiles in CSF from primary brain tumor patients and controls
Comparison of the CBB- and the silver-stained gels of the CSF samples of the 14 controls yielded almost identical protein expression profiles. The gels from the primary brain tumor patients were compared to those of the controls. A diagonal train of spots consisting of glycosylated protein isoforms was found in 7/10 of the CSF of the glioma patients but absent from the medulloblastomas and the controls (Fig. 1A and B; Table 1). Three out of four spots of this train were identified by MALDI-TOF-MS as low molecular weight caldesmon (*l*-CaD). The *p*I and mass shifts represent the various states of glycosylation of this protein (16). In the CSF from 9/12 primary brain tumor patients, another specific spot was detected which was absent from the control samples (Fig. 2A and B; Table) and the MS cases (data not shown). MALDI-TOF-MS analysis revealed that this spot was a truncated *N-myc* oncoprotein (data not shown).

Immunohistochemistry
The presence of *l*-CaD and *N-myc* in tissue samples of the primary brain tumors from the corresponding patients was verified by immunohistochemistry. *l*-CaD was expressed in all cells (endothelial cells, smooth muscle cells and pericytes) of proliferated vascular clusters of the gliomas (Fig. 1C), and also in the blood vessels of normal brain tissue (Fig. 1D). The immunostaining for *l*-CaD was stronger in the tumor vessels as compared to the normal capillaries in normal brain tissue (Fig. 1C and D). Immunostaining for *N-myc* yielded nuclear immunoreactivity in the tumor cellsin variable percentages of tumor cells ranging from 30% to 90% (Fig 2C, D; Table). Positive immunostaining was not seen in the tissue sections of the control surgical specimens or in any of the sections of the various brain regions of the autopsy cases.

Discussion

Changes in the protein components of CSF may be indicative of disease-related alterations in CNS protein expression patterns (11) . Because of the relative absence of cellular and macromolecular components, CSF is a potential, and also easily accessible source of disease-related proteins. *N-myc* oncoprotein and *l*-CaD were selectively identified by 2D PAGE followed by MALDI-TOF-MS in CSF obtained from primary brain tumors covering different histology and biological behavior.The proteins identified in the CSF sample were related to the tumor samples using immunohistochemistry. *N-myc* onoprotein and *l*-CaD were not present in theCSF of the MS patients, indicatve of the fact that the findng of these proteins does not simply reflect disruption of the BBB. The application of the techniques for proein anaysis used in this study also enable to identify protein degradation (e.g, truncated *N-myc*) and protein modification (e.g, *l*-CaD glycosylation).

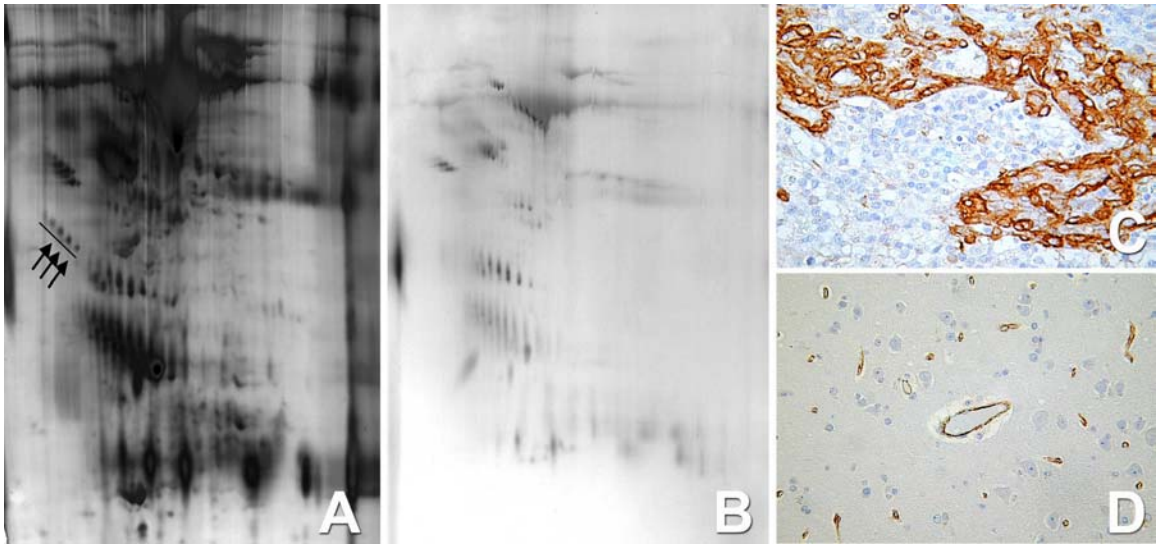

Fig 1. A representative silver-stained 2D master gel and immunohistochemical staining for *l*-CaD. **A ,B**: Silver-stained 2D PAGE gels of an anaplastic oligodendroglioma (A, case 3 in the Table) and a control CSF (B). The train of four spots in A (underlined) is absent from the corresponding gel site in (B). Three out of the four spots (indicated by arrows) were identified as *l*-CaD (MW 61,176 Da; *pI* 4.30) by MALDI-TOF-MS analysis. The fourth spot was not identified by MALDI-TOF-MS. **C**: Strong immunopositivity is appreciated in all constituents of the proliferated blood vessels (endothelial cells, smooth muscle cells and pericytes) (anaplastic oligodendroglioma, case 3 in the Table; immunostaining for *l*-CaD, magnification 250 x). D: Immunopositivity is restricted to capillaries in the normal control brain tissue (immunostaining for *l*-CaD, magnification 250 x).

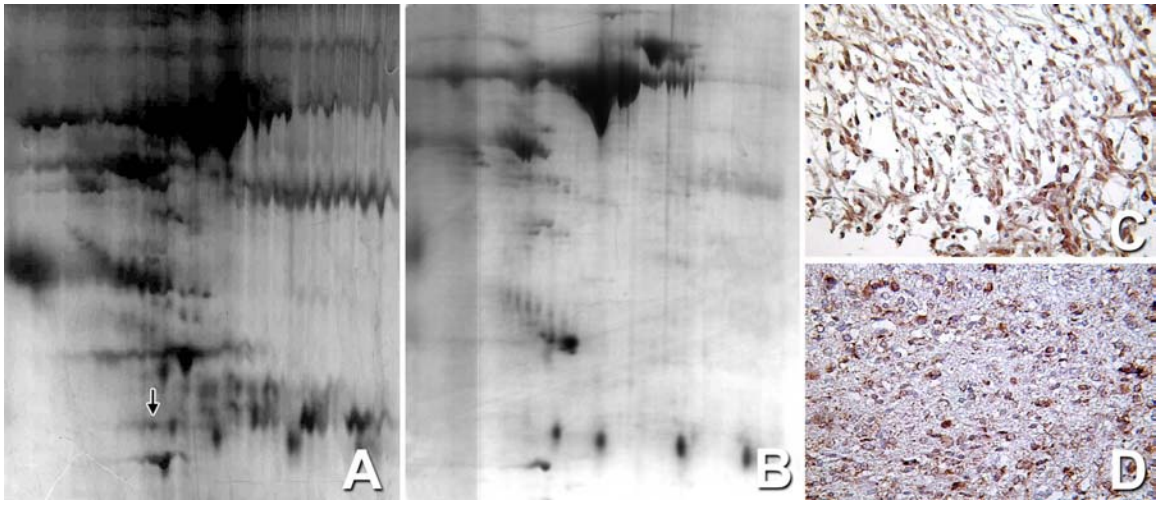

Fig 2. Representative silver-stained 2D master gel and immunohistochemical staining for *N-myc*. **A , B**: Silver-stained 2D PAGE gels from a pilocytic astrocytoma (**A**, case 8 in the Table) and a control CSF (**B**). The spot in **A** (arrowed) was identified as truncated *N-myc* oncoprotein (MW 19,584 Da; *pI* 5.28). **C.** Immunoreactivity in the tumor cell nuclei in a pilocytic astrocytoma (case 8 in the Table; immunohistochemistry for *N-myc*; magnification 250 x). **D.** Immunoreactivity in the nuclei of an anaplastic oligodendroglioma (case 5 in the Table; immunohistochemistry for *N-myc*; magnification 250 x).

Caldesmon is a microfilament binding protein with 2 high-molecular- and 4 low-molecular weight isoforms, which are produced by alternative splicing from a single gene (17). High-molecular caldesmon (*h*-CaD) is specifically present in smooth muscle cells while the low-molecular (*l*-CaD) molecule is expressed more ubiquitously (18) . Non-muscle *l*-CaD blocks cellular contractility through interactions with actin and myosin (18) . Phosphorylation of *l*-CaD (e.g. by mitosis-linked cdc2 kinase) results in the dissociation of *l*-CaD from the microfilaments which are required for mitosis (19) . Little is known about the role of *l*-CaD in human disease and cancer (20, 21) . In the present study the

expression of *l*-CaD was confined to the blood vessel components of normal and proliferated tumor vessels. Immunostaining of the tumor vessels was stronger as compared of that in the blood vessels in normal brain. This is suggestive of a ole of this protein in vascularization and angiogenesis. The presence of *l*-CaD in the CSF seems unrelated to glioma subtype or grade. Microvascular proliferation is characteristically seen in anaplastic gliomas. Although pilocytic astrocytomas are low-grade lesions, they harbor notoriously proliferated blood vessels, which explains the presence of *l*-CaD in the CSF of patients with these tumors. A possible explanation for the finding of *l*-CaD in the CSF of patients with low-grade diffuse gliomas may be that the generastion of this protein is already enhanced in the angiogenesis of the low-grade lesions. In gliomas, neovascularization and endothelial proliferation are closely associated with breakdown of the blood-brain barrier (BBB) and increased endothelial permeability (22-24). Regulation of the endothelial cell barrier is highly dependent on the actomyosin cytoskeleton (25) . Protein kinase C (PKC) is involved in endothelial cell barrier function via a signaling pathway that includes the phosphorylation of *l*-CaD (26) . It may very well be that PKC isoforms, overexpressed by malignant gliomas, contribute to BBB disruption through phosphorylation of *l*-CaD (27) . The finding of *l*-CaD in CSF of the patients with primary brain tumors exemplifies that proteins related to the tumor-host microenvironment may be detected by proteomics.

N-myc oncoprotein was found in the CSF samples of almost all patients with primary brain tumors (Fig. 2A, B). *N-myc* is one of the nuclear oncoproteins that undergo rapid ubiquitin-mediated degradation (28). The finding of truncated *N-myc* reflects this fast intracellular degradation. Immunostaining for *N-myc* confirmed the presence of this protein in part of the nuclei of the corresponding primary brain tumor tissue sections (Fig. 2C, D). With only few exceptions like normal human breast tissue (29) normal tissues do not express the *N-myc* oncogene (30). Various percentages of immuopositive cells were encountered in the 2 medulloblastomas.

The *myc* oncogene family encodes a group of nuclear phosphoproteins that play a role in cell growth and in the development of human tumors (31) . Activation and amplification of the *N-myc* oncogene and its subsequent overexpression has been found in various primary brain tumors, including glioblastomas and anaplastic astrocytomas (32, 33), but most commonly in members of the PNET group such as medulloblastomas (34) and neuroblastomas (35) .The expression of *N-myc* was not previously reported in oligodendrogliomas or pilocytic astrocytomas. Additional studies of CSF and serum are required to further investigate the practical value of *N-myc* protein as a primary brain tumor marker.

It is concluded that the application of the combination of 2D PAGE and MALDI-TOF-MS is successful in the unbiased global screening for tumor-related proteins in CSF. The identified proteins *N-myc* oncoprotein and *l*-CaD have not yet been reported in previous CSF studies. The practical value of these proteins as possible tumor markers, prognosticators or their utility in monitoring response to chemotherapy urges further investigation.

Acknowledgements

Mr. M. van der Weiden is kindly thanked for his technical assistance. Mr. F. van de Panne is acknowledged for his assistance with the photography.

References

1. Fishman RA. Cerebrospinal fluid in diseases of the nervous system. Philadephia: W. B. Saunders Company, 1992

2. Wasserstrom WR, Glass JP, Posner JB. Diagnosis and treatment of leptomeningeal metastases from solid tumors: experience with 90 patients. Cancer 1982; 49:759-72.

3. van Zanten AP, Twijnstra A, Ongerboer de Visser BW, van Heerde P, Hart AA, Nooyen WJ. Cerebrospinal fluid tumour markers in patients treated for meningeal malignancy. J Neurol Neurosurg Psychiatry 1991; 54:119-23.

4. Liotta LA, Kohn EC. The microenvironment of the tumour-host interface. Nature 2001; 411:375-9.

5. Klose J. Protein mapping by combined isoelectric focusing and electrophoresis of mouse tissues. A novel approach to testing for induced point mutations in mammals. Humangenetik 1975; 26:231-43

6. Patterson SD. Mass spectrometry and proteomics. Physiol Genomics 2000; 2:59-65.

7. Siuzdak G. The emergence of mass spectrometry in biochemical research. Proc Natl Acad Sci U S A 1994; 91:11290-7.

8. Mann M, Talbo G. Developments in matrix-assisted laser desorption/ionization peptide mass spectrometry. Curr Opin Biotechnol 1996; 7:11-9.

9. Bonk T, Humeny A. MALDI-TOF-MS analysis of protein and DNA. Neuroscientist 2001; 7:6-12.

10. Sickmann A, Dormeyer W, Wortelkamp S, Woitalla D, Kuhn W, Meyer HE. Identification of proteins from human cerebrospinal fluid, separated by two-dimensional polyacrylamide gel electrophoresis. Electrophoresis 2000; 21:2721-8.

11. Rohlff C. Proteomics in molecular medicine: applications in central nervous systems disorders. Electrophoresis 2000; 21:1227-34.

12. Kleihues P, Louis DN, Scheithauer BW, et al. The WHO classification of tumors of the nervous system. J Neuropathol Exp Neurol 2002; 61:215-25; discussion 226-9.

13. Petty MA, Lo EH. Junctional complexes of the blood-brain barrier: permeability changes in neuroinflammation. Prog Neurobiol 2002; 68:311-23.

14. Morrissey JH. Silver stain for proteins in polyacrylamide gels: a modified procedure with enhanced uniform sensitivity. Anal Biochem 1981; 117:307-10.

15. Perkins DN, Pappin DJ, Creasy DM, Cottrell JS. Probability-based protein identification by searching sequence databases using mass spectrometry data. Electrophoresis 1999; 20:3551-67.

16. Packer NH, Lawson MA, Jardine DR, Sanchez JC, Gooley AA. Analyzing glycoproteins separated by two-dimensional gel electrophoresis. Electrophoresis 1998; 19:981-8.

17. Ciechanover A, DiGiuseppe JA, Bercovich B, Orian A, Richter JD, Schwartz AL, Brodeur GM. Degradation of nuclear oncoproteins by the ubiquitin system in vitro. Proc Natl Acad Sci U S A 1991; 88:139-43.

18. Hershko A. Ubiquitin-mediated protein degradation. J Biol Chem 1988 ; 263:15237-40.

19. Huber PA. Caldesmon. Int J Biochem Cell Biol 1997; 29:1047-51.

20. Hayashi K, Fujio Y, Kato I, Sobue K. Structural and functional relationships between h- and l-caldesmons. J Biol Chem 1991; 266:355-61.

21. Yamashiro S, Yamakita Y, Hosoya H, Matsumura F. Phosphorylation of non-muscle caldesmon by p34cdc2 kinase during mitosis. Nature 1991; 349:169-72.

22. Yamamura H, Yoshikawa H, Tatsuta M, Akedo H, Takahashi K. Expression of the smooth muscle calponin gene in human osteosarcoma and its possible association with prognosis. Int J Cancer 1998; 79:245-50.

23. Porter RM, Holme TC, Newman EL, Hopwood D, Wilkinson JM, Cuschieri A. Monoclonal antibodies to cytoskeletal proteins: an immunohistochemical investigation of human colon cancer. J Pathol 1993; 170:435-40.

24. Earnest Ft, Kelly PJ, Scheithauer BW, et al. Cerebral astrocytomas: histopathologic correlation of MR and CT contrast enhancement with stereotactic biopsy. Radiology 1988; 166:823-7.

25. Roberts HC, Roberts TP, Brasch RC, Dillon WP. Quantitative measurement of microvascular permeability in human brain tumors achieved using dynamic contrast-enhanced MR imaging: correlation with histologic grade. AJNR Am J Neuroradiol 2000; 21:891-9.

26. Jackson A, Kassner A, Annesley-Williams D, Reid H, Zhu XP, Li KL. Abnormalities in the recirculation phase of contrast agent bolus passage in cerebral gliomas: comparison with relative blood volume and tumor grade. AJNR Am J Neuroradiol 2002; 23:7-14.

27. Liu F, Verin AD, Borbiev T, Garcia JG. Role of cAMP-dependent protein kinase A activity in endothelial cell cytoskeleton rearrangement. Am J Physiol Lung Cell Mol Physiol 2001; 280:L1309-17.

28. Ishii I, Tomizawa A, Kawachi H, et al. Histological and functional analysis of vascular smooth muscle cells in a novel culture system with honeycomb-like structure. Atherosclerosis 2001; 158:377-84.

29. Sharif TR, Sharif M. Overexpression of protein kinase C epsilon in astroglial brain tumor derived cell lines and primary tumor samples. Int J Oncol 1999; 15:237-43.

30. Mizukami Y, Nonomura A, Takizawa T, et al. N-myc protein expression in human breast carcinoma: prognostic implications. Anticancer Res 1995; 15:2899-905.

31. Schwab M, Ellison J, Busch M, Rosenau W, Varmus HE, Bishop JM. Enhanced expression of the human gene N-myc consequent to amplification of DNA may contribute to malignant progression of neuroblastoma. Proc Natl Acad Sci U S A 1984; 81:4940-4.

32. Zajac-Kaye M. Myc oncogene: a key component in cell cycle regulation and its implication for lung cancer. Lung Cancer 2001; 34 Suppl 2:S43-6.

33. Herms JW, von Loewenich FD, Behnke J, Markakis E, Kretzschmar HA. c-myc oncogene family expression in glioblastoma and survival. Surg Neurol 1999; 51:536-42.

34. Mapstone TB, Galloway PG. Expression of glial fibrillary acidic protein, vimentin, fibronectin, and N-myc oncoprotein in primary human brain tumor cell explants. Pediatr Neurosurg 1991; 17:169-74

35. Moriuchi S, Shimizu K, Miyao Y, Hayakawa T. An immunohistochemical analysis of medulloblastoma and PNET with emphasis on N-myc protein expression. Anticancer Res 1996; 16:2687-92.

36. Borriello A, Roberto R, Della Ragione F, Iolascon A. Proliferate and survive: cell division cycle and apoptosis in human neuroblastoma. Haematologica 2002; 87:196-214.

Chapter 3

Differential expression of splicing variants of the human caldesmon gene (*CALD1*) in glioma neovascularization versus normal brain microvasculature

Am J Pathol. 2004 Jun;164(6):2217-28.

Ping-Pin Zheng, Anieta M. Sieuwerts, Theo M. Luider, M. van der Weiden, Peter A.E. Sillevis-Smitt, Johan M. Kros

Abstract

Caldesmon is a cytoskeleton-associated protein which has not yet been related to neoplastic angiogenesis. In this study we investigated the expression of the caldesmon gene (*CALD1*) splicing variants and the protein expression level in glioma microvessels versus normal brain microvasculature. In order to exclude sources of splice variant expression from non-vascular components all possible cellular components present in control and glioma samples were pre-screened by laser capture microdissection followed by RT-PCR prior to the cohort study. We discovered differential expression of the splicing variants of *CALD1* in the tumor microvessels in contrast to normal brain microvasculature. Missplicing of exons 1, 1 + 4 and 1' + 4 of the gene is exclusively found in glioma microvessels. To exclude the possibility that this missplicing results from splice-site mutations, mutation scanning was performed by a coupled in vitro transcription/translation assay (IVTT). No premature stop mutations were traced by the IVTT. The transcriptional changes consequently resulted in up-regulation at the protein expression level. The up-regulated expression of caldesmon was coincident with the down-regulated expression of tight junction proteins (occludin and ZO-1). The results support the notion that missplicing of the *CALD1* gene in glioma microvasculature is an independent epigenetic event regulated at the transcriptional level. The event coexists with TJ breakdown of the endothelial cells in glioma microvasculature. The data reveal a novel mechanism contributing to dysfunctionality of glioma neovascularization.

Introduction

Genome-wide analyses have revealed that 40 to 60% of human genes undergo alternative splicing [1]. Alternative splicing, therefore, seems to contribute considerably to enable the highly complex and diverse functions encoded by the human genome. Alternative splicing permits vertebrate pre-mRNA to be processed into multiple mRNAs differing in their precise combination of exon sequences, resulting in the encoding of different protein isoforms [2]. Multiple modes of alternative splicing exist, such as alternative 5' or 3'splice-site usage, differential inclusion or skipping of particular exons, mutually exclusion of exons, and more [3]. Importantly, alternative splicing is often tightly regulated in a cell type- or developmental stage-specific mode [3]. The essential nature of this process is underscored by the fact that misregulation (missplicing events) is often related to human disease[4-6]. The caldesmon gene (*CALD1*) is a single gene with transcriptional variance characterized by the recombination of different alternative splicing modes regulated by specific promoter activities [7]. The human *CALD1* shares common structural and expressional properties through mammals [8,9]. The gene is located on chromosome 7q33-34, consists of at least 15 exons and gives rise to two major classes of protein isoforms, i.e., high molecular weight caldesmon (120-150 kDa, *h*-CaD) and low molecular weight caldesmon (70-80 kDa, *l*-CaD) [7,10]. The conserved regions of all isoforms encoded by exon 2, 3a and 5 to 15 contain caldesmons' capacity to bind to actin, tropomyosin, Ca (2+)-calmodulin, myosin and phospholipids [11]. The exons 1, 3b and 4 are alternatively spliced. Exon 3b encodes the central alpha helix which is absent from *l*-CaD. *h*-CaD isoforms are restricted to fully differentiated smooth muscle cells (SMCs) and regulate the smooth muscle tone. *l*-CaD consists of at least four splicing variants (WI-38 *l*-CaDs I and II, Hela *l*-CaDs I and II) which are expressed via differential inclusion of the variable alternative spliced exons 1, 1' and 4 of the gene [7]. The exons 1 and 1' encode the short amino terminus specific for Hela *l*-CaDs and WI-38 *l*-CaDs or *h*-CaD, respectively [7]. The *l*-CaD isoforms are ubiquitously distributed in various cells and dedifferentiated SMCs. They play roles in the regulation of cell contractility, adhesion-dependent signaling and cytoskeletal organization, influencing granule movement, hormone secretion and reorganization of microfilaments during mitosis via mitosis-specific phosphorylation by cdc2 protein kinase [10-12]. The distinct functions of different cell types must involve different isoforms of caldesmon. However, the expression of the various *CALD1* splicing variants and protein isoforms has only been investigated in a limited selection of normal human tissues[8]. In human aorta, all splicing variants of the gene have been investigated. The expression was restricted to *h*-CaD (exon 1, 3b and 4) and WI-38 *l*-CaD II (exon 1') [8].

In glioma, microvascular proliferation or hyperplasia is a notorious event. Microvascular architecture and density in low-grade gliomas are similar to that in normal brain tissue. In anaplastic gliomas and glioblastomas however, microvascular hyperplasia such as glomeruloid and branching or

sprouting proliferation, is a common event. Leakage of these vessels leads to perivascular edema and shows in neuroradiologic presentations of high-grade gliomas. The proliferated or hyperplastic vessels are dysfunctional in that there is a disruption of the blood-brain barrier.

In a previous study we found the low molecular isoform of caldesmon (*l*-CaD) in the cerebrospinal fluid (CSF) of glioma patients[13]. It was noticed by immunohistochemistry on tissue sections of the very gliomas that the expression of caldesmon was restricted to the blood vessels while no immunopositivity was obtained in glial cells. In the present study, we further investigated the *CALD1* splicing variants, focusing on *l*-CaD in tissue samples of 68 patients with gliomas. In order to exclude the possibility that *CALD1* transcripts manifest translationally repressed or silent [14,15] in the glial cells, the glial cells were captured from control and tumor samples by laser capture microdissection (LCM) prior to the cohort study. In addition, any possible or minor cellular components present in the normal controls and glioma samples were pre-screened by LCM/RT-PCR and immunohistochemistry. Missplicings in glioma microvessels are revealed by RT-PCR. The transcriptional changes consequently result in an up-regulated protein expression level. Alterations of splicing patterns could result from splice-site mutations via activation of cryptic splice site usage[16,17]. The phenotypic effects of such mutations on mRNA splicing often cause codon frame-shifts or single base substitution consequently resulting in premature termination codons [18,19]. Such splice site mutations account for at least 15% of point mutations causing disease in human [16,20]. To rule out the presence of splice site mutations resulting in the missplicing events of the *CALD1* gene in our tumor cases, the samples were scanned by coupled in vitro transcription/translation assay (IVTT, also known as the protein truncation test PTT). The principle of IVTT is based on targeting mutations that generate truncated proteins induced by premature translation termination [21]. IVTT enables to pinpoint the site of a mutation, offers good sensitivity and a low false-positive rate [22]. Further tight junction proteins (occludin and ZO-1) were co-investigated in this study. Interestingly, the up-regulated expression of *l*-CaD resulting from *CALD1* missplicing was coincident with the down-regulation of occludin and ZO-1, causing TJ breakdown of the endothelial cells in glioma microvasculature.

Material and Methods

Samples and Histology

The study was conducted on 68 snap-frozen specimens of glioma stored in the archives of the Department of Pathology, Erasmus Medical Center, Rotterdam, the Netherlands. Histopathologic typing and grading of the tumors was performed on the corresponding paraffin sections based on the latest WHO classification of tumors of the central nervous system [23]. Frozen section screening was to get rid of those samples with massive necrosis, hemorrhage and contaminating normal tissues. Finally, the tumors analyzed included 26 glioblastomas, 23 oligodendrogliomas (among which 18 anaplastic oligodendrogliomas) and 19 pilocytic astrocytomas. Six samples of white matter obtained from patients without neurological or systemic disease served as controls.

Light Microscopy/Immunohistochemistry

To determine the site and distribution of the *l*-CaD protein expression in the tumors and control samples, tissue sections were immunohistochemically stained with a monoclonal anti-*l*-CaD antibody at a 1: 40 dilution (BD Biosciences). The immunohistochemical procedure was described previously[13].

Pre-screening CALD1 expression in all of the cellular components possibly present in the tissue samples used by laser Capture Micodissection (LCM)/RT-PCR and immunohistochemistry

The main purpose for the pre-screening experiments was to determine whether unfractional samples can be used for analysis. The white matter controls predominantly consist of glial cells and blood vessels with minor blood cell components. In glioma, the major cellular components are neoplastic glial cells (glioma cells) and hyperplastic or proliferated microvessels with possible or minor contaminating cells such as inflammatory cells, fibroblasts and leptomeningeal cells. Normal glial cells and normal vessels were captured from the control samples (4 cases), while glioma cells and glioma vessels were captured from glioma cases (10 cases), respectively. Fibroblasts and leptomeningeal cells were captured from normal dura and arachnoid (each 2 from autopsy cases), respectively. Since all kinds of inflammatory cells are derived from transmigration of leukocytes from blood vessels into the brain tissue, 20 normal blood samples were used for screening of possible

CALD1 expression in leukocytes. LCM was performed by using a Robot Microbeam laser microscope as the manufacture instructed (P.A.L.M, Microlaser Technologies, Germany). Frozen sections for LCM were prepared by using Rnase-free conditions. The used frozen tissue blocks were sectioned at 5 μm in cryostat, mounted on noncoated clean glass sliders, and stored at -80°C until use. The staining procedures of the sections were mainly based on the published protocol at http://pathbox.wustl.edu/~tisscore/protocols.htm [24]. A little modification of the protocol was made by skipping "automation buffer" and using the stainer (HisGene™ , Arcturus) instead of Mayer's hemotoxylin and eosin. For Robot Microbeam laser microdissection the tissue area of interest was selected and positioned (Figures 1A, C and E), and cut out using a focused, pulsed laser beam. The dissected areas were collected in the cap of a microcentrifuge tube containing 18 μl TRIZOL (Invitrogen) via laser pressure catapulting. The object of interest was catapulted off the slide using a high-energy, defocused, short-duration laser pulse (Figures 1B, D and F). The cap with the procured tissues was immediately placed on a microcentrifuge tube containing 200μl TRIZOL (Invitrogen) and lysed by mixing for further RNA isolation.

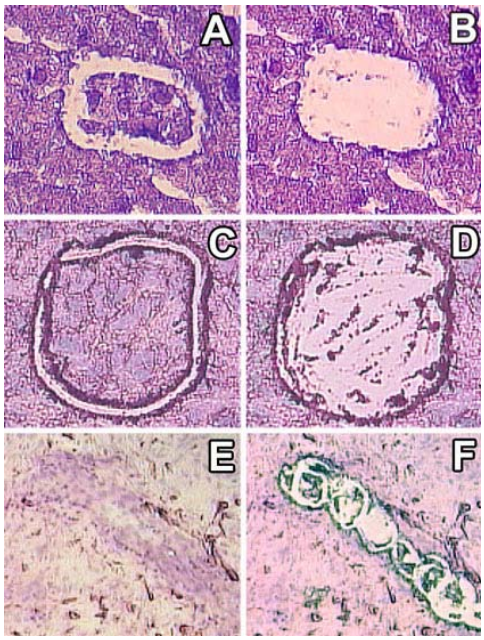

Figure 1. Laser-capture microdissection of glial cells and vessels**. A**: The target normal glial cell population was dissected with ultraviolet laser. **B**: The dissected cells were photoablated within the laser focus and then directly collected into a microcentrifuge tube cap filled with Trizol for RNA isolation by laser pressure catapulting. **C**: The target tumor cell population (glioblastoma) was dissected with ultraviolet laser. **D**: The dissected cells were photoablated and collected as mentioned under B. **E**: The targeted hyperplastic vessel in pilocytic astrocytoma was positioned. **F**: The dissected vessel was photoablated and collected as mentioned in (**B**).

CALD1 Transcript Analysis

Total cellular RNA was extracted from the selected specimens using TRIZOL as the Manufacturer's protocol (Invitrogen). First strand complementary DNA (cDNA) was generated with an oligo $(dT)_{23}$ primer and DuraScript™ reverse transcriptase (Sigma). The resulting cDNA was amplified by PCR using CALD1 specific primer sets spanning the splice-sites of this gene toward all the four splicing variants of *l*-CaD as described elsewhere [7]. A primer set for the CALD1, designed to amplify all the splicing variants [25], was used for initial examining the microdissected samples (the product size for *l*-CaD isoforms is 744bp). Glyceraldehyde 3-phosphate dehydrogenase (GAPD) fragment [26] was prepared by PCR as an internal control. All the primers used in this study were commercially synthesized (Invitrogen). The amount of each RNA sample used was selected on the basis of identical amounts of GAPD cDNA amplified from each sample. At a 2 min initial denaturation at 94°C, amplification conditions were as follows: 94°C for 15 s, 66°C (60°C for GAPD) for 30 s and 68°C for 1 min for 36 cycles (40 cycles for the microdissected samples), and final extension at 68°C for 5 min. GAPD transcripts were amplified by 30 cycles (36 cycles for the microdissected samples). Negative controls, consisting of one sample without reverse transcriptase and one without template, were included in each experiment. The PCR products were resolved by electrophoresis on a 1% agarose gel containing ethidium bromide, and viewed under ultraviolet illumination. At least three experiments were performed for reproducibility.

Immunoblotting
Total cellular protein was co-isolated and lysed during RNA isolation by TRIZOL according to the manufacturer's protocol (Invitrogen). Protein concentrations in the extracts was determined by the BCA protein assay (Pierce Chemical Co). Protein samples (15 μg/lane) were separated on a 12% SDS-polyacrylamide gel and transferred to nitrocellulose. Electroblotting was performed on a nitrocellulose membrane in 25 mM Tris and 192 mM glycine containing 20% methanol. The membrane was then pretreated with 5% skim milk in TBST overnight at 4°C. The membrane was incubated with monoclonal anti-*l*-CaD antibody (BD Biosciences, dilution 1: 1000) in TBST or anti-α,β-tublin cocktail (Lab Vision, dilution 1: 1000) in TBST for 1 h at room temperature. The membrane was further incubated with horseradish peroxidase (HRP)-conjugated goat anti-mouse IgG antibody (Zymed Laboratory Inc, dilution 1:10,000) for 1 h at room temperature. The peroxidase was finally activated with enhanced chemiluminescence (ECL kit, Amersham) and the immunoreactivity was visualized with Kodak® X-Omat AR X-ray film. For quantitative analysis of *l*-CaD, the bands on films were scanned by using a UMAX PowerLook II scanner (Genomic Solutions, Hundingdon, UK) at 750dpi. Densitometric analysis was performed with the ONE-Dscan software (Scanalytics, Billerica). Each experiment was repeated at least twice. The average change in band intensities was normalized against tubulin.

IVTT
The specimens used by a coupled in vitro transcription/translation assay (IVTT) were pre-treated by puromycin (200μg/ml) (Sigma) for 6 hr at room temperature prior to RNA isolation. Puromycin is a translation inhibitor known to suppress nonsense-mediated mRNA decay (NMD), thus allowing mutation screening at the RNA level [27]. The PCR products suitable for IVTT analysis were generated with sense primers containing a T7 RNA polymerase promoter, a start condon, and the Kozak translation initiation sequence [28]. The transcripts were amplified by 40 cycles. Since the normal transcripts containing exons 1, 1 + 4 and 1' + 4 were not detected in the control white matter, the corresponding transcripts used in IVTT were retrieved from normal stomach, prostate and thyroid, respectively. 2.5 μl of the PCR product amplified from each transcript was incubated in the TNT/T7 non-radioactive coupled transcription and translation system (TNT® Quick for PCR DNA, Promega) for 90 min at 30°C in a total volume of 50 μl in the presence of biotinylated lysine residues. The biotinylated lysine residues are incorporated into nascent protein during translation, eliminating the need for labelling with [^{35}S] methionine or other radioactive amino acids, and allowing non-radioactive detection of protein synthesized in vitro by binding either Streptavidin-Alkaline Phosphatase (Streptavidin-AP) or Streptavidin-Horseradish Peroxidase (Streptavidin-HRP). In our experiments, the in vitro synthesized proteins were size fractionated on 12% SDS-polyacrylamide minigels. The fractionated proteins were electroblotted onto nitrocellulose at a constant voltage of 100V for 60 min. Streptavidin-HRP binding (dilution at 1: 20,000) was used for visualization with enhanced chemiluminescence ((ECL kit, Amersham) as the protocol (Promega).

Expression of occludin and ZO-1 in Glioma Microvasculature detected by Immunofluorescence and Immunohistochemistry
Cryostat sections (5μm) were cut onto non-coated microscope slides (Menzel-Glaser). Slides were fixed in 100% ice-acetone at room temperature for 10 min and air dried.
After washes with PBS, indirect immunofluorescence was carried out by using the anti-occludin polyclonal antibody (Zymed Laboratories Inc, dilution 1:100) and anti-ZO-1 polyclonal antibody (Zymed Laboratories Inc, dilution 1:100) with incubation for 1 hour at room temperature. The FITC-conjugated swine anti-rabbit IgG (Dako, dilution1:100) was used for 1 hour at room temperature for visualization. Slides were washed with PBS, and were mounted in imselmount (Klinipath) and covered with Pertex and covering glass. A CCD video camera (Leica) mounted on a Leica (DMRXA) fluorescence microscope was used to capture digital images on a Leica computer (Q550 CW) running the software (Leica CW 4000 FISH Version V 1.0)
For immunohistochemistry, paraffin sections (5μm) were cut onto aminopropyltriethoxysilane (APES)-coated glass slides (Knittel Glaser). Dewaxed sections were pretreated in 0.1% pronase (Sigma) for 10 minutes at 37ºC. After the pre-treatment of the slides were washed with PBS and

incubated with anti-occludin polyclonal antibody (Zymed Laboratories Inc, dilution 1:100) for two hour at room temperature. The biotinylated goat anti-rabbit (Dako, dilution1: 200) was used for 1 hour at room temperature for visualization. Again the slides were washed in PBS and incubated with StreptABC complex/AP (Dako, dilution 1:100) for one hour at room temperature. After the slides were washed with PBS, enzyme detection was performed by using a solution of Tris-HCl pH 8.0 containing 1% new fuchsin, 1% natriumnitriet, 0.03% Napthol AS-MX phosphate (Sigma) and 0.025% Levamisol (Acros)) for one hour at room temperature. The slides were washed again with PBS, mounted in imselmount (Klininpath) and covered with Pertex and covering glass for examination under a light microscope.

Results

Confirmation of Absent Expression of CALD1 Transcript and Protein in Glial Cells

Immunohistochemistry showed that the expression of the caldesmon protein was restricted to the blood vessels. The immunoreactivity for the caldesmon protein was stronger in the hyperplastic microvessels of the gliomas as compared to normal brain microvasculature (Figures 2A-E). The enhanced immunoreactivity was confirmed by immunoblotting analysis showing a higher expression of total *l*-CaD in the tumor samples (see below). At the light microscopical level no immunopositivity was observed in neoplastic and normal glial cells in the specimens. Neither the neoplastic-, nor the normal glial cells captured by LCM showed expression of CALD1 transcripts, in contrast to the positive controls (tumor vessels) (Figures 1 and 3).

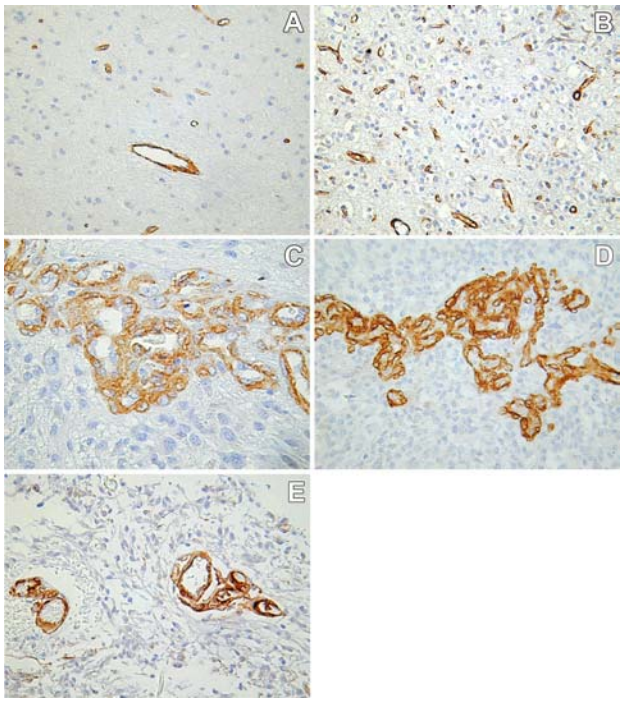

Figure 2. Immunohistology of a series of representative glioma subtypes and normal control. Immunohistochemistry showed that the expression of the protein was restricted to the blood vessels and stronger immunoreactivity was noticed in the hyperplastic vessels of the gliomas. No immunopositivity was obtained in normal glial cells and their neoplastic counterparts. A: Immunopositivity for *l*-CaD is observed in the normal blood vessels in control white matter (x 250). B: Immunopositivity for *l*-CaD is seen in the oligodendroglioma vessels without hyperplasia (x 250). C: Strong immunopositivity for *l*-CaD is found in the hyperplastic microvessels in a glioblastoma (x 400). D: Strong immunopositivity for *l*-CaD is seen in the hyperplastic microvessels in an anaplastic oligodendroglioma (x 250). E: Strong immunopositivity for *l*-CaD is noticed in the hyperplastic microvessels in a pilocytic astrocytoma (x 250).

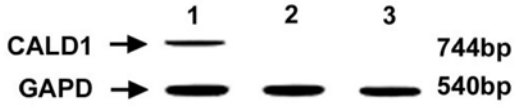

Figure 3. Analysis of *CALD1* transcript expression in purified glial cells by LCM. The used primer set was designed to amplify all the splicing variants. Lane 1 represents the positive control (tumor vessels; Figure 1 E and F) showing *CALD1* transcript expression (744bp). Lane 2 (normal glial cells) and lane 3 (neoplastic glial cells) show no expression of *CALD1* transcripts. The housekeeping gene (*GAPD*) was identically amplified in all the samples.

Expression Profiles of CALD1 in Microdissected Normal Brain Vessels and Other Possible or Minor Cellular Components in Normal Controls and Gliomas

The microdissected microvessels from the normal controls showed expression of exon 1'(WI-38 II) (Figure 4). Fibroblasts express *CALD1* with restriction to exon 1' and with immunopositivity of caldesmon (Figure 5).

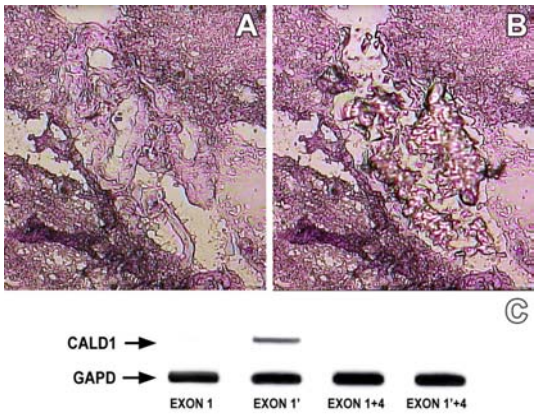

Figure 4. Laser-capture microdissection of normal brain vessels. **A**: Normal brain vessels prior to microdisection. **B**: The target vessels from A after microdissection. **C:** The RT-PCR result from the microdissected vessels. These normal vessels express exon 1'only.

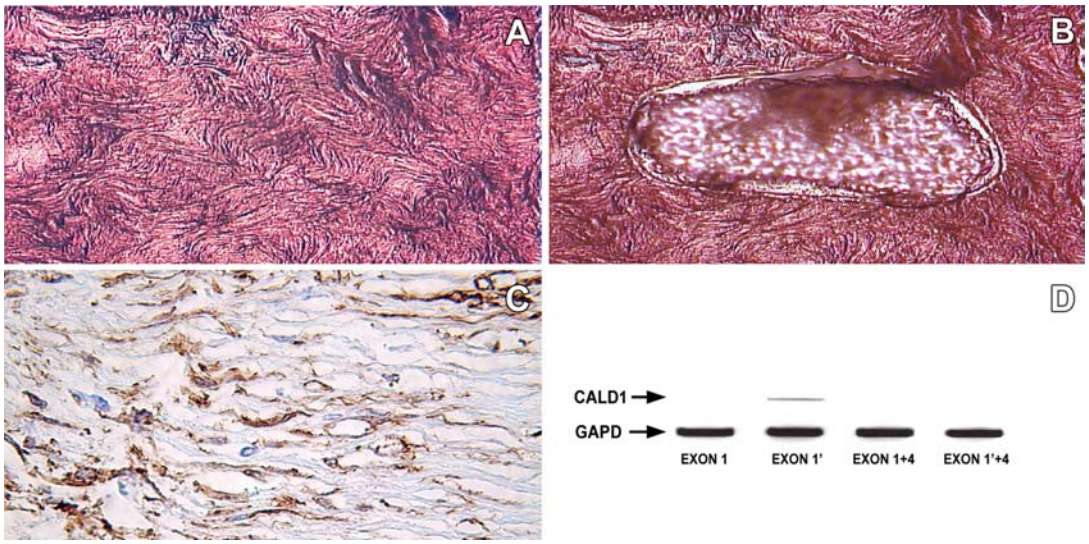

Figure 5. Laser-capture microdissection of fibroblasts from normal dura. A: Normal dura prior to microdissection. B: The microdissected target cell population from A. C: Positive immunoreactivity for caldesmon is shown in the fibroblasts. D: The RT-PCR result from the micodissected fibroblasts. The fibroblasts show *CALD1* expression with restriction to exon 1'.

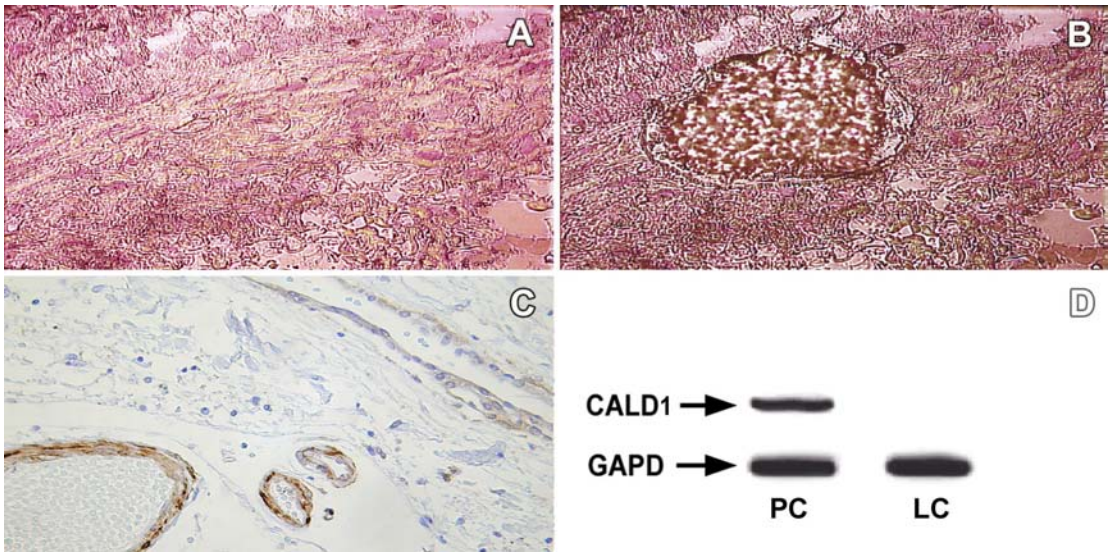

Figure 6. Laser-capture microdissection of normal leptomeningeal cells from the arachnoid. **A**: Normal arachnoid prior to microdissection. **B**: The microdissected target leptomeningeal cell population from A. **C**: No immunoreactivity for caldesmon is seen in the leptomeningeal cells. **D**: The RT-PCR result from the micodissected leptomeningeal cells. PC = positive control; LC = leptomingeal cells. The housekeeping gene (*GAPD*) was identically amplified in the PC and LC. No expression of *CALD1* transcript in leptomeningeal cells was found.

Further, no *CALD1* expression was found in leptomeningeal cells by LCM/RT-PCR and immunohistochemistry (Figure 6). No *CALD1* expression in leukocytes or inflammatory cells was detected (Figure 7).

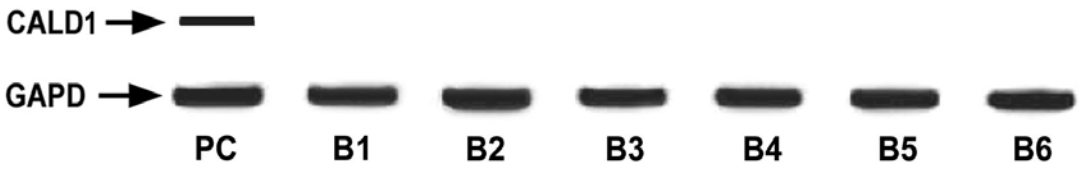

Figure 7. Examination of *CALD1* expression in leukocytes or inflammatory cells. A representative RT-PCR result of the blood samples is shown. (PC = positive control; B1 to B6 = blood samples examined). The housekeeping gene (*GAPD*) was identically amplified in all the samples examined. No *CALD1* expression was found in the leukocytes or inflammatory cells.

Differential Expression of CALD1 Transcripts and Protein in Glioma Microvessels Versus Normal Brain Microvasculature

The results of immunohistochemistry and the LCM data revealed that there was no expression of protein and transcript of the CALD1 gene in normal and neoplastic glial cells. In addition, the pre-screening experiments show that no differential expression patterns of CALD1 were detected in any of these cell types. Thus, it is feasible to use unfractional samples of control tissue (white matter) and glioma samples. Sixty-eight glioma samples were assessed by RT-PCR. The transcript containing exon 1' (752bp, WI-38 *l*-CaD II) was invariably detected in all tumors and control samples, while the transcripts containing the exons 1 (731bp, Hela *l*-CaD II), 1 + 4

(670bp, Hela *l*-CaD I) and 1' + 4 (691bp, WI-38 *l*-CaD I) were exclusively detected in the tumors (Figure 8 and Table 1). The transcript of the ubiquitously expressed housekeeping gene GAPD (540bp) was uniformly amplified in all the used samples. The splicing patterns show various frequencies and combinations of the expressed transcripts (Table 1). The expression pattern of *l*-CaD in normal brain vessels is similar to that of the human normal aorta cDNA [8]. The expression of the additional transcripts in the gliomas appears to be tightly linked with the presence of microvascular hyperplasia or proliferation in the sample examined. The samples with normal-looking microvessels retained normal expression patterns of CALD1. The findings in the microdissected vessels (4/6 controls and 10/68 gliomas) further confirmed the results from these unfractional samples. To determine whether the change in *l*-CaD transcription would be manifested as changes in the protein quantity, immunoblotting analysis was performed on total cell lysates of the glioma and control samples. Densitometric analysis revealed an average 3.6-fold enhancement of caldesmon protein levels in the tumor samples as compared to the normal controls (Figure. 9), indicating that the transcriptional changes were translated into altered protein levels.

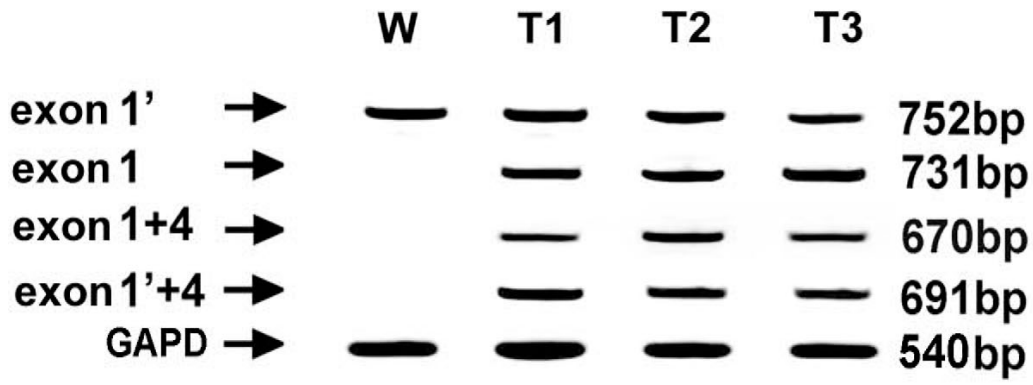

Figure 8. Analysis of *CALD1* splicing transcripts. Total RNA was isolated from the tumors and controls, and subjected to RT-PCR analysis. The expressed transcript variants and the corresponding sizes are indicated on the left and right, respectively. Each lane was labeled as W (white matter), T1 (glioblastoma), T2 (anaplastic oligodendroglioma) and T3 (pilocytic astrocytoma), respectively. The housekeeping gene (*GAPD*) was identically amplified in all samples. The transcript containing exon 1' is invariably co-detected in the control and tumors, while the transcripts containing exon 1, 1 + 4 and 1' + 4 are exclusively expressed in the tumor samples.

Table 1. Summary of differential expression patterns of CALD1 transcripts in gliomas versus the controls

Case No	Glioma subtypes	Expression Patterns			
		Hela II (exon 1)	WI-38 II (exon 1')	Hela I (exon 1+4)	WI-38 I (exon 1'+4)
Controls			+		
1--8	glioblastoma	+	+	+	+
9--17	glioblastoma	+	+		+
18--26	glioblastoma		+		+
27--32	anaplastic oligodendroglioma	+	+	+	+
33--34	anaplastic oligodendroglioma	+	+	+	
35--38	anaplastic oligodendroglioma	+	+		+
39--40	oligodendroglioma	+	+		+
41	oligodendroglioma	+	+		
42--47	anaplastic oligodendroglioma		+		+
48--49	oligodendroglioma		+		
50--56	pilocytic astrocytoma	+	+	+	+
57--58	pilocytic astrocytoma	+	+		+
59--61	pilocytic astrocytoma	+	+		
62--63	pilocytic astrocytoma		+		+
64--68	pilocytic astrocytoma		+		

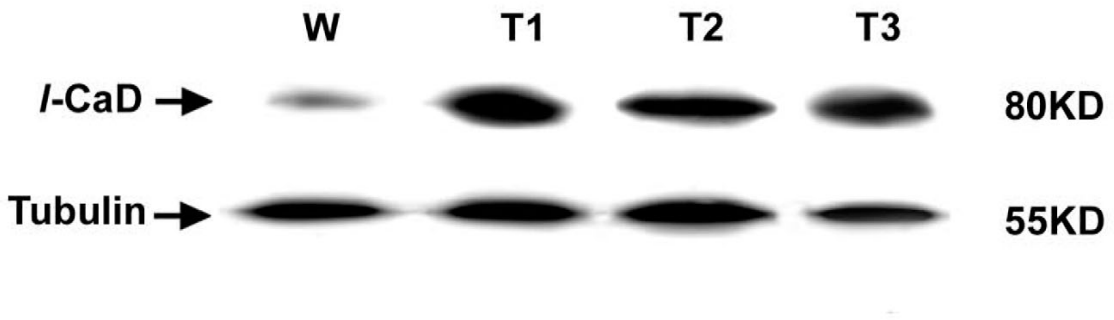

Figure 9. Immunoblotting analysis of *I-CaD*. The labels of the consecutive lanes correspond to those in Figure 8. Enhanced *I-CaD* protein expression is revealed in the tumors as compared to the control. Tubulin expression was used as a total protein loading control. The average change in band intensities was normalized against tubulin signal.

Splice-Site Mutation Scanning

Mutation screening was carried out on 20 glioma cases by applying the IVTT to exon 1, exon 1' and exon 4, spanning all splice-sites for each transcript. No mutations leading to premature protein terminations were observed in these target exons (Figure 10).

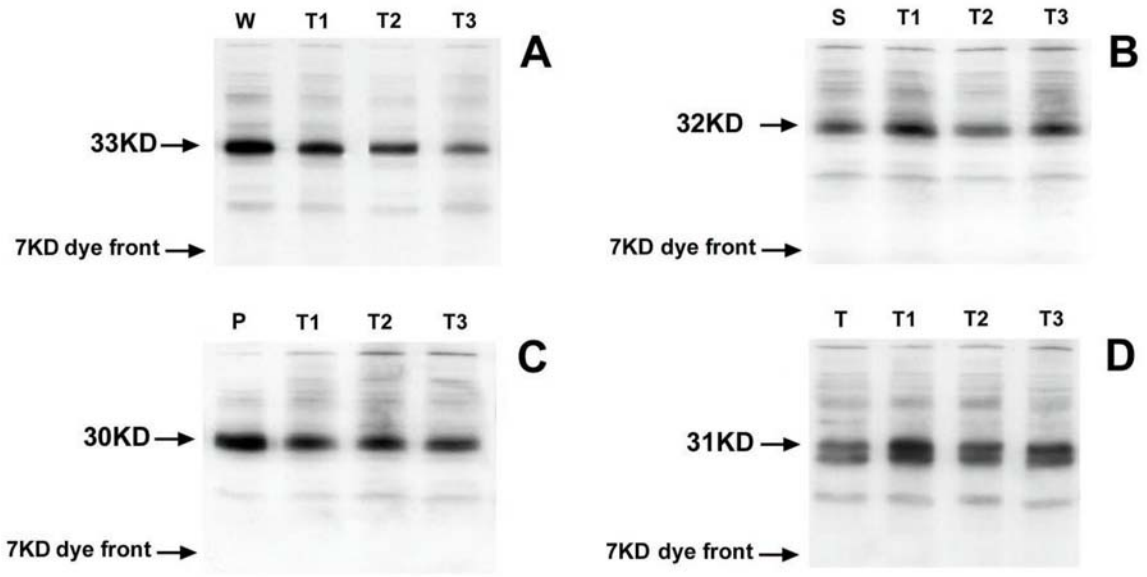

Figure 10. Scanning of splice-site mutations. The four panels show the IVTT analysis of the representative cases corresponding to Figures 8 and 9. The wild polypeptides synthesized in vitro contain exon 1' from white matter indicated as "W" (Panel A), exon 1 from stomach indicated as "S" (Panel B), exon 1 + 4 from prostate indicated as "P" (Panel C) and exon 1' + 4 from thyroid indicated as "T" (Panel D). The predicted MWs of these polypeptides are indicated in KD. No truncated polypeptides are observed in the glioma cases as compared to the controls. Panel D displays a mass heterogeneity by two bands. This mass heterogeneity is possibly caused by the in- or exclusion of exon 4, or alternatively, by an internal ATG initiation site.

Tight Junction breakdown in glioma microvasculature

The expression of TJ proteins (occludin and ZO-1) was detected by immunohistochemistry (IH) and immunofluorescence (IF). Occludin and ZO-1 in our study showed similar expression patterns (data from ZO-1 not shown). In longitudinally sectioned normal blood vessels the staining patterns for occludin and ZO-1 were predominantly axial and linear, with occasional anastomoses/bifurcations (Figure 11A1 and A2). In transversely sectioned vessels, however, the staining revealed short, radial or near-radial, continuous staining bands (Figure 11B1 and B2). In the proliferated and/or hyperplastic glioma microvessels abnormalities in expression of occludin and ZO1 were observed. The abnormalities include reduced clarity of TJ bands (Figure 11C1 and C2), interruption or discontinuity (Figure 11D1 and D2), beading or spot-like pattern of the TJ staining (Figure 11E), diffuse intra-cytoplasmic staining or absence or complete loss of immunostaining (Figure 11F).

Correlation of up-regulation of l-CaD resulting from CALD1 missplicing and TJ breakdown in glioma microvasculature

The up-regulation of *l*-CaD resulting from *CALD1* missplicing in hyperplastic glioma microvasculature is coincident with down-regulation of occludin (Figure 12) and ZO-1. In our study, strong immunopositivity of *l*-CaD in hyperplastic glioma microvasculature was always concomitant with complete or near-complete loss of occludin and ZO-1 expression.

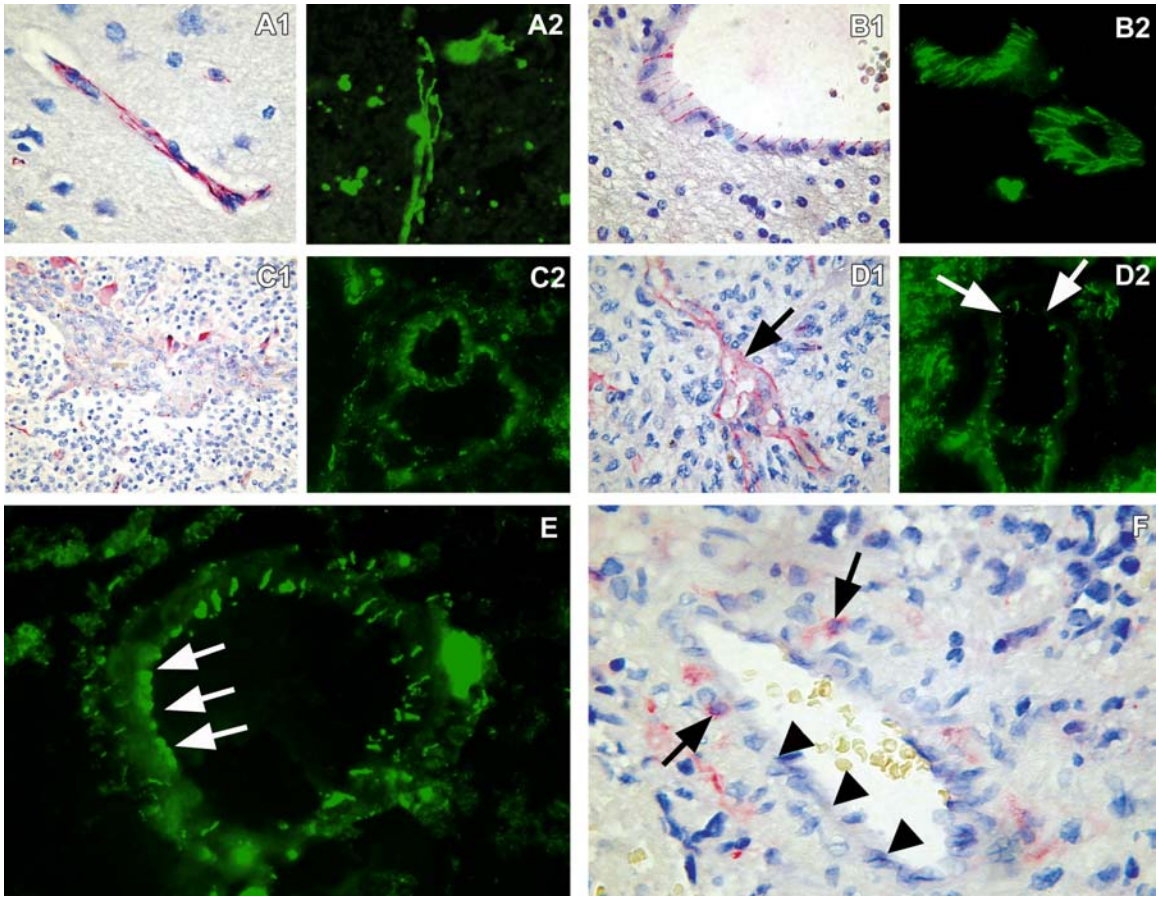

Figure 11. Immunofluorescence (IF) and immunohistochemical (IH) staining of occludin. **A1, B1, C1, D1** and **E** show IH images, while **A2, B2, C2, D2 and F** exhibit IF images. **A1 and A2:** Immunoreactive pattern for occludin in a longitudinal section of normal brain vessels (x 250). The vessels show an axial and linear staining pattern with occasional anastomoses or bifurcations. **B1 and B2:** Immunoreactive pattern for occludin in a transverse section of normal brain vessels, characterized by short, radial or near-radial, continuous staining bands (x 250). **C1 and C2:** Hyperplastic glioma vessels immunostained for occludin, showing reduced clarity of TJ patterns (C1 x 100; C2 x 250). **D1 and D2:** Discontinous immunostaining for occludin in a glioma vessel (**arrows**) (x 250). **E:** Glioma vessel with spot-like or beading immunostaining pattern for occluding (**arrows**)(x 250). **F:** Redistribution of occludin immunoreactivity in the endothelial cytoplasm (**arrows**) and complete loss of occludin staining (**arrowheads**)(x 400).

Discussion

Tumor vessels are morphologically and functionally different from normal vasculature [29]. The endothelial cells are mitotically active and there is enhanced permeability of the micovascular walls [30]. Nevertheless, there is substantial difference in neoplastic angiogenesis between tumor types, depending on the organ system involved and differential expression of cytokines by organ-specific stroma [31,32]. In the brain, the microvascular system is composed of endothelial cells surrounded by a layer of pericytes [33]. The lack of smooth muscle cells in brain tissue suggests that any contractile activity must be performed by either endothelial cells, pericytes, or both. The development of glioma microvasculature may serve as a typical model of neoplastic angiogenesis. In particular, glioblastoma are among the best-vascularized tumors in humans with highest endothelial cell proliferation indices [23,32]. Numerous factors such as angioproteins and their Tie receptors [34], PDGF-B [35], monocyte chemotactic protein 1 [36], ephrins and Eph-B receptors [37,38] are likely candidates for the activation of various modes of angiogenesis, and mediation of endothelial-endothelial and endothelial-pericyte interactions in the adaptation to physiological and pathological stimuli [39]. So far, the caldesmon protein has not yet been implicated in angiogenesis.

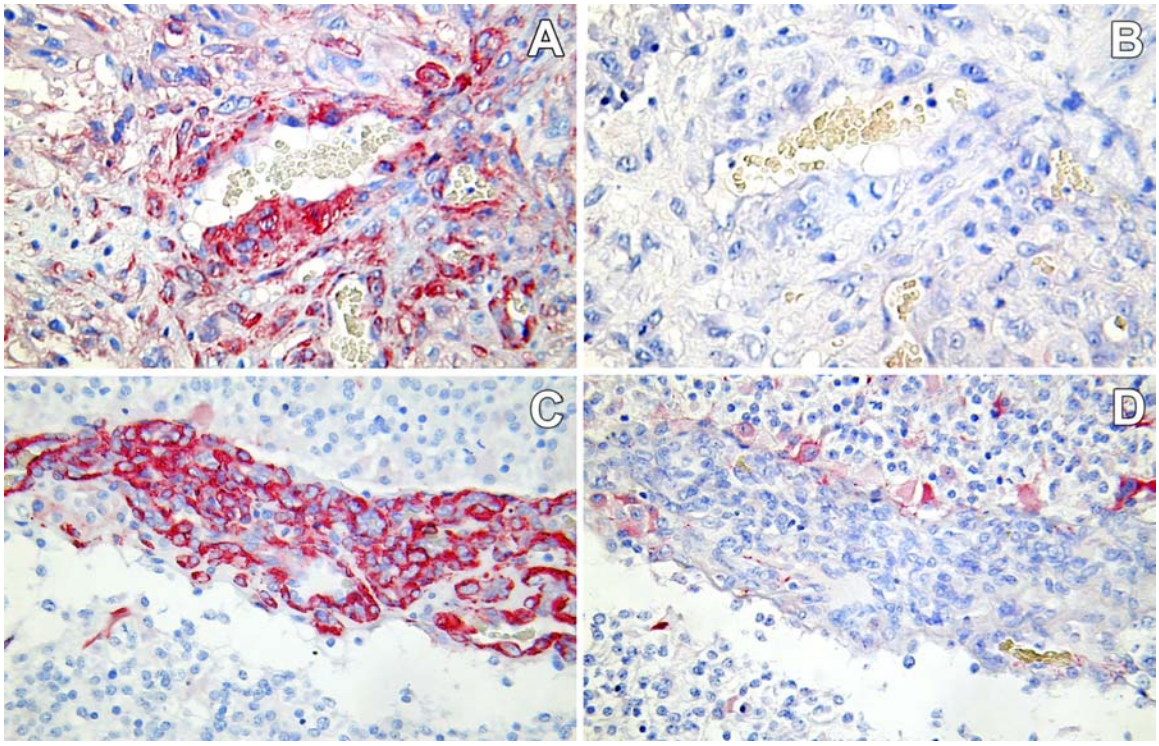

Figure 12. Up-regulation of *l-CaD* resulting from *CALD1* missplicing coincident with down-regulation of occludin. **A**: A glioblastoma with expression of four splice variants of *CALD1* (Case 6, Table 1). The strong immunoreactivity of *l-CaD* is observed (x 250). **B**: An adjacent section from A was immunostained for occludin. Complete loss of occludin immunoreactivity is observed (x 250). **C**: An anaplastic oligodendroglioma with expression of four splice variants of *CALD1* (Case 28, Table 1). Strong immunoreactivity of *l-CaD* is noticed in this section (x 250). **D**: An adjacent section immunostained for occludin. Near-complete loss of occludin expression is observed (x 250). In addition, the occludin redistribution in endothelial cytoplasm and ingestion by glial cells are shown.

Caldesmon is an actomyosin-associated cytoskeletal protein residing in contractile microfilaments (MFs) [10]. The actin cytoskeleton in eukaryotic cells operates as a tension-sensing molecular device and has an important regulatory role on cellular contractility and adhesion-dependent signalling via caldesmon modulation [40]. The contractile functions are carried out by modulating cellular tensional integrity (tensegrity) without disrupting the cellular structural integrity [41]. However, alterations of *CALD1* expression and the molecular mechanisms leading to such alterations in the context of neoplastic angiogenesis remain unexplored. Based on our previous findings [13], we hypothesized that the enhanced protein expression in glioma cases is regulated at the transcriptional level, not just simply reflecting posttranslational modifications of the protein. Definitely, the analysis of transcriptional changes could potentially lead to the identification of novel transcription-dependent and –independent molecular contributors to the process of neoplastic neovascularization. To address this issue, we investigated the *CALD1* splicing transcripts and expression level of this protein. Our data indicate that the transcriptional changes of *CALD1* in splicing variants are translated into altered protein levels, and both the expression of the splicing variants and the protein are up-regulated during the process of neo-angiogenesis in gliomas. In non-muscle cells, simulation of *CALD1* overexpression by transfection of full-length *l*-CaD results in the inhibition of cell contractility and interferes with Rho A-mediated formation of stress fibers and focal adhesions [40]. The co-activated caldesmon isoforms induce an overexpression of the protein and could have a synergetic effect on the cellular contractility of the vascular components, enhancing the permeability of microvessels, and consequently facilitate the extravasation and migration of cancer cells. Moreover, both an increase in cellular calcium

concentration and caldesmon phosphorylation cause dissociation of caldesmon from actin and results in weakening most of caldesmons' properties [10]. Thus, it seems that caldesmon carries out a regulatory role in endothelial cell spread and elongation, two properties related to vascular development [42-44]. There is evidence from in vitro experiments that the expression of *CALD1* both at the transcriptional and translational level was markedly and reproducibly down-regulated during vascular tube formation[45]. Taken together, caldesmon appears to be a target in a variety of signaling pathways that modulate its function and thereby its effect on cell contractility and adhesion-dependent signaling [40].

Alternative splicing of specific pre-mRNAs is controlled by *cis-acting* regulatory elements (exonic splicing enhancers) and *trans-acting* factors (SR proteins) [3]. The alternative exons are commonly weakened as compared to constitutive exons by having sub-optimal splice sites and length but are strengthened by the presence of exon enhancers that bind to putative splicing regulators [46] and/or activation of cryptic splice sites by mutation [16]. We did not trace any splice-site mutations in the examined cases. It appears that an alternative mechanism may alter the interaction between an exonic splice enhancer and mRNA splicing factors of the *CALD1* via a signalling pathway modifying the splicing apparatus [2,47,48]. The regulation of the transcriptional activation of *CALD1* splicing variants could have far-reaching epigenetic effects on the development of molecular targeted anti-angiogenic therapies.

The tight junction (TJ) is the most apical located element of the junctional complex in epithelial and endothelial cells[49]. The TJ between endothelial cells of brain capillaries form the structural basis of the blood-brain barrier (BBB), which controls the exchange of molecules between blood and CNS. The endothelial cells of the normal blood-brain barrier possess tight junctions which maintain a severely restricted permeability. In the hyperplastic glioma microvasculature morphological alterations such as fenestrations, the increase of caveolae, pericyte detachment and thickening and alteration of the extracellular matrix (ECM) exist[50-52]. These changes result in a dramatic increase of the permeability of these vessels. Occudin and ZO-1 are well-studied TJ proteins. In particular, occludin was the first identified transmembrane protein that is exclusively localized at TJ[53]. Therefore, occludin is considered a sensitive and reliable marker of TJs [54]. The inverse relationship between the regulation of *l*-CaD and occludin or ZO-1 found in our study has not yet been reported so far. Our data clearly reveal the up-regulation of *l*-CaD resulting from *CALD1* missplicing in hyperplastic glioma microvessels with a concomitant loss of TJ integrity of the endothelial cells. Although the molecular basis for this correlation remains unclear, our data are indicative of a specific contribution of *CALD1* expression patterns to glioma angiogenesis and generate hypotheses regarding the mechanisms contributing to the dysfunctionality of glioma neovascularization.

Acknowledgements
The authors would like to thank Mr. F. van de Panne for his assistance with the photography.

References

1. Modrek B, Lee C: A genomic view of alternative splicing. Nat Genet 2002, 30:13-19.

2. Grabowski PJ, Black DL: Alternative RNA splicing in the nervous system. Prog Neurobiol 2001, 65:289-308.

3. Smith CW, Valcarcel J: Alternative pre-mRNA splicing: the logic of combinatorial control. Trends Biochem Sci 2000, 25:381-388.

4. Philips AV, Cooper TA: RNA processing and human disease. Cell Mol Life Sci 2000, 57:235-249.

5. Stoss O, Stoilov, O., Daoud, R., Hartmann, A.M., Olbrich, M. and Stamm, S.: Misregulation of pre-mRNA splicing that causes human diseases. Gene Ther Mol Biol 2000:9-28

6. Stoilov P, Meshorer E, Gencheva M, Glick D, Soreq H, Stamm S: Defects in pre-mRNA processing as causes of and predisposition to diseases. DNA Cell Biol 2002, 21:803-818.

7. Hayashi K, Yano H, Hashida T, Takeuchi R, Takeda O, Asada K, Takahashi E, Kato I, Sobue K: Genomic structure of the human caldesmon gene. Proc Natl Acad Sci U S A 1992, 89:12122-12126.

8. Payne AM, Yue P, Pritchard K, Marston SB: Caldesmon mRNA splicing and isoform expression in mammalian smooth- muscle and non-muscle tissues. Biochem J 1995, 305:445-450.

9. Haruna M, Hayashi K, Yano H, Takeuchi O, Sobue K: Common structural and expressional properties of vertebrate caldesmon genes. Biochem Biophys Res Commun 1993, 197:145-153.

10. Huber PA: Caldesmon. Int J Biochem Cell Biol 1997, 29:1047-1051.

11. Bryan J: Caldesmon: fragments, sequence, and domain mapping. Ann N Y Acad Sci 1990, 599:100-110

12. Yamakita Y, Yamashiro S, Matsumura F: Characterization of mitotically phosphorylated caldesmon. J Biol Chem 1992, 267:12022-12029.

13. Zheng PP, T.M. Luider, P. Rob, C.J.J. Avezaat, M.J. van den Bent, P.A.E. Sillevis Smitt, and J.M. Kros.: Identification of tumor-related proteins by proteomic analysis of cerebrospinal fluid from patients with primary brain tumors. J Neuropathol & Exp Neurol 2003, 62:855-862

14. Garcia-Sanz JA, Mikulits W, Livingstone A, Lefkovits I, Mullner EW: Translational control: a general mechanism for gene regulation during T cell activation. Faseb J 1998, 12:299-306.

15. Steger K: Haploid spermatids exhibit translationally repressed mRNAs. Anat Embryol (Berl) 2001, 203:323-334.

16. Krawczak M, Reiss J, Cooper DN: The mutational spectrum of single base-pair substitutions in mRNA splice junctions of human genes: causes and consequences. Hum Genet 1992, 90:41-54.

17. Stamm S: Signals and their transduction pathways regulating alternative splicing: a new dimension of the human genome. Hum Mol Genet 2002, 11:2409-2416.

18. Cooper TA, Mattox W: The regulation of splice-site selection, and its role in human disease. Am J Hum Genet 1997, 61:259-266.

19. van der Luijt RB, Khan PM, Vasen HF, Tops CM, van Leeuwen-Cornelisse IS, Wijnen JT, van der Klift HM, Plug RJ, Griffioen G, Fodde R: Molecular analysis of the APC gene in 105 Dutch kindreds with familial adenomatous polyposis: 67 germline mutations identified by DGGE, PTT, and southern analysis. Hum Mutat 1997, 9:7-16

20. Nakai K, Sakamoto H: Construction of a novel database containing aberrant splicing mutations of mammalian genes. Gene 1994, 141:171-177.

21. Bateman JF, Freddi S, Lamande SR, Byers P, Nasioulas S, Douglas J, Otway R, Kohonen-Corish M, Edkins E, Forrest S: Reliable and sensitive detection of premature termination mutations using a protein truncation test designed to overcome problems of nonsense-mediated mRNA instability. Hum Mutat 1999, 13:311-317

22. Den Dunnen JT, Van Ommen GJ: The protein truncation test: A review. Hum Mutat 1999, 14:95-102

23. Kleihues P, Louis DN, Scheithauer BW, Rorke LB, Reifenberger G, Burger PC, Cavenee WK: The WHO classification of tumors of the nervous system. J Neuropathol Exp Neurol 2002, 61:215-225; discussion 226-219.

24. Luzzi V, Holtschlag V, Watson MA: Expression profiling of ductal carcinoma in situ by laser capture microdissection and high-density oligonucleotide arrays. Am J Pathol 2001, 158:2005-2010.

25. Yamamura H, Yoshikawa H, Tatsuta M, Akedo H, Takahashi K: Expression of the smooth muscle calponin gene in human osteosarcoma and its possible association with prognosis. Int J Cancer 1998, 79:245-250.

26. Shibuta K, Begum NA, Mori M, Shimoda K, Akiyoshi T, Barnard GF: Reduced expression of the CXC chemokine hIRH/SDF-1alpha mRNA in hepatoma and digestive tract cancer. Int J Cancer 1997, 73:656-662.

27. Andreutti-Zaugg C, Scott RJ, Iggo R: Inhibition of nonsense-mediated messenger RNA decay in clinical samples facilitates detection of human MSH2 mutations with an in vivo fusion protein assay and conventional techniques. Cancer Res 1997, 57:3288-3293.

28. Hogervorst FB, Cornelis RS, Bout M, van Vliet M, Oosterwijk JC, Olmer R, Bakker B, Klijn JG, Vasen HF, Meijers-Heijboer H, et al.: Rapid detection of BRCA1 mutations by the protein truncation test. Nat Genet 1995, 10:208-212.

29. Krylova NV: Characteristics of microcirculation in experimental tumours. Bibl Anat 1969, 10:301-303

30. Carmeliet P, Jain RK: Angiogenesis in cancer and other diseases. Nature 2000, 407:249-257.

31. Brat DJ, Van Meir EG: Glomeruloid microvascular proliferation orchestrated by VPF/VEGF: a new world of angiogenesis research. Am J Pathol 2001, 158:789-796.

32. Eberhard A, Kahlert S, Goede V, Hemmerlein B, Plate KH, Augustin HG: Heterogeneity of angiogenesis and blood vessel maturation in human tumors: implications for antiangiogenic tumor therapies. Cancer Res 2000, 60:1388-1393.

33. Ehler E, Karlhuber G, Bauer HC, Draeger A: Heterogeneity of smooth muscle-associated proteins in mammalian brain microvasculature. Cell Tissue Res 1995, 279:393-403.

34. Folkman J, D'Amore PA: Blood vessel formation: what is its molecular basis? Cell 1996, 87:1153-1155.

35. Hellstrom M, Kal n M, Lindahl P, Abramsson A, Betsholtz C: Role of PDGF-B and PDGFR-beta in recruitment of vascular smooth muscle cells and pericytes during embryonic blood vessel formation in the mouse. Development 1999, 126:3047-3055.

36. Shyy YJ, Hsieh HJ, Usami S, Chien S: Fluid shear stress induces a biphasic response of human monocyte chemotactic protein 1 gene expression in vascular endothelium. Proc Natl Acad Sci U S A 1994, 91:4678-4682.

37. Gale NW, Baluk P, Pan L, Kwan M, Holash J, DeChiara TM, McDonald DM, Yancopoulos GD: Ephrin-B2 selectively marks arterial vessels and neovascularization sites in the adult, with expression in both endothelial and smooth- muscle cells. Dev Biol 2001, 230:151-160.

38. Shin D, Garcia-Cardena G, Hayashi S, Gerety S, Asahara T, Stavrakis G, Isner J, Folkman J, Gimbrone MA, Jr., Anderson DJ: Expression of ephrinB2 identifies a stable genetic difference between arterial and venous vascular smooth muscle as well as endothelial cells, and marks subsets of microvessels at sites of adult neovascularization. Dev Biol 2001, 230:139-150.

39. Burri PH, Djonov V: Intussusceptive angiogenesis--the alternative to capillary sprouting. Mol Aspects Med 2002, 23:1-27.

40. Helfman DM, Levy ET, Berthier C, Shtutman M, Riveline D, Grosheva I, Lachish-Zalait A, Elbaum M, Bershadsky AD: Caldesmon inhibits nonmuscle cell contractility and interferes with the formation of focal adhesions. Mol Biol Cell 1999, 10:3097-3112.

41. Ingber DE: Tensegrity I. Cell structure and hierarchical systems biology. J Cell Sci 2003, 116:1157-1173.

42. Alessandro R, Masiero L, Lapidos K, Spoonster J, Kohn EC: Endothelial cell spreading on type IV collagen and spreading-induced FAK phosphorylation is regulated by Ca2+ influx. Biochem Biophys Res Commun 1998, 248:635-640.

43. Masiero L, Lapidos KA, Ambudkar I, Kohn EC: Regulation of the RhoA pathway in human endothelial cell spreading on type IV collagen: role of calcium influx. J Cell Sci 1999, 112:3205-3213.

44. King WG, Mattaliano MD, Chan TO, Tsichlis PN, Brugge JS: Phosphatidylinositol 3-kinase is required for integrin-stimulated AKT and Raf-1/mitogen-activated protein kinase pathway activation. Mol Cell Biol 1997, 17:4406-4418.

45. Grove AD, Prabhu VV, Young BL, Lee FC, Kulpa V, Munson PJ, Kohn EC: Both protein activation and gene expression are involved in early vascular tube formation in vitro. Clin Cancer Res 2002, 8:3019-3026.

46. Humphrey MB, Bryan J, Cooper TA, Berget SM: A 32-nucleotide exon-splicing enhancer regulates usage of competing 5' splice sites in a differential internal exon. Mol Cell Biol 1995, 15:3979-3988.

47. Hoffmeyer S, Nurnberg P, Ritter H, Fahsold R, Leistner W, Kaufmann D, Krone W: Nearby stop codons in exons of the neurofibromatosis type 1 gene are disparate splice effectors. Am J Hum Genet 1998, 62:269-277.

48. Messiaen L, Callens T, De Paepe A, Craen M, Mortier G: Characterisation of two different nonsense mutations, C6792A and C6792G, causing skipping of exon 37 in the NF1 gene. Hum Genet 1997, 101:75-80.

49. Wittchen ES, Haskins J, Stevenson BR: Protein interactions at the tight junction. Actin has multiple binding partners, and ZO-1 forms independent complexes with ZO-2 and ZO-3. J Biol Chem 1999, 274:35179-35185

50. Hirano A, Matsui T: Vascular structures in brain tumors. Hum Pathol 1975, 6:611-621

51. Dinda AK, Sarkar C, Roy S, Kharbanda K, Mathur M, Khosla AK, Banerji AK: A transmission and scanning electron microscopic study of tumoral and peritumoral microblood vessels in human gliomas. J Neurooncol 1993, 16:149-158

52. Bertossi M, Virgintino D, Maiorano E, Occhiogrosso M, Roncali L: Ultrastructural and morphometric investigation of human brain capillaries in normal and peritumoral tissues. Ultrastruct Pathol 1997, 21:41-49

53. Furuse M, Hirase T, Itoh M, Nagafuchi A, Yonemura S, Tsukita S: Occludin: a novel integral membrane protein localizing at tight junctions. J Cell Biol 1993, 123:1777-1788

54. Vorbrodt AW, Dobrogowska DH: Molecular anatomy of intercellular junctions in brain endothelial and epithelial barriers: electron microscopist's view. Brain Res Brain Res Rev 2003, 42:221-242

Chapter 4

Hela-type caldesmon: a novel marker of angiogeneic endothelial cells identified in glioma neovascularization

Submitted for publication

Ping-Pin Zheng, Marcel van der Weiden, Peter A.E. Sillevis Smitt, Theo.M. Luider, Johan M. Kros

Abstract

In a previous study, we found that Hela-type transcripts of the caldesmon gene (*CALD1*) are specifically present in glioma microvasculature, while not in normal cerebral vessels. Caldesmon (CaD) is a major actomyosin-binding protein distributed in various cell types. There are at least two high-molecular-weight isoforms (*h*-CaD) and four low-molecular-weight isoforms (*l*-CaD) produced by alternative splicing. The splice variants for the *l*-CaD class are further differentiated by inclusion (Hela-type) or exclusion (WI-38-type) of exon 1. Since differential expression of Hela *l*-CaDs has never before been studied in relation to tumor neovascularization, in this study we address the question whether the differentially expressed Hela-type transcripts in glioma microvasculature are translated into genuine proteins; in which stage of neovascularization this occurs; and we attempt to relate the expression to endothelial cell functionality. Our data indicate that the Hela *l*-CaDs are exclusively expressed in glioma vessels with preference for the early stages of glioma neovascularization. Disassembly of focal adhesion and remodeling of F-actin with formation of podosome-like structures were observed in the Hela *l*-CaD-expressing ECs. The findings support the notion that activation of motility of quiescent endothelial cells is necessary for creating an ubiquitous neovascularization in glial tumors. The data indicate that the protein could be considered as a new marker of angiogenic ECs during early stages of glioma neovascularization.

Introduction

Endothelial cells (ECs) are normally quiescent, but when triggered may become capable of rapidly sending out sprouts in a coordinated and directional manner (1). Normal vascular development and maturation involves a sequence of events consisting of the formation, stabilization, branching, remodeling, pruning and specialization of blood vessels (2). Tumor vessels, however, follow these events in chaotic order. Most tumor vessels are structurally and functionally different from normal vessels in that they lack tissue-specific perivascular cells (3), are more permeable(4) and may undergo progressive regression (5), while some tumor vessels are even partially composed of neoplastic cells (6). Capillary ECs switch from growth to differentiation by altering their focal adhesion and thereby, modulate their shapes (7). Shape-dependent control of cell growth and function is mediated by tension-dependent changes in the actin cytoskeleton (8). Thus, actin cytoskeleton (CSK)-associated proteins play an important role in EC physiology and pathology. However, only little attention has been drawn to the role of CSK-associated proteins in the regulation of tumor neovascularization.

Caldesmon (CaD) is a major CSK associated-protein and serves as a target for a variety of signaling pathways that modulate cell contractility and cell adhesion in fully differentiated smooth muscle cells (*h*-CaD, 120-150kDa) and a variety of other cell types (*l*-CaD, 70-80 kDa) (9, 10). The Hela-type splicing variants and protein isoforms were initially cloned from Hela S3 cell lines, further subdivided into Hela *l*-CaD I (exon 1 + 4) and Hela *l*-CaD II (exon 1)(9) So far, expression of the protein isoforms was only examined in cell lines(11, 9). In a previous study we found that the Hela-type transcripts are differentially expressed in glioma microvasculature while not in the blood vessels of and glial cells of normal brain tissue (12).

In the present study we address the question whether the Hela-type *l*-CaD transcripts expressed in glioma microvessels are translated into genuine proteins or whether they are translationally repressed; in which stages of glioma neovascularization this occurs; and what the functional implications of this expression are. To this aim, we examined the expression of Hela *l*-CaDs in glioma microvasculature by immunohistochemistry using a specific antibody raised against Hela *l*-CaDs in a large cohort of glioma cases. The identity of the individually distributed Hela *l*-CaDs$^+$ ECs was confirmed by immuno-double-labeling studies with endothelial markers. In situ expression of the transcripts in glioma microvasculature was confirmed by nonradioactive in situ hybridization. To determine the Hela *l*-CaD isoform diversity, the microvessels were microdissected by laser capture microdissection (LCM) for immunoblotting analysis. In addition, morphological features, focal adhesion and F-actin of the Hela *l*-CaDs$^+$ ECs were compared with those observed in motile cells (13-18). The findings support that Hela *l*-CaD-expressing ECs undergo activation of motility.

Materials and Methods

Clinical Samples
The paraffin-embedded tissue samples of 68 gliomas, including 26 glioblastomas, 23 oligodendrogliomas (among which 18 anaplastic oligodendrogliomas) and 19 pilocytic astrocytomas, and 16 control white matter samples from patients free of neurological diseases or tumors, were taken from the archives of the Department of Pathology, Erasmus Medical Center, Rotterdam, The Netherlands. Histopathologic typing and grading of the tumors was performed based on the latest WHO classification of Tumors of the Central Nervous System (19). Corresponding frozen samples were used for *in situ* hybridization and laser capture microdissection for immunoblotting analysis. The use of human tissue samples was approved by the Ethical Review Board of the Erasmus Medical Center.

Defining stages/patterns of glioma neovascularization
Tumor vessels may develop from various sources and pass various stages of development. The initial stage of neovascularization consists of *de novo* vessel formation (vasculogenesis) through single endothelial cells (ECs) or endothelial precursor/progenitor cells (EPCs)(20), or non-canalized endothelial cell chains (NCECCs) (5) shed from the vessel walls or mobilized from the bone marrow (21). The endothelial cells proliferate and differentiate *in situ* within previously avascular tissue to coalesce and form primitive tubular networks (22). In the early stage, vessels sprout either from the newly formed vessels or from host vessels, a process called angiogenesis (23, 22). Also, tumor cells may take over host vessels (cooption)(5), or form perivascular cuffs around host vessels (1). Intussusceptive vascular growth (IVG), i.e., partitioning of the vessel lumen by insertion of interstitial tissue columns (24), forms the main source of tumor vessels at later stages of neovascularization (25). One important characteristic of IVG is that it is achieved by an exceedingly low rate of EC proliferation (26). The end stage, vessels show fibrosis and hyalinization of their walls.

Production of the Antibody
The antibody (CUK-0129) to the Hela-type isoforms was generated against the synthetic peptide which corresponds to the N-terminal 18 residues encoded by exon 1 of *CALD1* (GenBank**,** Accession NM_033139). Production, characterization and demonstration of the specificity of the antibody were commercially performed (CovalAB). Briefly, the target peptide was synthesized, purified, and verified by amino acid analysis. Two rabbits were immunized subcutaneously with the peptide. Immunopurification of the specific antibody was performed by loading the antisera onto the peptide-coupled Sepharose column. The immunoreactivity of the antibody was validated by enzyme-linked immunosorbent assay (ELISA).

Immunohistochemistry (IHC)
Paraffin sections (5µm) were mounted onto aminopropyltriethoxysilane (APES)-coated glass slides (Knittel Glaser). Dewaxed sections were pretreated in 0.1% pronase (Sigma) for 10 minutes at 37ºC, and incubated with CUK-0129 (CovalAB) at 1:40 for two hour at RT. The biotinylated goat-anti-rabbit (Dako) at 1:200 was incubated for 1 hour at RT, followed by incubation with StreptABC complex/AP (Dako) at 1:100 for one hour at RT. Standard enzyme development procedures were performed for final visualization of the immunoreactivity.

Double and triple immunofluorescence labeling (IF)
We used the endothelial cell markers CD31 and CD34 in IF double-labeling experiments to confirm the EC identity of individually distributed cells or NCECCs with Hela *l*-CaDs expression. Cryostat sections (5 µm) were mounted onto non-coated microscope slides (Menzel Glaser), fixed in acetone for10 minutes and air dried. Sections were then incubated with mouse- anti-CD34 (Lab Vision) at 1:20 or mouse-anti-CD31 (Dako) at 1:40, and CUK-0129 (CovalAb) at 1:10

for one hour, respectively. After washing, FITC-conjugated goat-anti-mouse (Southern Biotech) at 1:50 and swine-anti-rabbit-biotin (Dako) at 1:100 were applied for 1 hour, respectively. Further, TRITC-conjugated avidine (Jackson ImmunoResearch) at 1:100 was applied for 1 hour. Nuclei were counterstained with DAPI (Sigma). After a final washing, sections were mounted with covering glass, and examined under a laser scanning confocal microscope. TRITC-phalloidin was used to visualize F-actin in vinculin-labeled cells. For this double-labeling, the frozen sections were permeabilized in PBS containing 0.2 % Triton X-100, followed by incubation with mouse monoclonal anti-human vinculin (Serotec) at 1: 40 for one hour. After washing , the sections were incubated with a solution of 50 μg/ml TRITC-Phalloidin (Sigma) for 40 min. DAPI counterstaining was as above. All steps were performed at RT.

Triple staining of vinculin, CD34 and CUK-0129 allowed us to visualize the FA status of Hela *l*-CaD$^+$ ECs. For simultaneous detection of two antigens by two monoclonal antibodies, we used the protocol by CSA kit (27). Briefly, the antigen-retrieved paraffin sections were soaked in a block peroxidase solution (CSA kit, Dako) for 5 min, followed by incubation with protein blocking solution (CSA kit, Dako) for 5 min. The sections were incubated with the highly diluted monoclonal mouse-anti-human vinculin as first primary antibody at 1:1,280 dilution for one hour. This dilution does not allow direct visualization by the second detection system for the second mouse monoclonal antibody (CD34) (Lab Vision), which was verified by a series of dilutions and examined by a laser scanning confocal microscope (CLSM). The HRP-conjugated-goat anti-mouse antibody (1:50) (Dako) was incubated for the detection for 30 min. Subsequently, the slides were incubated with the amplification reagent (CSA kit, Dako) for 30 min to generate the biotinylated tyramid deposits. Afterwards, the sections were washed and incubated for one hour with mouse monoclonal antibody CD 34 (1:20) as second primary antibody. The biotin-tyramide deposits corresponding to the first Mab and the second Mab were detected simultaneously by incubating one hour by a mixture of FITC-conjugated streptavidin (Jackson ImmunoResearch) and TRITC-conjugated sheep anti-mouse immunoglobulin (Chemicon), respectively. Subsequently, the sections were incubated with the polyclonal antibody CUK-129 (1:25) for one hour. Cy5-conjugated donkey anti- rabbit (1:50) (Jackson ImmunoResearch) was incubated for 30 min for detection. The sections were washed twice with PBS between the different staining steps. Nuclei were counterstained with DAPI (Sigma). All steps were performed at RT. Sections were mounted with covering glass and examined under CLSM.

Confocal Laser Scanning Microscope (CLSM)

CLSM was performed using a Zeiss LSM 510 META system (Karl Zeiss). The laser diode 405 nm, Argon 488 nm, HeNe1 543 and HeNe2 633 were switched on and set at 50% output intensity. The multiple track standard DAPI/FITC/TRITC, or DAPI/FITC/TRITC/Cy5 configurations were selected. We used korr C-Apochromat 63x objective to generate a single image for each sample. DAPI, FITC, TRITC and Cy5 preparation was scanned triple or quadruple, using changes of filters among: one pass 405 nm light emitted by the laser diode (DAPI channel), second one pass with 488 nm light emitted by the argon (FITC channel), and the third one pass with 543 nm light emitted by HeNe1 laser (TRITC channels) and the fourth one pass with 633 nm light emitted by HeNe2 laser (Cy5 channel). The three or four signals were detected by the same detector and stored separately in the computer memory.

Laser Capture Microdissection (LCM)

LCM was basically performed as described previously(12). For this study only Trizol was replaced by the lysis buffer. Vessels from normal controls and gliomas were captured by LCM. The dissected areas were collected in the cap of a microcentrifuge tube containing 20 μl of lysis buffer (7M urea, 2M thiourea, 4% CHAPS, 40 Mm Tris base) and the cells solubilized by inversion of the tube for 10 min at RT, followed by votex-mixing for 15 s and a brief centrifugation at 12,000g. Tissue from multiple caps was extracted into the same aliquot of lysis buffer until sufficient material had been collected.

Immunoblotting Analysis (IB)

IB was performed as described before (12). Briefly, the protein samples (20μg/lane) from LCM were separated on a 12% SDS-PAGE and transferred to a nitrocellulose membrane. The

membrane was incubated with the CUK-0129 (CovalAB) at 1:500 in TBST. Detection was performed by incubation with HRP-conjugated goat-anti-rabbit IgG antibody (Zymed) at 1:5000 for 1 h at RT, respectively. The immunoreactivity was visualized with enhanced chemiluminescence (Amersham).

RNA Isolation and cDNA Cloning
Total cellular RNA was extracted from normal organs which express the Hela-type transcripts as described in our previous study (12) using Trizol (Invitrogen) as the Manufacturer's protocol. cDNA was generated with an oligo $(dT)_{23}$ primer and DuraScript™ reverse transcriptase (Sigma). RT-PCR was used to clone the cDNA fragments as described before (12). The full-length integrity of the PCR products was examined by gel electrophoresis. Further, the PCR products were purified using the QIA quick-spin columns (QIAGEN), pheno-extracted, ethanol-precipitated and resuspended in DEPC-treated water, and used as template in an *in vitro* transcription assay reaction.

In Vitro Transcription and cRNA Probe Labeling
cRNAs were generated by *in vitro* transcription using T7 RiboMAX™ Express Large Scale RNA Production System (Promega) following the Manufacturer's protocol, using the cloned cDNAs as templates. Briefly, approximately 1 µg of cDNA was used as template and incubated the T7 RiboMAX™ system at 37°C for 30 minutes in total volume of 20µl. The in vitro synthesized transcripts (cRNAs) were extracted using Trizol (Invitrogen). The full-length integrity of the cRNAs was examined by gel electrophoresis. The cRNAs were fragmented, and labeled with FastTag™ Biotin Labeling Kit (Vector Laboratories) as the manufacturer's instructions.

Nonradioactive in situ Hybridization (ISH)
Briefly, frozen tissue sections of 5 µm were fixed in 4% paraformaldehyde and digested by proteinase K (50 µg/ml), followed by acetylation in 250 ml 0.1 M RNAse-free triethanolamine-HCl (pH 8.0) and 0.625 ml acetic anhydride. Prehybridization was done by the addition of 100 µl of hybridiation solution (50% formamide, 5x SSC, 2.5% yeast tRNA, 1x Denhardt's Solution, 5% bovine serum albumin, 0.1% Tween 20 and 10% dextran sulfate) without a probe and incubating the slides in a 5X SSC humidified chamber at 60°C for 2 hours. The hybridization mixture was prepared by adding 2µg probe per ml of hybridization buffer, heating at 95°C and chilling on ice. The prehybridization solution was replaced by the hybridization mixturer for subsequent incubation overnight at 60°C. After hybridization, the sections were washed, blocked, and incubated in alkaline phosphatase streptavidin (Vector Laboratories) at 1: 200 for 1 hour at RT. BCIP/NBT solution (Vector Laboratories) was prepared for color developing as recommended by the manufacturer.

Results

Differential expression of Hela I-CaDs in glioma microvasculature versus normal counterparts by IHC
Fig. 1A-F show representative IHC profiles of the differential expression of Hela *I*-CaDs in different stages of glioma neovascularization. In general, we found that the Hela *I*-CaDs are predominantly expressed in individual ECs/EPCs, NCECCs and sprouting/branching microvessels. There was low or absent expression expression of the protein in vessels showing intussusception or fibrosis. No immunoreactivity of this protein was observed in normal-looking vessels (coopted vessels) within the gliomas or in normal vessels of the control samples. The coopted vessels appear as normal vessels characterized by the absence of vascular sprouts, branches, hyperplasia or NCECCs (5). These vessels may progressively regress as manifested by detachment of endothelial cells from the surrounding supporting cells or tight junction breakdown (data not shown). No immunoreactivity was observed in normal or neoplastic glial cells (glioma cells).

Cell shape change, focal adhesion (FA) disassembly and remodeling of F-actin

Significant changes in cell shape, FA and actin cytoskeletal organization were observed in Hela *l*-CaD$^+$ ECs. Cellular enlargement, multinucleation, protrusions or free cellular fragments were often observed in the Hela *l*-CaDs$^+$ ECs (Figure 1G-J). FAs were visualized by immunofluorescence labeling with anti-vinculin monoclonal antibody. The vinculin-containing FAs show dense dash-like or oval bands localized in the basal membrane region of the endothelium of normal vessels (Figure 2A and B). These vinculin bands diminish or disappear in Hela *l*-CaD$^+$ ECs and form dot-like structures associated with Hela *l*-CaD (Figure 2C) or are diffusely redistributed through the cytoplasm (Figure 2D).

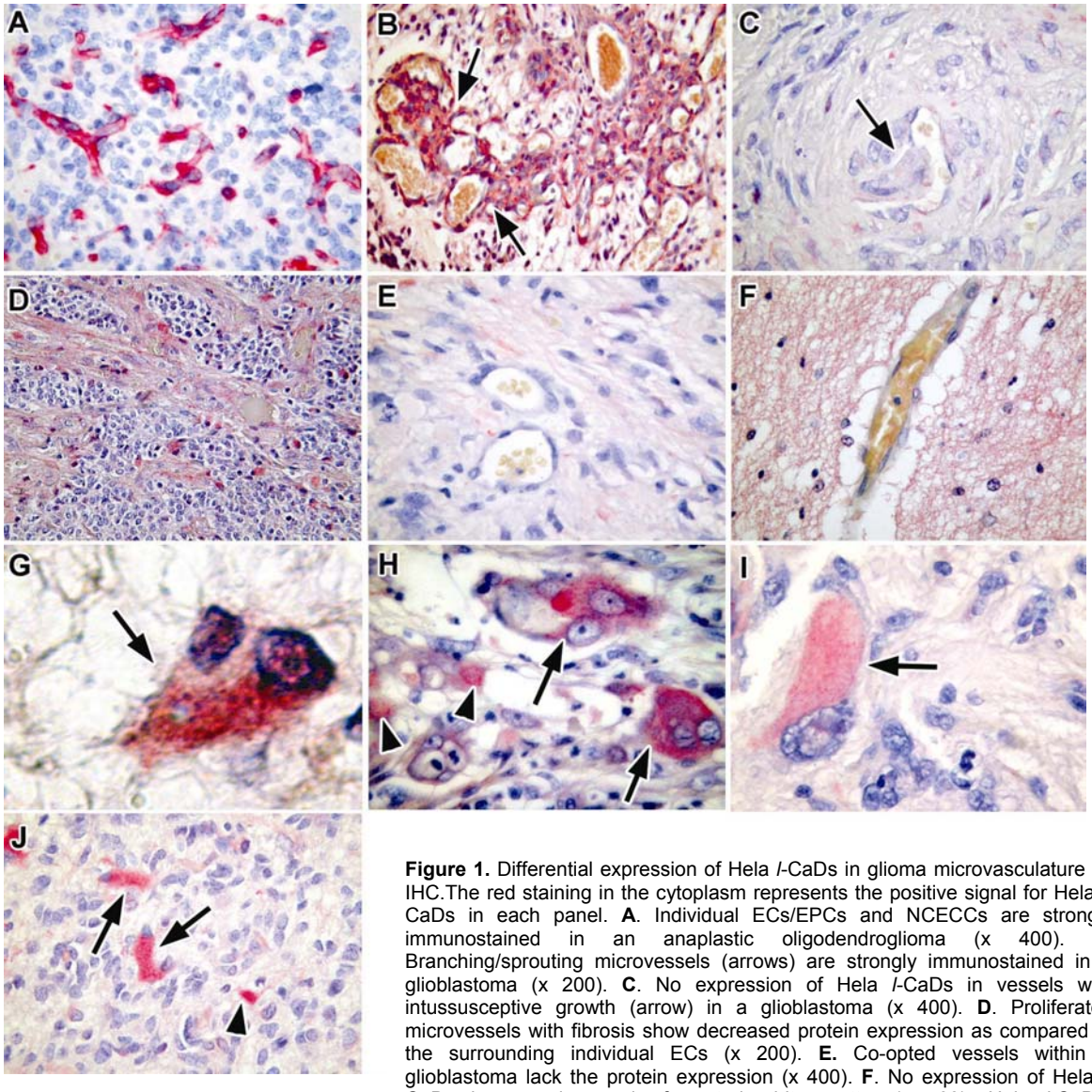

Figure 1. Differential expression of Hela *l*-CaDs in glioma microvasculature by IHC.The red staining in the cytoplasm represents the positive signal for Hela *l*-CaDs in each panel. **A**. Individual ECs/EPCs and NCECCs are strongly immunostained in an anaplastic oligodendroglioma (x 400). **B**. Branching/sprouting microvessels (arrows) are strongly immunostained in a glioblastoma (x 200). **C**. No expression of Hela *l*-CaDs in vessels with intussusceptive growth (arrow) in a glioblastoma (x 400). **D**. Proliferated microvessels with fibrosis show decreased protein expression as compared to the surrounding individual ECs (x 200). **E.** Co-opted vessels within a glioblastoma lack the protein expression (x 400). **F**. No expression of Hela *l*-CaDs in normal vessel of control white matter (x 400). Hela *l*-CaDs$^+$ multinucleated cells (arrows) are observed in pilocytic astrocytoma (G), anaplastic oligodendroglioma (H) and glioblastoma (I). Elongated cellular protrusions of individual Hela *l*-CaDs$^+$ ECs (I and J x 400, arrows), as well as scattered Hela *l*-CaDs$^+$ cellular fragments (H and J x 400, arrowheads) are seen.

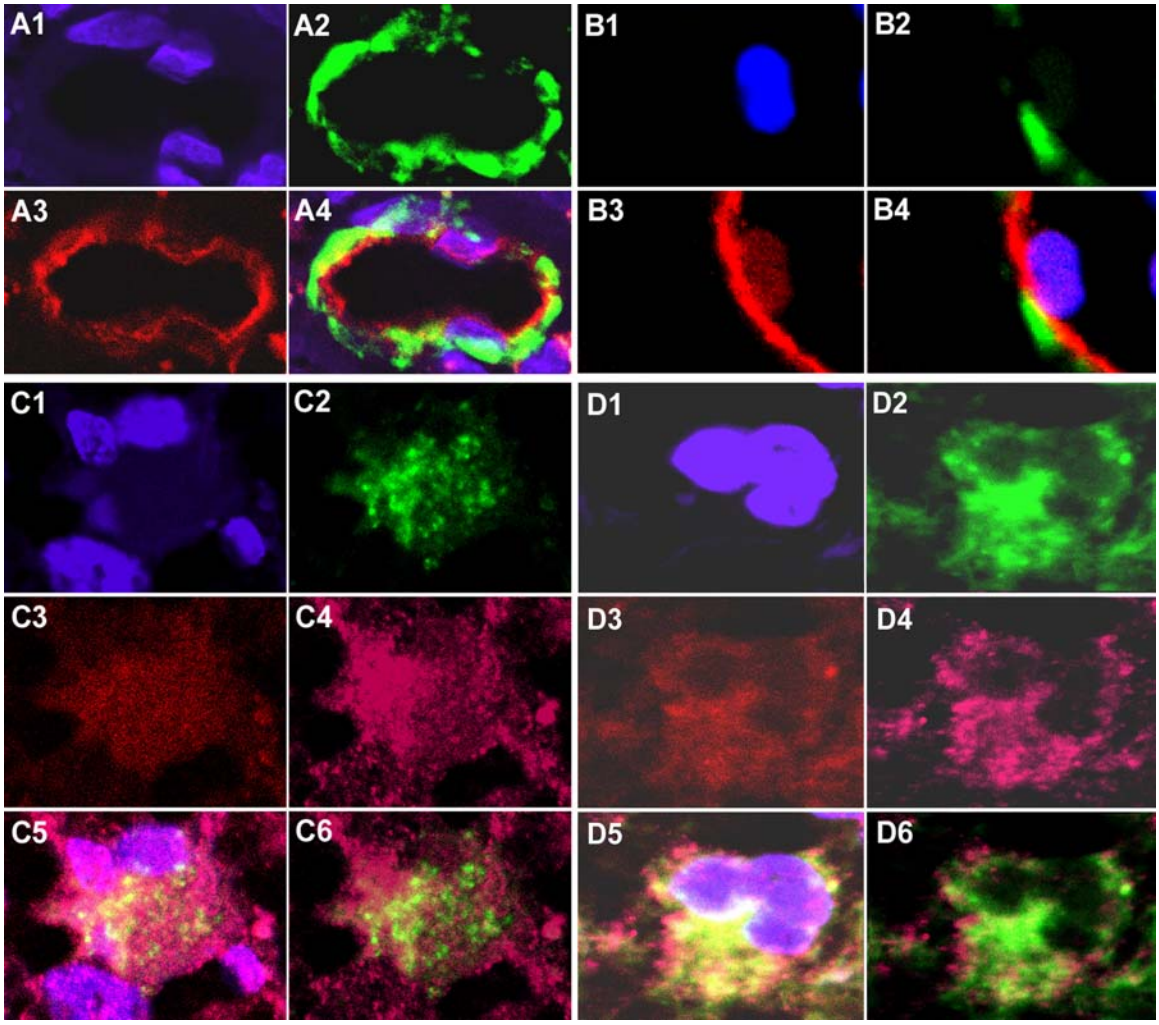

Figure. 2. Disassembly of vinculin-containing FA in Hela *l*-CaD^{+} ECs. **A** Vinculin is localized along the basal membrane region of the endothelium in a capillary of normal brain, appearing as dense dash-like or oval bands (A2). The endothelium is labeled with CD34 (A3). Nuclei are counterstained with DAPI (A1). A merged image is shown in A4. **B.** A single EC, cropped from normal endothelium, is double-labeled with vinculin (B2) and CD34 (B3). The vinculin bands are present at the periphery of the EC (B4). **C**. An individually deposited multinucleated EC was captured from glioma tissue and is triply labeled with vinculin (C2), CD34 (C3) and CUK-0129 (C4). A merged image is shown in C5. A merged image of the expression pattern of vinculin and Hela-*l*-CaD is shown in C6. As compared to the normal EC shown in panel B, the vinculin bands have disappeared at the cell periphery and form dot-like structures in cytoplasm. **D**. The labeling of these panels are similar to those used in panel C. Diffuse. not dot-like, distribution of vinculin is observed in this cell. Co-localization of vinculin and Hela-*l*-CaD is shown in D6.

The F-actin was visualized with TRITC-phalloidin staining. In normal ECs stress fibers (normal actin-containing structures) are well-developed (Figure 3A), while in Hela *l*-CaDs^{+} ECs the F-actin exhibits disorganization with formation of dot-like structures (Figure 3B), or is found diffusely distributed through the cytoplasm where it is associated with vinculin (Figure 3C).

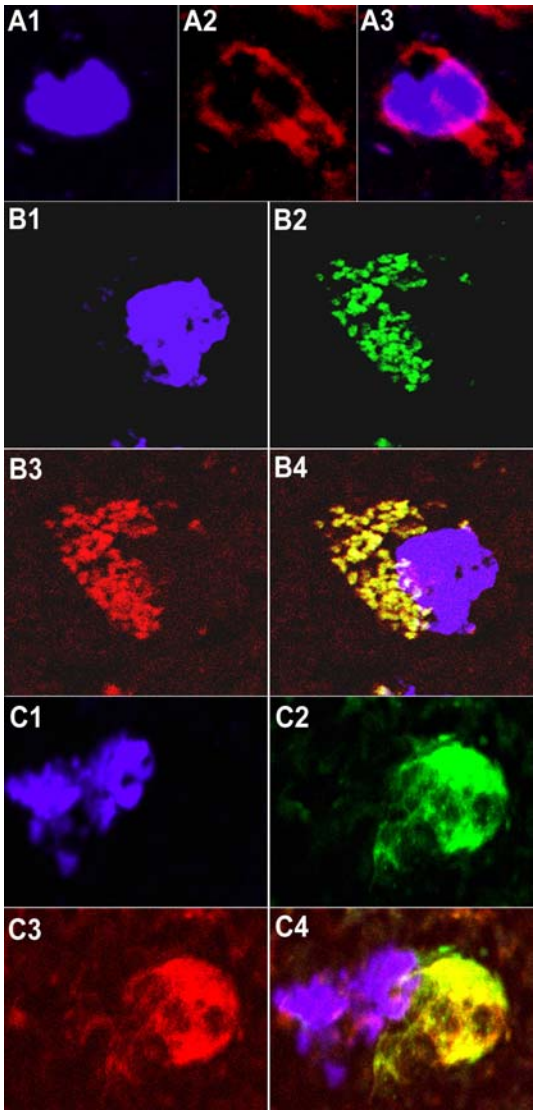

Figure 3. F-actin remodeling of Hela *I*-CaD-expressing ECs. **A.** F-actin is well-developed in a normal EC (A2). The nucleus is counterstained with DAPI (A1). A3 is a merged image. **B.** An
EC, captured from a branching vessel of glioma, triply labeled with vinculin (B2), F-actin (B3) and CUK-0129 (not shown). A merged image of the immunostaining for vinculin and F-actin is shown in B4. In contrast to A, well-organized F-actin has disappeared and dot-like structures are seen. These proteins appear accumulated at the leading edge of the EC, the moving direction of motile cells (15). **C.** Multiple labeling similar to panel B. Vinculin and F-actin show diffuse distribution through the cell body (C2 and C3). Also these proteins are clustered at the leading edge of this EC.

Confirmation of the EC Lineage of Individually Distributed ECs/EPCs or NCECCs

The endothelial markers (CD31/CD34) were used for gross (IHC, data not shown) and elaborate (IF) confirmation of the lineage of the individual Hela *I*-CaDs^{+} cells by double immunolabeling. Figure 4 shows a single cell double IF-stained with CUK-129 and CD34. The co-localization of the two antigens was adjudged in a merged image of two colors within the same cell(s) (Figure 4D). The images were taken by CLSM using triple laser scanning for a target cell or cell population.

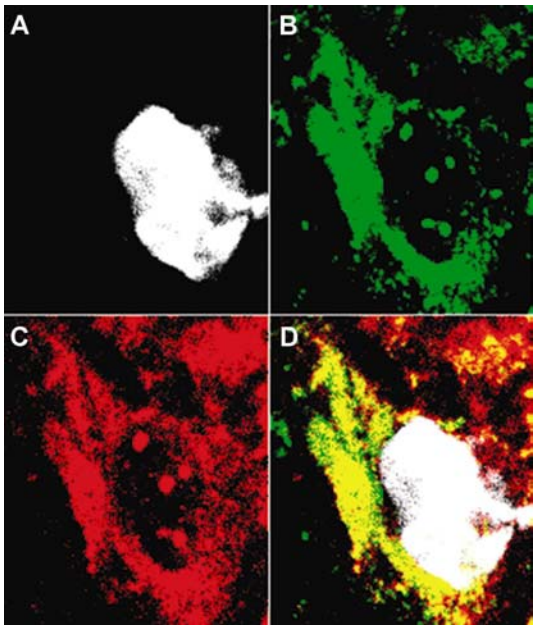

Figure 4. Determination of the EC lineage of the individual Hela *I*-CaD^{+} cells. The images show IF double-labeling of CD34 and CUK-0129 in a single cell examined under CLSM. A single nucleus is stained by DAPI in white (A), and cytoplasm is co-stained by CD34 in green (B) and by CUK-0129 (C) in red. Co-localization of the two antigens is shown in the merged image in yellow (D).

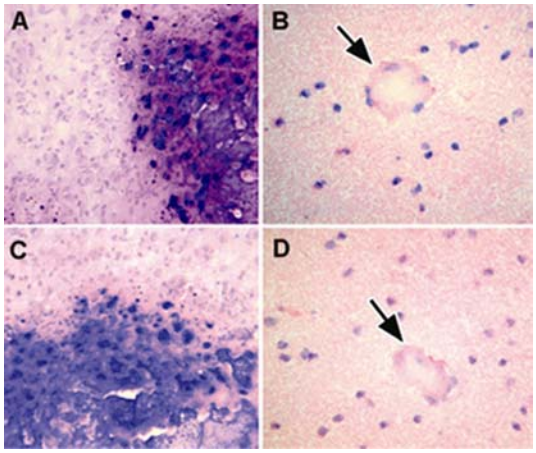

Figure 5. Expression of the Hela-type transcripts in situ. The figure shows a representative paired glioma/control corresponding to the lanes 1 and 4 in Figure 6. The cytoplasmic dark blue staining represents the positive signal for Hela *I*-CaD transcripts in ISH. The Hela I and II transcripts were detected in hyperplastic multilayered microvascular tufts in an glioblastoma, respectively (A and C x 200) with HE counterstaining, but not observed in glioma cells. The transcripts are undetectable both in glial cells and vessels of the control (B and D x 400).

Confirming the Expression of Hela I-CaD Transcripts in situ

In situ expression of the Hela-type transcripts was determined by ISH. The transcripts are exclusively detected in glioma microvasculature, while not in normal blood vessels nor in normal glial or glioma cells (Figure 5).

Determination of Hela l-CaD isoform diversity in glioma microvessels
To determine whether both isoforms of Hela *l*-CaD are expressed in glioma microvessels, a combination of LCM and IB was performed. Two isoforms were present in glioma vasculature and expression variaton between different gliomas was noticed. In figure 6 the results from representative glioma subtypes are shown. Hela *l*-CaD II appears to be more often expressed in the glioma cases examined, consistent with data obtained from RT-PCR in our previous study (12) and in situ hybridization data. The isoforms were absent from the normal controls.

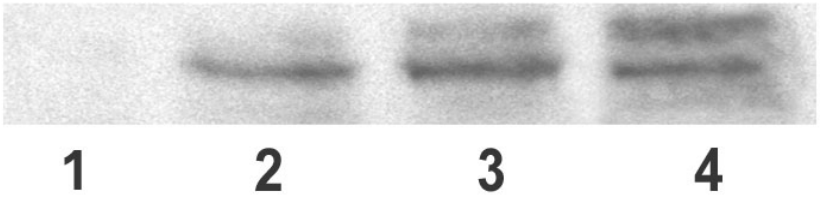

Figure 6. Immunoblot analysis of the isoform diversity in glioma microvessels. This figure shows a single band migrated at 70-80 kDa in a pilocytic astrocytoma (lane 2) while two bands migrated in an oligodendroglioma (lane 3) and a glioblastoma (lane 4). The bands detected in these glioma subtypes are undetectable in control white matter (lane 1). Hela *l*-CaD I contains amino acids (aa) encoded by both exon 1 and 4 and therefore, the top band is characteristic of Hela *l*-CaD I, while the lower band indicates Hela *l*-CaD II (no aa encoded by exon 4).

Discussion

Caldesmon (CaD) is expressed from a single gene (*CALD1*) located on chromosome 7q33-q34. It is composed of at least 15 exons of which exons 1, 1', 3b and 4 are alternatively spliced (9, 28, 29). Biochemical studies have shown that the actomyosin system in smooth muscle cells and other cells is dually regulated by myosin- and actin-linked mechanisms (30). CaD and tropomyosin are crucial components in the actin-linked mechanism (31). In quiescent non-muscle cells *l*-CaD is periodically associated with actin filaments (stress fibers) as well as with tropomyosin (10). These associations change during activation by specific receptor ligand interactions or change during mitosis (10). There is evidence that *l*-CaD is implicated in glucocorticoid-induced actin reorganization (32) and is associated with signaling receptor complexes (33), intracellular granule movement (34) and with the mitosis-specific regulation of actin dynamics (35). All of this demonstrates a crucial role of *l*-CaD in the organization of the actin cytoskeleton (CSK) dynamics and architecture. We found that the Hela *l*-CaD is strongly expressed in early stages of neovascularization, i.e., the stages of vasculogenesis and angiogenesis. In the late stages of neovascularization, in which intussusception and fibrosis/hyalinization of the vessels occur, the expression of Hela *l*-CaD tapers off. Hela *l*-CaD is not expressed in normal-looking vessels (coopted vessels) in the gliomas, nor in normal vessels of the control samples. The findings suggest that the expression of Hela *l*-CaDs appears tightly associated with glioma neovascularization-triggered differential splicing of *CALD1* during activation of quiescent ECs. The differential splicing contributes to upregulation or overexpression of the entire *l*-CaD class in the tumor microvasculature (12). Hela *l*-CaD II is found more often as compared to Hela *l*-CaD I, consistent with the findings at mRNA level (12). No transcripts or isoforms of Hela *l*-CaD were detected in normal or neoplastic glial cells and so the expression appears to be specific for glioma microvasculature.

In vivo functions of *l*-CaD have not been well characterized. In vitro overexpression of the actin-binding domain, or full length, of *l*-CaD stabilizes actin microfilaments by polymerization (36-38). The stabilized microfilaments enhance cell spreading and arborization/branching of cell

processes as well as inhibit cell contractility and decrease in the number of focal adhesions in cultured and transfected cells (36, 37). These *l*-CaD-mediated phenomena probably result in remodelling of actomyosin-associated molecules to form podosomes, a type of highly dynamic cell adhesive structure (15, 39). A distinct feature of podosomes is the accumulation of actin-associated proteins such as myosin, caldesmon and tropomyosin. These proteins are not detected in stable or immotile adhesive structures (focal adhesions) of normal cells (15, 39). Focal adhesions are sites of transmembrane linkage between the actin microfilament bundles and the extracellular matrix (ECM), where stress fibers terminate (40, 39). Podosomes are typically found in highly motile cells with the ability to cross tissue boundaries under various normal and pathological conditions (15). Only recently it was discovered that podosomes can be induced in endothelial cells in vitro (16). Intriguingly, the formation of podosomes seems to be associated with cell enlargement and multinucleation, elongation of cytoplasm protrusions or free cellular fragments (14-18). All of these morphologic changes were frequently observed in Hela *l*-CaD^+ ECs (Figure 1). More interestingly, we found FA disassembly and F-actin remodeling in Hela *l*-CaD^+ ECs. The dot-like structures of actin and vinculin fit well with the distribution and structure of podosomes (15). The Hela *l*-$CaDs^+$ ECs may, therefore, very well be involved in the formation of podosomes. Also, the finding that Hela *l*-$CaDs^+$ ECs/EPCs and NCECCs are ubiquitously present in the glioma tissues hints to the high motility of such cells. The cells appear to be capable of robust vasculogenesis and angiogenesis serving survival and growth of the tumors in which they are present. It appears that the differential expression of Hela *l*-CaDs has a potent effect on endothelial cell function. It has been observed that most of Hela *l*-CaD in Hela S3 cells only have a C-terminal actin-binding domain (41). Although the majority of the C-terminal fragments is released from the microfilaments during mitosis, some may incompletely dissociate, resulting in the formation of multinuclear cells (38). This may explain the frequently observed Hela *l*-CaD^+ multinucleated ECs in our gliomas.

In conclusion, the differential expression of the Hela *l*-CaD displays an *in situ* specificity during glioma neovascularization. It could serve as a novel marker in the early stage of glioma neovascularization. The expression of Hela *l*-CaD is associated with activation of motility of ECs taking part in neovascularization.

References

1. Carmeliet P, Jain RK (2000) Angiogenesis in cancer and other diseases. *Nature* 407:249-257.

2. Jain RK (2003) Molecular regulation of vessel maturation. *Nat Med* 9:685-693.

3. Mentlein R, Held-Feindt J (2003) Angiogenesis factors in gliomas: a new key to tumour therapy? *Naturwissenschaften* 90:385-394.

4. Carmeliet P (2003) Angiogenesis in health and disease. *Nat Med* 9:653-660.

5. Holash J, Maisonpierre PC, Compton D, Boland P, Alexander CR, Zagzag D, Yancopoulos GD,Wiegand SJ (1999) Vessel cooption, regression, and growth in tumors mediated by angiopoietins and VEGF. *Science* 284:1994-1998.

6. Chang YS, di Tomaso E, McDonald DM, Jones R, Jain RK, Munn LL (2000) Mosaic blood vessels in tumors: frequency of cancer cells in contact with flowing blood. *Proc Natl Acad Sci U S A* 97:14608-14613.

7. Ingber DE, Prusty D, Sun Z, Betensky H,Wang N (1995) Cell shape, cytoskeletal mechanics, and cell cycle control in angiogenesis. *J Biomech* 28:1471-1484.

8. Huang S, Ingber DE (2000) Shape-dependent control of cell growth, differentiation, and apoptosis: switching between attractors in cell regulatory networks. *Exp Cell Res* 261:91-103.

9. Hayashi K, Yano H, Hashida T, Takeuchi R, Takeda O, Asada K, Takahashi E, Kato I, Sobue K (1992) Genomic structure of the human caldesmon gene. *Proc Natl Acad Sci U S A* 89:12122-12126.

10. Huber PA (1997) Caldesmon. *Int J Biochem Cell Biol* 29:1047-1051.

11. Castellino F, Ono S, Matsumura F, Luini A (1995) Essential role of caldesmon in the actin filament reorganization induced by glucocorticoids. *J Cell Biol* 131:1223-1230.

12. Zheng PP, Sieuwerts AM, Luider TM, van der Weiden M, Sillevis-Smitt PA, Kros JM (2004) Differential expression of splicing variants of the human caldesmon gene (CALD1) in glioma neovascularization versus normal brain microvasculature. *Am J Pathol* 164:2217-2228.

13. DeFife KM, Jenney CR, Colton E, Anderson JM (1999) Cytoskeletal and adhesive structural polarizations accompany IL-13-induced human macrophage fusion. *J Histochem Cytochem* 47:65-74.

14. Euteneuer U, Schliwa M (1984) Persistent, directional motility of cells and cytoplasmic fragments in the absence of microtubules. *Nature* 310:58-61.

15. Linder S, Aepfelbacher M (2003) Podosomes: adhesion hot-spots of invasive cells. *Trends Cell Biol* 13:376-385.

16. Moreau V, Tatin F, Varon C, Genot E (2003) Actin can reorganize into podosomes in aortic endothelial cells, a process controlled by Cdc42 and RhoA. *Mol Cell Biol* 23:6809-6822.

17. Parast MM, Aeder S, Sutherland AE (2001) Trophoblast giant-cell differentiation involves changes in cytoskeleton and cell motility. *Dev Biol* 230:43-60.

18. Verkhovsky AB, Svitkina TM, Borisy GG (1999) Self-polarization and directional motility of cytoplasm. *Curr Biol* 9:11-20.

19. Kleihues P, Louis DN, Scheithauer BW, Rorke LB, Reifenberger G, Burger PC, Cavenee WK (2002) The WHO classification of tumors of the nervous system. *J Neuropathol Exp Neurol* 61:215-225; discussion 226-219.

20. Goldbrunner RH, Bernstein JJ, Plate KH, Vince GH, Roosen K, Tonn JC (1999) Vascularization of human glioma spheroids implanted into rat cortex is conferred by two distinct mechanisms. *J Neurosci Res* 55:486-495.

21. Rafii S (2000) Circulating endothelial precursors: mystery, reality, and promise. *J Clin Invest* 105:17-19.

22. Yancopoulos GD, Davis S, Gale NW, Rudge JS, Wiegand SJ, Holash J (2000) Vascular-specific growth factors and blood vessel formation. *Nature* 407:242-248.

23. Plate KH, Mennel HD (1995) Vascular morphology and angiogenesis in glial tumors. *Exp Toxicol Pathol* 47:89-94.

24. Burri PH, Djonov V (2002) Intussusceptive angiogenesis--the alternative to capillary sprouting. *Mol Aspects Med* 23:1-27.

25. Vajkoczy P, Menger MD (2004) Vascular microenvironment in gliomas. *Cancer Treat Res* 117:249-262.

26. Djonov V, Baum O, Burri PH (2003) Vascular remodeling by intussusceptive angiogenesis. *Cell Tissue Res* 314:107-117.

27. Teramoto N, Szekely L, Pokrovskaja K, Hu LF, Yoshino T, Akagi T, Klein G (1998) Simultaneous detection of two independent antigens by double staining with two mouse monoclonal antibodies. *J Virol Methods* 73:89-97.

28. Humphrey MB, Bryan J, Cooper TA, Berget SM (1995) A 32-nucleotide exon-splicing enhancer regulates usage of competing 5' splice sites in a differential internal exon. *Mol Cell Biol* 15:3979-3988.

29. Yano H, Hayashi K, Momiyama T, Saga H, Haruna M, Sobue K (1995) Transcriptional regulation of the chicken caldesmon gene. Activation of gizzard-type caldesmon promoter requires a CArG box-like motif. *J Biol Chem* 270:23661-23666.

30. Sobue K, Sellers JR (1991) Caldesmon, a novel regulatory protein in smooth muscle and nonmuscle actomyosin systems. *J Biol Chem* 266:12115-12118.

31. Humphrey MB, Herrera-Sosa H, Gonzalez G, Lee R, Bryan J (1992) Cloning of cDNAs encoding human caldesmons. *Gene* 112:197-204.

32. Castellino F, Heuser J, Marchetti S, Bruno B, Luini A (1992) Glucocorticoid stabilization of actin filaments: a possible mechanism for inhibition of corticotropin release. *Proc Natl Acad Sci U S A* 89:3775-3779.

33. McManus MJ, Lingle WL, Salisbury JL, Maihle NJ (1997) A transformation-associated complex involving tyrosine kinase signal adapter proteins and caldesmon links v-erbB signaling to actin stress fiber disassembly. *Proc Natl Acad Sci U S A* 94:11351-11356.

34. Hegmann TE, Schulte DL, Lin JL, Lin JJ (1991) Inhibition of intracellular granule movement by microinjection of monoclonal antibodies against caldesmon. *Cell Motil Cytoskeleton* 20:109-120.

35. Yamakita Y, Yamashiro S, Matsumura F (1992) Characterization of mitotically phosphorylated caldesmon. *J Biol Chem* 267:12022-12029.

36. Helfman DM, Levy ET, Berthier C, Shtutman M, Riveline D, Grosheva I, Lachish-Zalait A, Elbaum M, Bershadsky AD (1999) Caldesmon inhibits nonmuscle cell contractility and interferes with the formation of focal adhesions. *Mol Biol Cell* 10:3097-3112.

37. Warren KS, Lin JL, Wamboldt DD, Lin JJ (1994) Overexpression of human fibroblast caldesmon fragment containing actin-, Ca++/calmodulin-, and tropomyosin-binding domains stabilizes endogenous tropomyosin and microfilaments. *J Cell Biol* 125:359-368.

38. Warren KS, Shutt DC, McDermott JP, Lin JL, Soll DR, Lin JJ (1996) Overexpression of microfilament-stabilizing human caldesmon fragment, CaD39, affects cell attachment, spreading, and cytokinesis. *Cell Motil Cytoskeleton* 34:215-229.

39. Tanaka J, Watanabe T, Nakamura N, Sobue K (1993) Morphological and biochemical analyses of contractile proteins (actin, myosin, caldesmon and tropomyosin) in normal and transformed cells. *J Cell Sci* 104 (Pt 2):595-606.

40. Girard PR, Nerem RM (1993) Endothelial cell signaling and cytoskeletal changes in response to shear stress. *Front Med Biol Eng* 5:31-36.

41. Goncharova EA, Shirinsky VP, Shevelev AY, Marston SB, Vorotnikov AV (2001) Actomyosin cross-linking by caldesmon in non-muscle cells. *FEBS Lett* 497:113-117.

Chapter 5

Differential expression of Hela-type caldesmon in tumor neovascularization: A new marker of angiogenic endothelial cells

J Pathol 2004, 2005, 205: in press

Ping-Pin Zheng, M. van der Weiden, Johan M. Kros

Abstract

Caldesmon (CaD) is a major actomyosin-binding protein distributed in various cell types. There are at least two high-molecular-weight isoforms (*h*-CaD) and four low-molecular-weight isoforms (*l*-CaD) produced by alternative splicing. The alternatively spliced variants for the *l*-CaD class are further differentiated by inclusion (Hela *l*-CaD) or exclusion (WI-38 *l*-CaD) of exon 1. Currently, nothing is known about differential expression of the Hela *l*-CaD in tumor neovascularization. In a previous study, we found the Hela-type transcripts expressed in glioma blood vessels but not in the normal cerebral vasculature. To investigate if the differentially expressed transcripts are translated into protein, a specific antibody against the peptide encoded by the exon 1 was raised. We initially confirmed that the protein is exclusively expressed in glioma vasculature. To further determine whether these findings are generalizable to neovascularization in a wide variety of other tumor types, we examined a large cohort of cancers derived from various organs, including breast, lung, kidney, colon, stomach, ovary, uterus, prostate, thyroid, liver, up to a total of 180 cases. It was found that the expression of the Hela *l*-CaD was restricted to tumor vasculature but not found in normal blood vessels, and that Hela *l*-CaD is preferentially expressed in the early stage of tumor neovascularization. Also it was noticed that the Hela *l*-CaD$^+$ endothelial cells (ECs) frequently are enlarged, multinucleated and develop elongated cell projections or free fragments of cytoplasm, correlating with the features of motile cells. In the Hela *l*-CaD$^+$ ECs disassembly of focal adhesion and the formation of podosome-like structures was observed. Therefore, the findings support the notion that quiescent ECs undergo activation of motility, necessary for ubiquitous tumor-associated neovascularization. The data indicate that Hela *l*-CaD can be considered as a marker for angiogenic ECs during early stages of tumor neovascularization.

Introduction

Neovascularization is essential for tumor development, growth and metastasis. New blood vessel formation is a complex process that involves at least the classic triad of endothelial cell (EC) proliferation, migration, and extracellular matrix (ECM) degradation[1]. In addition, tumor cells may take over host vessels (an event designated as “co-option”)[2], or form perivascular cuffs around host vessels[3]. Neither in co-option, nor in the formation of perivascular cuffs, proliferation of ECs is involved. Currently, significant advances have been made in understanding the molecular mechanisms by the identification of the soluble angiogenic factors, insoluble ECM molecules, and receptor signaling pathways that mediate the control of angiogenesis [4]. Despite the increasing number of regulatory factors and receptors that are being focused on[3, 5-7], only little attention has been drawn to the role of the actin cytoskeleton (CSK)-associated proteins in the regulation of tumor neovascularization. In fact, actin polymerization and remodeling is involved in many cellular functions that include motility, migration, division and endocytosis[8]. All of the actin-binding proteins are regulated by a complex network of bi-directional outside-in and inside-out signaling cascades that lead to the proper organization and dynamics of the CSK[8]. Capillary ECs also have the ability to switch between different fates, including growth, apoptosis, differentiation and motility, through adhesive interactions with the ECM by modulating their cell shape and cytoskeletal structure [4].

Caldesmon (CaD) is a major actin-associated protein found in smooth muscle (high molecular weight (*h*-CaD), 120-150kDa) and nonmuscle cells (low molecular weight (*l*-CaD), 70-80 kDa)[9]. The Hela-type splicing variants and protein isoforms were initially cloned from Hela S3 cell lines [9]. So far, the expression of the Hela *l*-CaD was only examined in cancer cell lines[9, 10], and was not previously investigated in tumor neovascularization.

In the present study, we examined Hela *l*-CaD expression in a variety of cancers derived from various organs to determine whether the protein is differentially expressed in neovascularization among a wide variety of tumor types. In addition, the cell shape of the Hela *l*-CaD-expressing ECs and focal adhesion (FA) was compared with that of motile cells.

Materials and methods

Clinical Samples
Paraffin-embedded tissue samples, taken from the archives of the Department of Pathology, Erasmus Medical Center, Rotterdam, The Netherlands, were used for this study. The use of human tissue samples was approved by the Ethical Review Board at the Erasmus Medical Center. Since it is known that gliomas are richly vascularized tumors harbouring all known patterns of neovascularization, we first examined 30 glioma samples and 15 control brain samples from autopsy cases free of neurological diseases or tumors. Subsequently, a total of 150 resection samples containing cancers derived from other organs as listed in Table 1 were examined (Table 1). For each case, tumor-free tissues taken from the tumor surrounding were used as normal controls.

Defining stages/patterns of tumor neovascularization
Neovascularization of tumors usually undergoes various stages encompassing multiple vascularization patterns. The initial stage consists of *de novo* vessel formation (vasculogenesis) through single ECs or endothelial precursor/progenitor cells (EPCs) [11], or non-canalized endothelial cell chains (NCECCs)[2] either shed from vessel walls or mobilized from bone marrow[12]. In the early stage, sprouting occurs either from the newly formed vessels or from host vessels, in a process called angiogenesis[7, 13]. At later stages of neovascularization, intussusceptive vascular growth (IVG), i.e., partitioning of the vessel lumen by insertion of interstitial tissue columns [14], forms the main source of tumor vessel growth[15]. An important characteristic of IVG is that it is achieved by an exceedingly low rate of EC proliferation[16]. The end stage vessels show fibrosis and hyalinization of their walls. Co-opted vessels lack vascular sprouts, branches, EC hyperplasia or NCECCs [2].

Table 1. **Scores of Hela *I*-CaD expression in various tumors**

Organ	Tumor type	Case No	Hela+EC scores			
			0	1+	2+	3+
Brain	glioma	30	0	0	5	25
Thyroid	adenocarcinoma	15	0	13	2	0
Lung	adenocarcinoma / adenosquamous carcinoma	15	1	12	2	0
Liver	hepatocellular - / metastatic adenocarcinoma	15	0	12	3	0
Kidney	renal cell carcinoma	15	0	3	10	2
Stomach	adenocarcinoma	15	0	5	10	0
Colon	adenocarcinoma	15	5	7	3	0
Breast	invasive carcinoma	15	0	0	9	6
Ovary	malignant surface epithelial-stromal tumors	15	10	5	0	0
Uterus	endometrial carcinoma	15	5	10	0	0
Prostate	adenocarcinoma	15	4	8	3	0

Raising the antibody
The antibody (CUK-0129) to the Hela *l*-CaD was generated against the synthetic peptide which corresponds to the N-terminal 18 residues encoded by exon 1 of the human caldesmon gene (*CALD1*) (GenBank, Accession NM_033139). Production, characterization and demonstration of the specificity of the antibody were commercially carried out (CovalAB, Lyon, France). Briefly, the target peptide was synthesized, purified, and verified by amino acid analysis. Two rabbits were immunized subcutaneously with the peptide. Immunopurification of the specific antibody was performed by loading the antisera onto the peptide-coupled Sepharose column. The immunoreactivity of the antibody was validated by enzyme-linked immunosorbent assay (ELISA). The specificity of CUK-0129 used in this study was monitored by the combination of immunoprecipitation and immunoblotting on positive control samples.

Immunohistochemistry (IHC)
Paraffin sections (5µm) were mounted onto aminopropyltriethoxysilane (APES)-coated glass slides (Knittel Glaser, Braunschweig, Germany). Dewaxed sections were pretreated in 0.1% pronase (Sigma, St Louis, USA) for 10 minutes at 37ºC, and incubated with CUK-0129 (CovalAB, Lyon, France) at 1:40 for two hour at RT. The biotinylated goat-anti-rabbit (Dako, Glostrup, Denmark) at 1:200 was incubated for 1 hour at RT, followed by incubation with StreptABC complex/AP (Dako, Glostrup, Denmark) at 1:100 for one hour at RT for visualization of the immunoreactivity.

Scoring Hela l-CaD-positive ECs/vessels
Based on the average percentages of Hela$^+$ ECs/vessels present in 10 HPFs, a scoring scheme was applied as follows (Table 1): no Hela$^+$ ECs/vessels present: score 0; few scattered positive ECs/vessels: score 1; less than 50% positive ECs/vessels: score 2 and more than 50% positive ECs/vessels: score 3. The individual ECs were recognized by double-labeling with CD34.

Double and triple immunofluorescence labeling (IF)
We used the endothelial cell markers CD34/CD31 together with CUK-0129 for IF double-labeling to confirm the EC identity of Hela *l*-CaD$^+$ cells. Cryostat sections (5 µm) were mounted onto non-coated microscope slides (Menzel Glaser, Braunschweig, Germany), fixed in acetone for10 minutes at RT and air dried. For double-labeling, sections were then incubated with mouse- anti-CD34 (Lab Vision Corporation) at 1:20 or mouse-anti-CD31 (Dako, Glostrup, Denmark) at 1:40, and CUK-0129 (CovalAb, Lyon, France) at 1:10 for one hour at RT, respectively. After washing, FITC-conjugated goat-anti-mouse (Southern Biotech) at 1:50 and swine-anti-rabbit-biotin (Dako, Glostrup, Denmark) at 1:100 were applied for 1 hour at RT, respectively. Further, Cy3-conjugated avidine (Jackson ImmunoResearch) at 1:100 was applied for 1 hour at RT. Triple staining of vinculin, CD34 and CUK-0129 allowed us to visualize the FA status of Hela *l*-CaD$^+$ ECs. For simultaneous detection of two antigens by two monoclonal antibodies, we used the protocol by CSA kit[17]. Briefly, the antigen-retrieved paraffin sections were soaked in a block peroxidase solution (CSA kit, Dako,Glostrup,Denmark) for 5 min, followed by incubation with protein blocking solution (CSA kit, Dako, Glostrup, Denmark) for 5 min. The sections were incubated with the highly diluted monoclonal mouse-anti-human vinculin as first primary antibody at 1:1,280 dilution for one hour. This dilution does not allow direct visualization by the second detection system for the second mouse monoclonal antibody (CD34) (Lab Vision Corporation), which was verified by a series of dilutions and examined by a laser scanning confocal microscope (CLSM). The HRP-conjugated-goat anti-mouse antibody (1:50) (Dako, Glostrup, Denmark) was incubated for the detection for 30 min. Subsequently, the very slides were incubated with the amplification reagent (CSA kit, Dako, Glostrup, Denmark) for 30 min to generate the biotinylated tyramid deposits. Afterwards, the sections were washed and incubated for one hour with mouse monoclonal antibody CD 34 (1:20) as second primary antibody. The biotin-tyramide deposits corresponding to the first Mab and the second Mab itself were detected simultaneously by incubating one hour by a mixture of FITC-conjugated streptavidin (Jackson ImmunoResearch) and TRITC-conjugated sheep anti-mouse immunoglobulin (Chemicon International,Inc), respectively. Subsequently the sections were incubated with the polyclonal antibody CUK-129 (1:25) for one hour. Cy5-conjugated donkey anti- rabbit (1:50) (Jackson ImmunoResearch) was incubated for 30 min. for

detection. All the sections were washed twice with PBS between the different staining steps. Nuclei were counterstained with DAPI (Sigma Aldrich,st Louis,USA). All steps were performed at RT. Sections were mounted with covering glass and examined under CLSM.

Confocal Laser Scanning Microscope (CLSM)
CLSM was performed using a Zeiss LSM 510 META system (Karl Zeiss, Gottingen, Germany). The laser diode 405nm, Argon 488 nm and HeNe 543 or 633 were switched on and set at 50% output intensity. We used korr C-Apochromat 63x objective to generate a single image for each sample. DAPI, FITC, Cy3/TRITC or Cy5 preparation was scanned triple or quadruple by using changes of the three or quadruple filters. The three signals were detected by the same detector and stored separately in the computer memory.

Results

Differential expression of Hela l-CaD in tumor vasculature versus normal blood vessels by IHC
All tumors included in this study harbored Hela *l*-CaD$^+$ ECs or vessels. However, the Hela *l*-CaD$^+$ ECs/vessels were variably present in the different tumor types (Table 1). The gliomas contained the highest percentages of Hela *l*-CaD$^+$ ECs/vessels, followed by breast cancer, gastric adenocarcinoma and renal cell carcinoma. Cancers of the ovary, prostate and endometrium contained relatively low percentages of Hela *l*-CaD$^+$ ECs/vessels. Cancers of thyroid, lung, liver, colon and breast were intermediate regarding the expression. Hela *l*-CaD was predominantly found to be expressed in individual ECs/EPCs, NCECCs and sprouting/branching microvessels.
There was low or absent expression of the protein in vessels showing IVG or fibrosis. No immunoreactivity of the protein was observed in co-opted vessels within the tumors or in normal vessels of the control samples. The Hela *l*-CaD$^+$ ECs often show alterations in cell shape, such as cell enlargement or elongated protrusions (Figure 1A), multinucleation or free fragments of cytoplasm (Figure 1B), or an epithelioid phenotype with round nuclei (Figure 1G), as compared to quiescent ECs with flat nuclei (Figure 1D, H, J and L).

Confirmation of the EC lineage of individual Hela l-CaD$^+$ cells or cell population
The endothelial markers (CD34/CD31) were used for gross (IHC, data not shown) and elaborate (IF) confirmation of the EC lineage of the individually deposited Hela *l*-CaDs$^+$ cells or cell populations by double immunolabeling. The co-localization of the two antigens was confirmed in merged images of two colors within the same cell(s). The images were taken by using triple laser scanning under CLSM for a target cell or cell population as representatively shown in Figure 2.

Focal adhesion (FA) disassembly/decrease coexisting in Hela l-CaD$^+$ ECs
FAs were readily visualized by immunofluorescence labeling with anti-vinculin monoclonal antibody. The vinculin-containing FAs show dense dash-like or oval bands in normal vessels as shown in Figure 3A and B. Vinculin bands disappear or diminish in Hela *l*-CaD$^+$ ECs and are diffusely redistributed through the cell body with the formation of dot-like structures associated Hela *l*-CaD. The redistributed viculin appears associated with Hela *l*-CaD and accumulated in protrusions of the ECs at their cell protrusions (Figure 3C and D).

Orthotopic expression of Hela l-CaD in epithelial cells
Except for tumor vessels, we found that the Hela *l*-CaD is also expressed in some types of normal epithelial cells and carcinomas derived from these epithelial cells as representatively shown in Figure 1G and I. This finding matches with the initial cloning of the transcript and protein in Hela S3 epithelial, not fibroblastic, cell lines.

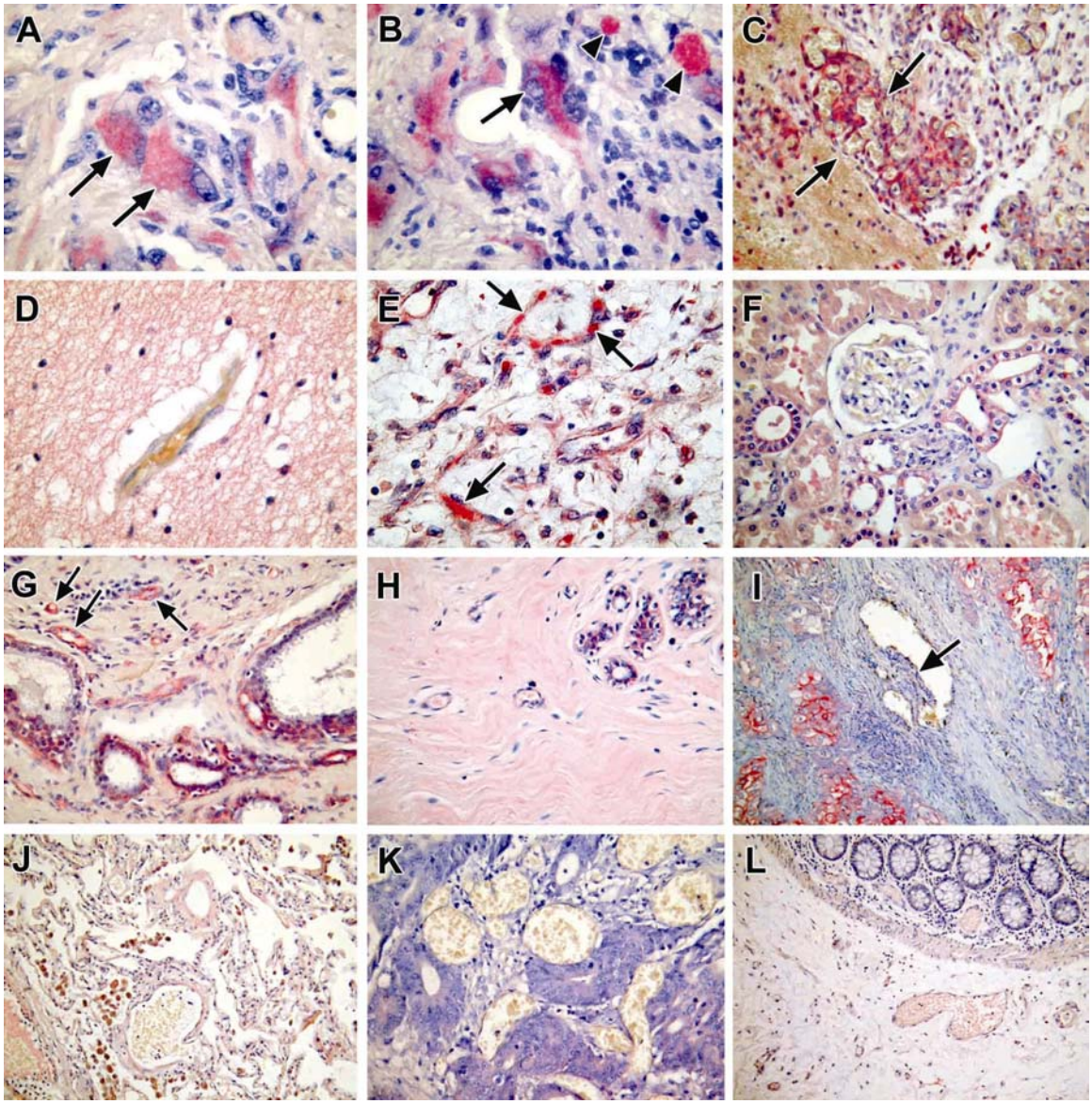

Figure 1: Differential expression of Hela *I*-CaD in tumor vasculature by IHC **A.** In a glioblastoma (GBM), the individual Hela *I*-CaD^{+} giant ECs (arrows) show cell enlargement with elongated protrusions. **B.** A Hela *I*-CaD^{+} multinucleated giant cell (arrow) and free fragments of cytoplasm (arrowheads) are noticed in a GBM. **C.** Immunopositivity is noted in microvascular sprouting/branching (arrows) in an anaplastic oligodendroglioma. **D.** Normal white matter in which the blood vessels and glial cells are immunonegative. **E.** The immunopositive NCECCs (arrows) are seen in a renal cell carcinoma (RCC, clear cell type). **F.** In a normal kidney cortex, the glomerulus is immunonegative while tubular epithelial cells exhibit immunostaining. **G.** In mammary ductal carcinoma (MDC), both the newly-formed capillaries with epithelial phenotype (arrows), and cancerous ducts demonstrate immunopositivity. **H.** In normal breast tissue, the capillaries are negative while epithelial cells in the duct lobule display immunopositivity. **I.** The inserted tissue column within a vessel (IVG) (arrow) in a lung adenocarcinoma remains immunonegative, in contrast to the surrounding immunopositive cancer cells. **J.** The vessels of normal lung tissue remain immunonegative, while epithelial cells in bronchi show immunopositivity (data not shown). **K.** No immunostaining was noted in the co-opted vessels within colon adenocarcinoma. **L.** The vessels in normal colon mucosa remain immunonegative.

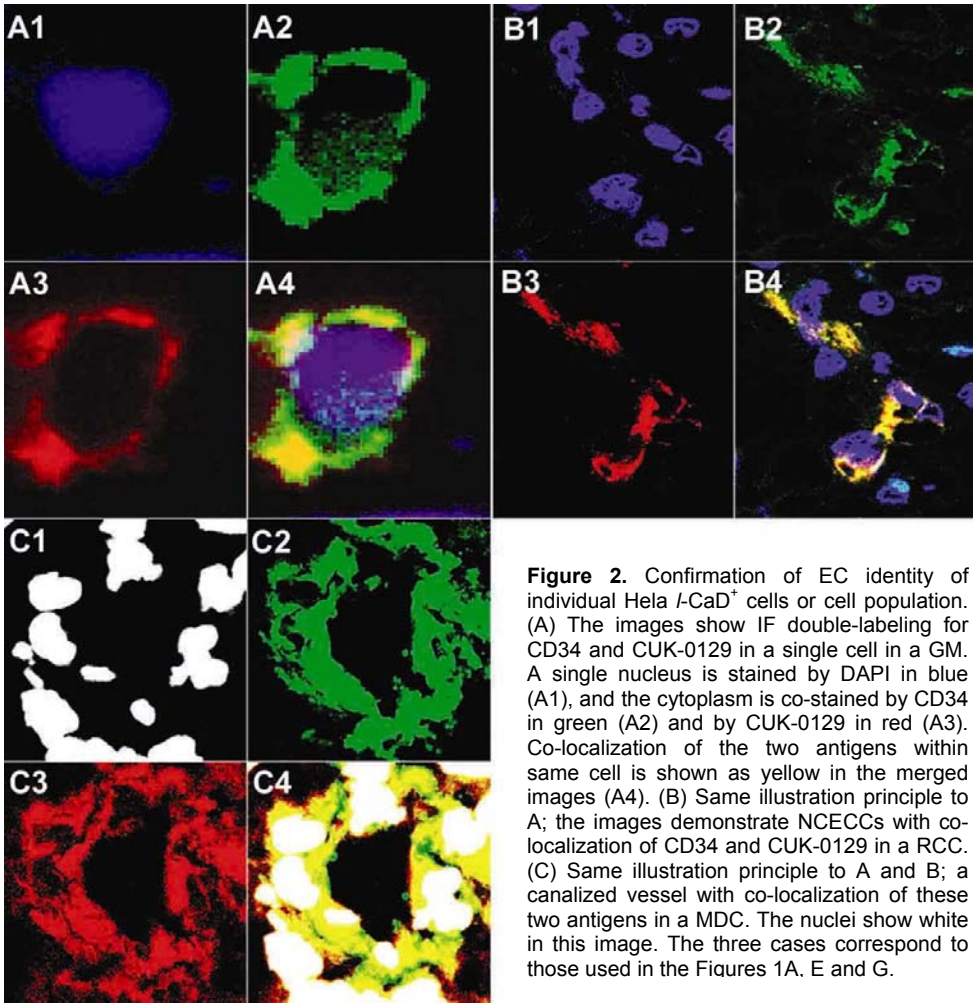

Figure 2. Confirmation of EC identity of individual Hela *I*-CaD^{+} cells or cell population. (A) The images show IF double-labeling for CD34 and CUK-0129 in a single cell in a GM. A single nucleus is stained by DAPI in blue (A1), and the cytoplasm is co-stained by CD34 in green (A2) and by CUK-0129 in red (A3). Co-localization of the two antigens within same cell is shown as yellow in the merged images (A4). (B) Same illustration principle to A; the images demonstrate NCECCs with co-localization of CD34 and CUK-0129 in a RCC. (C) Same illustration principle to A and B; a canalized vessel with co-localization of these two antigens in a MDC. The nuclei show white in this image. The three cases correspond to those used in the Figures 1A, E and G.

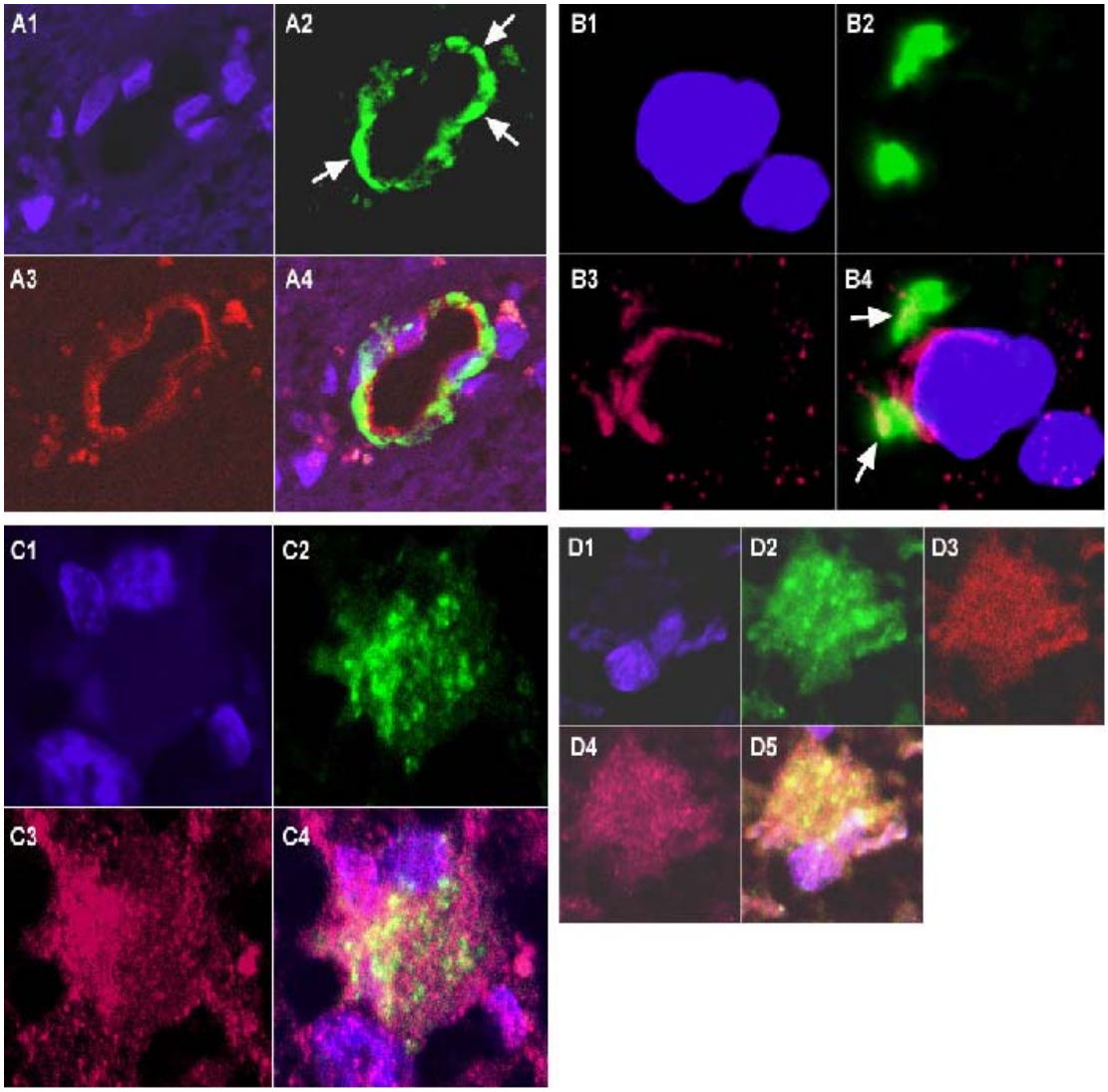

Figure 3. Disassembly of vinculin-containing FA in Hela *I*-CaD$^+$ ECs. (A) Vinculin is localized along the basal membrane region of the endothelium in a capillary of normal brain, showing dense bands (A2, arrows). The endothelium is labeled with CD34 (A3). Nuclei are counterstained with DAPI (A1). A merged image is shown in A4. (B) A single EC, cropped from normal endothelium, is double-labeled with vinculin (B2) and CD34 (B3). The vinculin bands are present at the periphery of the EC and are positioned perpendicularly to the ECM at the leading edge of the EC (B2, arrows), indicating the polarity of the EC. The merged image is shown in B4. (C) An individually distributed multinucleated EC was captured from glioma tissue and is triply labeled with vinculin (C2), CD34 (not shown) and CUK-0129 (C3). As compared to the normal EC shown in panel B, the vinculin bands have disappeared at the cell periphery and are diffusely redistributed to cytoplasm with formation of dot-like structures. The dot-like structures appears associated with Hela *I*-CaD as shown in C4. (D) This panel shows a triple labeling for vinculin (D2), CD34 (D3) and CUK-129 (D4) in a single multinucleated EC from glioma tissue. The findings are similar to those shown in panel C.

Discussion

In endothelium, the cytoskeletal structure regulates adhesive interactions with neighboring cells and the ECM [18, 19], which control endothelial permeability and vessel wall integrity. There is evidence that in nonmuscle cells *I*-CaD plays a crucial role in the cytoskeletal dynamics and architecture[20]. ECs are usually quiescent, but when triggered may become capable of rapidly sending out sprouts in a coordinated and directional manner [21]. Table 1 summarizes the percentage of Hela *I*-CaD$^+$ECs in the various tumor types. The highest percentages of Hela-*I*-

CaD-positive ECs were found in the gliomas, which are well-known for their exuberant vascularization. We found that Hela *l*-CaD is predominantly expressed in the early stages of neovascularization, while in the late stages the expression dramatically diminishes. Hela *l*-CaD is not expressed in co-opted vessels within the tumors, nor in normal vessels of the control samples. The findings suggest that the expression of Hela *l*-CaD is tightly associated with the differential splicing of *CALD1* during activation of ECs as part of the process of tumor neovascularization. The ectopic splicing contributes to the upregulation of the entire *l*-CaD class in tumor microvasculature[22].

In cultured and transfected non-muscle cells overexpression of *l*-CaD results in enhanced cell spreading, inhibition of cell contractility and a decrease in the number of focal adhesions (FAs)[20, 23]. These *l*-CaD-mediated phenomena probably result from the disassembly of stable FAs to form motile adhesions (podosomes). Podosomes are considered as a type of highly dynamic cell adhesive structures[24, 25], and is typically found in highly motile cells showing the ability to cross tissue boundaries under various normal and pathological conditions[24], including cells of mesenchymal and epithelial origin[24, 26]. Only recently it was discovered that podosomes can be induced in ECs in vitro[18]. Coincidentally, there is evidence that with podosome formation and increased motility, the cells become enlarged, multinucleated, and actively form protrusions and free fragments of cytoplasm[18, 27-30]. Hela *l*-CaD$^+$ ECs with these features were frequently observed in this study. Vinculin, a focal adhesion protein, is normally found at the periphery of ECs perpendicular to adhesion substrate in vitro [18], and along the region of the basal membrane of the endothelium of vessels [31] as dense dash-like or oval bands [32]. FA destablization is a typical feature of activated cell motility [24]. In this study, we found that the vinculin bands disassemble at FA sites and diffusely redistribute into the cytoplasm with dot-like structures together with Hela *l*-CaD. The dot-like structures represent podosome-like structures [24]. These structures are often localized at the leading-edges of cell protrusions, directing cell migration [24]. The findings suggest an activation of motility of quiescent ECs. The locomotion of the individual Hela *l*-CaD$^+$ ECs or cell groups in the tumors seems to be reflected by the ubiquitous presence of these cells, particularly in the gliomas. Taken together, the findings support the notion that the Hela *l*-CaDs$^+$ ECs may be involved in the formation of podosomes. Consequently, such ECs appear to be capable of ubiquitous and robust vasculogenesis and angiogenesis serving survival and growth of the tumors. Vasculogenesis is normally limited to early embryogenesis and is believed not to occur in the adult[33]. Tumor vasculogenesis is reminiscent of vasculogenesis in the embryo. The embryonic ECs are able to alter their phenotypes into epithelioid cell types as a response to growth factors[34]. Such a metamorphosis seems to be reflected by the epithelioid Hela *l*-CaD$^+$ ECs found in the present study.

In conclusion, the Hela *l*-CaD is differentially expressed in angiogenic ECs among a wide variety of tumors, and is associated with the motility activation of quiescent ECs. Hela *l*-CaD can be considered as a new marker of neovascularization in early stages of tumor neovascularization.

References

1. Wernert N, Okuducu AF,Pepper MS. Ets 1 is expressed in capillary blood vessels but not in lymphatics. *J Pathol* 2003;200:561-567.

2. Holash J, Maisonpierre PC, Compton D*, et al.* Vessel cooption, regression, and growth in tumors mediated by angiopoietins and VEGF. *Science* 1999;284:1994-1998.

3. Carmeliet P, Jain RK. Angiogenesis in cancer and other diseases. *Nature* 2000;407:249-257.

4. Ingber DE. Mechanical signaling and the cellular response to extracellular matrix in angiogenesis and cardiovascular physiology. *Circ Res* 2002;91:877-887.

5. Folkman J. Angiogenesis in cancer, vascular, rheumatoid and other disease. *Nat Med* 1995;1:27-31.

6. Wernert N. The multiple roles of tumour stroma. *Virchows Arch* 1997;430:433-443.

7. Yancopoulos GD, Davis S, Gale NW, Rudge JS, Wiegand SJ,Holash J. Vascular-specific growth factors and blood vessel formation. *Nature* 2000;407:242-248.

8. Houle F, Rousseau S, Morrice N*, et al.* Extracellular signal-regulated kinase mediates phosphorylation of tropomyosin-1 to promote cytoskeleton remodeling in response to oxidative stress: impact on membrane blebbing. *Mol Biol Cell* 2003;14:1418-1432.

9. Hayashi K, Yano H, Hashida T*, et al.* Genomic structure of the human caldesmon gene. *Proc Natl Acad Sci U S A* 1992;89:12122-12126.

10. Castellino F, Ono S, Matsumura F,Luini A. Essential role of caldesmon in the actin filament reorganization induced by glucocorticoids. *J Cell Biol* 1995;131:1223-1230.

11. Goldbrunner RH, Bernstein JJ, Plate KH, Vince GH, Roosen K,Tonn JC. Vascularization of human glioma spheroids implanted into rat cortex is conferred by two distinct mechanisms. *J Neurosci Res* 1999;55:486-495.

12. Rafii S. Circulating endothelial precursors: mystery, reality, and promise. *J Clin Invest* 2000;105:17-19.

13. Plate KH, Mennel HD. Vascular morphology and angiogenesis in glial tumors. *Exp Toxicol Pathol* 1995;47:89-94.

14. Burri PH, Djonov V. Intussusceptive angiogenesis--the alternative to capillary sprouting. *Mol Aspects Med* 2002;23:1-27.

15. Vajkoczy P, Menger MD. Vascular microenvironment in gliomas. *Cancer Treat Res* 2004;117:249-262.

16. Djonov V, Baum O,Burri PH. Vascular remodeling by intussusceptive angiogenesis. *Cell Tissue Res* 2003;314:107-117.

17. Teramoto N, Szekely L, Pokrovskaja K*, et al.* Simultaneous detection of two independent antigens by double staining with two mouse monoclonal antibodies. *J Virol Methods* 1998;73:89-97.

18. Moreau V, Tatin F, Varon C,Genot E. Actin can reorganize into podosomes in aortic endothelial cells, a process controlled by Cdc42 and RhoA. *Mol Cell Biol* 2003;23:6809-6822.

19. Zaidel-Bar R, Ballestrem C, Kam Z,Geiger B. Early molecular events in the assembly of matrix adhesions at the leading edge of migrating cells. *J Cell Sci* 2003;116:4605-4613.

20. Helfman DM, Levy ET, Berthier C*, et al.* Caldesmon inhibits nonmuscle cell contractility and interferes with the formation of focal adhesions. *Mol Biol Cell* 1999;10:3097-3112.

21. Carmeliet P. Angiogenesis in health and disease. *Nat Med* 2003;9:653-660.

22. Zheng PP, Sieuwerts AM, Luider TM, van der Weiden M, Sillevis-Smitt PA,Kros JM. Differential expression of splicing variants of the human caldesmon gene (CALD1) in glioma neovascularization versus normal brain microvasculature. *Am J Pathol* 2004;164:2217-2228.

23. Warren KS, Shutt DC, McDermott JP, Lin JL, Soll DR,Lin JJ. Overexpression of microfilament-stabilizing human caldesmon fragment, CaD39, affects cell attachment, spreading, and cytokinesis. *Cell Motil Cytoskeleton* 1996;34:215-229.

24. Linder S, Aepfelbacher M. Podosomes: adhesion hot-spots of invasive cells. *Trends Cell Biol* 2003;13:376-385.

25. Tanaka J, Watanabe T, Nakamura N,Sobue K. Morphological and biochemical analyses of contractile proteins (actin, myosin, caldesmon and tropomyosin) in normal and transformed cells. *J Cell Sci* 1993;104 (Pt 2):595-606.

26. Spinardi L, Rietdorf J, Nitsch L*, et al.* A dynamic podosome-like structure of epithelial cells. *Exp Cell Res* 2004;295:360-374.

27. DeFife KM, Jenney CR, Colton E,Anderson JM. Cytoskeletal and adhesive structural polarizations accompany IL-13-induced human macrophage fusion. *J Histochem Cytochem* 1999;47:65-74.

28. Euteneuer U, Schliwa M. Persistent, directional motility of cells and cytoplasmic fragments in the absence of microtubules. *Nature* 1984;310:58-61.

29. Parast MM, Aeder S,Sutherland AE. Trophoblast giant-cell differentiation involves changes in cytoskeleton and cell motility. *Dev Biol* 2001;230:43-60.

30. Verkhovsky AB, Svitkina TM,Borisy GG. Self-polarization and directional motility of cytoplasm. *Curr Biol* 1999;9:11-20.

31. Lee TY, Gotlieb AI. Microfilaments and microtubules maintain endothelial integrity. *Microsc Res Tech* 2003;60:115-127.

32. Katz BZ, Zamir E, Bershadsky A, Kam Z, Yamada KM,Geiger B. Physical state of the extracellular matrix regulates the structure and molecular composition of cell-matrix adhesions. *Mol Biol Cell* 2000;11:1047-1060.

33. Risau W, Flamme I. Vasculogenesis. *Annu Rev Cell Dev Biol* 1995;11:73-91.

34. Arciniegas E, Parada D,Graterol A. Mechanically altered embryonic chicken endothelial cells change their phenotype to an epithelioid phenotype. *Anat Rec* 2003;270A:67-81.

Chapter 6

Low-molecular weight caldesmon (*l*-CaD) as a potential serum marker for glioma

Submitted for publication

Ping-Pin Zheng, Wim C. Hop, Peter A.E. Sillevis Smitt, Martin J. van den Bent, Cees J.J. Avezaat, Theodorus M. Luider, Johan M. Kros

Abstract

Purpose: Testing the feasibility of using the serum *l*-CaD level as serum marker for the presence of glioma.
Experimental Design: Within a total of 230 serum samples the *l*-CaD level was measured in healthy volunteers (30), patients with gliomas (57), non-glial intracranial tumors (107) and non-tumor neurological diseases (36) by enzyme-linked immunosorbent assay (ELISA). The specificity of the assay was monitored by combination of immunoprecipitation and immunoblotting (IP/IB).
Results: The serum level of *l*-CaD is significantly higher in the group of glioma patients as compared to any of the other groups ($p<0.001$). The cut-off value of 45 yields optimal sensitivity and specificity of the assay (91% and 84%, respectively; AUC score = 0.91). The specificity of ELISA was confirmed by the IP/IB control experiments. There were no significant differences in serum *l*-CaD levels between patients with low- or high-grade gliomas.
Conclusions: The serum *l*-CaD level as determined by ELISA is a good discriminator between glioma patients versus patients with other intracranial tumors, other neurological diseases, and healthy people. Prospective studies are required to test the contribution of the assay in making the diagnosis of glioma, or its feasibility for monitoring the tumor during treatment.

Introduction

Over the last decade, significant progress has been made in unraveling genetic pathways underlying the large variety of glial neoplasms. In addition to histological parameters for biological aggressiveness of gliomas, lineage-specific genetic markers have been identified which by now play a role in therapeutic decision-making (1, 2). However, for genetic typing, grading and genetic profiling, tumor tissue samples from a craniotomy or brain biopsy are required, making its clinical usefulness in patient surveillance both cumbersome and difficult. Currently, neuroradiology is still the sole method for the surveillance of glioma progression or regression as response to therapeutic intervention. A drawback of such neuroradiological evaluation is the limited ability to delineate the tumor size and there is substantial subjectivity in the assessment of the images, particularly when only minor changes in tumor sizes have occurred. A serum marker of glioma would be easier to collect, quantify, reproduce and use in clinical practice as alternative means of measuring response to treatment or making diagnosis. A few angiogenesis-related growth factors such as VEGF, and the glycoprotein YKL-40 have been proposed as glial tumor markers in serum or CSF (3-5). Unfortunately, lack of specificity has invalidated the clinical application of these putative markers until now. So far, there is no a glioma marker established for guiding clinicians in making the diagnosis, or aiding neurooncologists in monitoring progress of glioma or measuring effects of irradiation or chemotherapy.

Low-molecular caldesmon (*l*-CaD) has not previously been mentioned as a potential marker for glioma. Caldesmon (CaD) is a major actomyosin-binding protein distributed in smooth muscle cells (high-molecular-weight isoforms (*h*-CaD), 120-150 kDa) and non-muscle cells (low-molecular-weight isoforms (*l*-CaD), 70-80 kDa). There are at least four protein isoforms of the *l*-CaD class generated by alternative splicing (Hela and WI-38 types)(6, 7). The conserved regions of all isoforms of *l*-CaD contain their ability of binding to actin, tropomyosin, Ca (2+)-calmodulin, myosin and phospholipids(8). The *l*-CaD protein is crucially involved in the assembly and stabilization of the microfilament network in non-muscle cells and therefore, *l*-CaD is an important regulator of various cell functions, among which cell motility (7) (9-11).

In previous studies we identified *l*-CaD in the cerebrospinal fluid (CSF) of glioma patients but not in normal controls by using 2-dimensional polyacrylamide gel electrophoresis (2D PAGE), followed by matrix-assisted laser desorption/ionization-time of flight-mass spectrometry (MALDI-TOF-MS) analysis, and by specific immunohistochemical staining of tissue slides of the corresponding tumors we showed that this protein is located in the glioma microvasculature (12). Gliomas are the most highly vascularized tumor type in human, and therefore, serve as an excellent model to elucidate the process of tumor neovascularization. Following RT-PCR and immunobloting to microdissected blood vessels from gliomas and normal brain tissue, we discovered that the differential expression of this protein is mainly a sequel of abnormal splicing

of the human caldesmon gene (*CALD1*) in glioma vasculature, which functionally result in up-regulation of the *l*-CaD whole class (13). It was further found that over-expression of this protein class in glioma vasculature connect to the activation of endothelial cell motility (14), an essential step for neovascularization-dependent glioma progression. Since *l*-CaD was differentially present in the CSF samples of the glioma patients investigated, we here test the feasibility of using *l*-CaD as a serum marker for glioma.

Patients and methods

Serum Samples and Tissue Materials
Samples were collected from patients admitted to the Departments of Neurosurgery and Neurology of the Erasmus Medical Center, Rotterdam. Four different groups of individuals were implicated in this study. The first group (Group A) consisted of 57 patients with gliomas (15 low-grade gliomas and 42 anaplastic gliomas). The second group (Group B) consisted of 107 patients with non-glial intracranial tumors. The third group (Group C) consisted of 36 patients with variety of neurological diseases without tumors. Blood samples from 30 healthy peoples (Group D) were obtained from the Sanguin Blood Bank, Rotterdam, The Netherlands. Informed consent was obtained from all patients and healthy controls prior to study. The use of human blood samples was approved by the Institutional Review Board of the Erasmus Medical Center. The blood samples of the tumor patients were all taken prior to surgery or any other treatment modalities. The blood samples were allowed to clot at RT for 30 min and centrifuged at 4,000 rmp for 10 min at 4C°. The supernatant was aliquoted and stored at -80 ºC until further analysis. The pathological diagnosis of the tumors was made by microscopical examination of the biopsy or resection tissues (Table 1).

l-CaD enzyme-linked immunosorbent assay (ELISA)
In brief, ELISA plates (Nunc Maxisorpe Bioscience, Inc, USA) were coated overnight at 4ºC with 100µl/well of the diluted sera (4-fold dilution) by coating buffer (0.1M carbonate/bicarbonate buffer, pH 9.6). Following blocking with 1% bovine serum albumin (BSA) in phophate-buffered saline + 0.05% Tween (PBST) for 1 hour at RT, three washes were performed in PBST (each 5 min) at RT. Plates were incubated with 100µl/well of the mouse anti *l*-CaD (Sigma-Aldrich, St Louis, MO, USA) at 1:250 dilution for 2 hours at RT and washed three times. The plates were further incubated with AP-conjugated swine anti-mouse IgG (Dako, Glostrup, Denmark) at 1:1,000 dilution for 2 hours at RT, followed by three washes in PBST. The wells were developed using p-nitrophenyl phosphate substrate (Sigma-Aldrich, St Louis, MO, USA) at RT for 20 min and the reaction was stopped by 3M NaOH as the manufacturer indicated. The yellow reaction product was read at 405 nm on a microtiter plate reader (Model 450 microplate reader, Bio-Rad). Each serum was tested in duplicate. A positive control (PC) from a glioma patient and a negative control (NC) from health subject verified by immunoprecipitation were the same on each plate. The index value was defined by the following formula (15): index value = $[(OD_{sample} – OD_{NC})/(OD_{PC} – OD_{NC})]$ X 100. The NC revealed the non-specific background noise of the system, which was subtracted from all values on the plate.
The precision of the assay was assessed using five serum samples. Each sample was tested in 10 different wells in the same assay plate and the coefficient of variation (CV) of 10 duplicates was used to determine intra-assay precision. Further, each sample was subjected to five independent assays using five different plates to assess inter-assay precision. The intra-assay CV and the inter-assay CV were 6.66 % and 10.86 %, respectively.

Immunoprecipitation / immunoblotting of l-CaD in human sera
To investigate the specificity of ELISA, all glioma cases (57), all the Groups C and D (66) and 40 cases from Group B were subjected to combined immunoprecipitation / immunoblotting (IP/IB). A pair of monoclonal anti-*l*-CaD antibodies recognizing two separate epitopes on the *l*-CaD molecule were used for IP followed by IB detection, respectively. Human serum samples (2 ml for each patient) were incubated with monoclonal anti-*l*-CaD (2µg/ml) (Clone 8, BD Biosciences, USA) for 1 hour on ice, followed by adding 10% rec-Protein A-Sepharose® 4B Conjugate (Zymed Laboratories, Inc, USA) in the lysis buffer containing 0.5% Triton X-100, 150 mM NaCl, 50 mM

Tris-HCl and cocktail protease inhibitors. The samples were incubated for 1 hour at 4ºC on a rocking platform. The beads were precipitated by centrifugation at 10,000 g for 15 sec at 4ºC. The supernatant was removed by gentle aspiration. The immune complexes on the beads were washed 3 times with the lysis buffer. After a final wash, 50µl of 1X SDS gel-loading buffer was added followed by denaturing the proteins on the beads at boiling for 5 min, centrifuging at 10,000 g for 15 sec at 4ºC and loading the supernatant on SDS-PAGE. The gel was blotted onto a nitrocellulose membrane followed by incubating with monoclonal anti-*l*-CaD at 1:1000 dilution (clone C21, Sigma-Aldrich, USA). The blot was incubated with HRP-conjugated anti-mouse IgG at 1:5000 dilution (Dako, Glostrup, Denmark). The target protein band was visualized by enhanced chemiluminescence (Amersham Biosciences Corp, USA). The criteria for evaluation of IP/IB data were defined as: definite band (+), smear (±), no band (-). The target protein band is located at 70-80KD.

Statistical analysis
Nonparametric tests (Kruskall-Wallis test or Mann-Whitney test) were used to compare median levels between groups. Comparisons of the fraction of cases with 0-values was done using Fisher's Exact test. Two-sided p-values < 0.05 were considered to be statistically significant. Sensitivities and specificities were calculated for all cut-off levels of the serum *l*-CaD values and graphically displayed in receiver-operating characteristic curves (ROC curves).

Results

Significantly elevated l-CaD levels in sera from glioma patients
Table 1 the ranges, mean and median values of the serum *l*-CaD values of the 57 patients with glioma and the three other groups B, C and D (viz., other intracranial tumors; neurological disease without tumors; healthy individuals) are listed. The distribution of the serum values for each group is shown in Fig. 1. Only seven percent of sera from glioma patients had a *l*-CaD value of 0 while these percentages were 59, 72 and 53 for Group B, C and D respectively. The median serum *l*-CaD values for the low- and high-grade gliomas were 100 and 123, respectively. The median values were zero in the subgroup of meningiomas, schwannomas, pituitary adenomas, and 15 in the group of 14 metastases. The differences of percentages of 0-values between the four groups was highly significant ($p<0.001$; Chi-Square test). The comparisons of these percentages of the glioma group versus each of the other groups yielded highly significant differences ($p<0.001$; Fisher's exact test). Pairwise testing of the percentages of 0-values between the other three groups B, C and D yielded non-significant *p*-values for each comparison ($p=0.170$; $p=0.677$ and $p=0.131$; respectively; Fisher's Exact test). The results prompted us to consider these three groups as one control group. The difference between the median values of the *l*-CaD serum values of the group of glioma patients versus this combined control group ($n=173$) was highly significant ($p<0.001$). Within the glioma group, there were 15 patients with low-grade tumors and 42 patients with high-grade tumors. The serum *l*-CaD values of the 15 patients with low-grade glioma ranged from 0 to 285 with a mean of 124 and a median of 100. The serum values of the 42 patients with high-grade gliomas ranged from 0 to 440 with a mean of 140 and a median of 123. There was no statistically significant difference in median serum *l*-CaD values between the two groups of different glioma malignancy grade ($p=0.329$).

Determination of cut-off values
A ROC analysis was performed to determine the cut-off value for differentiating between patients with or without a glioma. The serum *l*-CaD value which gave the highest sum of sensitivity (%) and specificity (%) was defined as the cut-off value. The serum *l*-CaD value as determined by ELISA has a very good discriminative power for identifying patients with gliomas as shown by the large area under the curve (AUC = 0.91) of the ROC curve (Fig 2). For a cut-off score of 45, the sensitivity and specificity of *l*-CaD are 91% and specificity 84%, respectively. For comparison, *l*-CaD cut-off value of 40 yields a sensitivity of 91% and specificity of 82%, and a cut-off value of 50 yields a sensitivity of 88% and a specificity of 85%.

Immunoprecipitation / immunoblotting of I-CaD in human sera

To determine the specificity of ELISA, combination of IP/IB was performed in a large portion of the serum samples (Table 2). Representative cases are shown in Fig. 3. The largest discrepancy is found in the group of healthy individuals. No *I*-CaD was detected in 93% of sera of the group. For the other groups, the results of the two techniques showed a good concordance. The IP/IB results were in agreement with the ELISA measurement of *I*-CaD in the sera, thus demonstrating the specificity of ELISA.

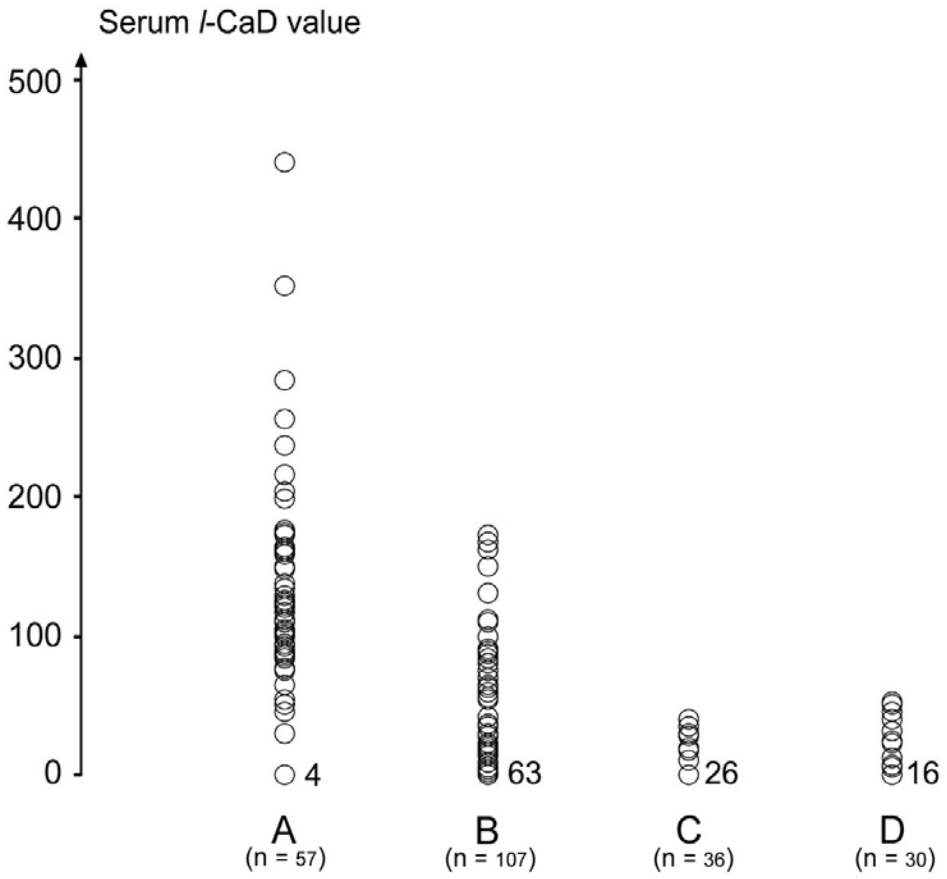

Fig 1. Serum *I*-CaD value in patients with glioma (A); patients with non-glial intracranial tumors (B); patients with various neurological diseases without tumors (C) and healthy subjects (D). The numbers 4, 63, 26 and 16 written at the basis of the columns indicate the number of patients with serum *I*-CaD levels of 0.

Table 1 Tumor diagnosis and *I*-CaD serum level values

Diagnosis	*N*	ELISA values		
		range	median	mean
A. Glioma	57	0-440	120	129
low-grade	15	0-285	100	124.1
high-grade	42	0-440	123	139.6
B. Non-glial intracranial tumors	107	0-173	0	25.6
meningioma	46	0-173	0	17.4
metastasis	14	0-150	15	48.8
schwannoma (CPA)	12	0-132	0	26.8
pituitary adenoma	23	0-100	0	28.9
non-glial intracranial tumors	12	0- 54	0	12.7
C. Non-tumor neurological disease	36	0- 40	0	5.5
D. Healthy individuals	30	0- 53	0	13.9

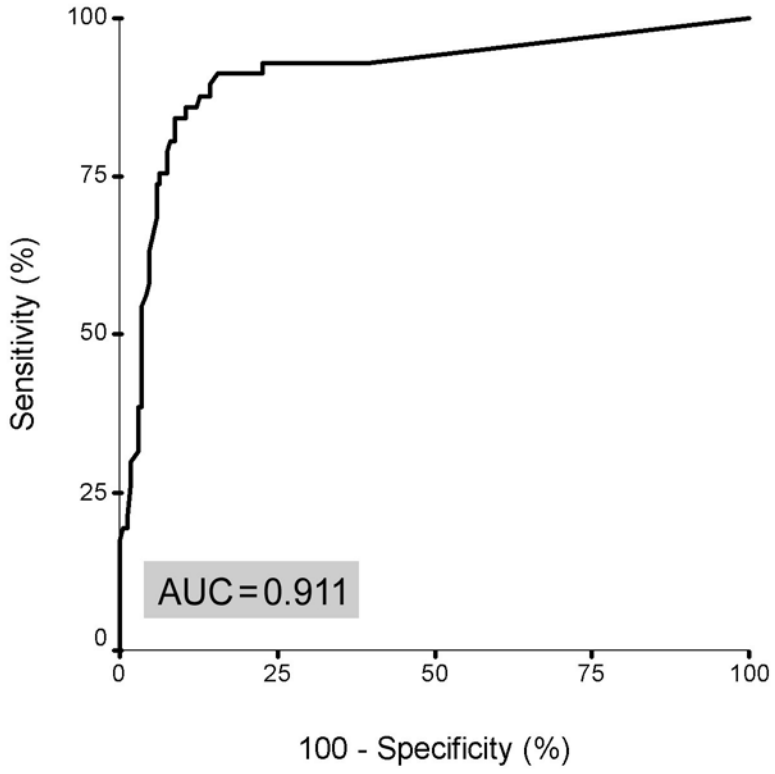

Fig 2. ROC curve. For the cut-off value of 45, the sensitivity and specificity of *I*-CaD are 91% and specificity 84%, respectively. For comparison, *I*-CaD cut-off value of 40 yields a sensitivity of 91% and specificity of 82%, and a cut-off value of 50 yields a sensitivity of 88% and a specificity of 85%. AUC = Area under the curve

Table 2 Results of immunoprecipitation/immunoblotting

Diagnosis	*N*	IP/IB results		
		+	±	-
A.Glioma	57	51		4
B.Non-glial intracranial tumors	40	11	8	21
C. Non-tumor neurological diseases	36	0	5	31
D.Healthy individuals	30	0	2	28

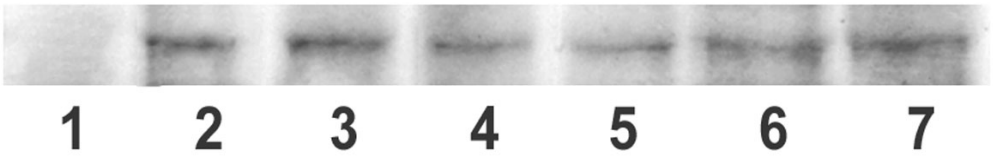

Fig 3. Example of immunoprecipitation / immunoblotting (IP/IB) experiment. The lanes 2 thru 7 represent the results from serum samples of glioma patients. Lane 1 is from a healthy control. In all of the lanes of the glioma patients bands located at 70-80 KD are present, representing *I*-CaD. The band is not detected in the healthy individual (lane 1). The results matched those obtained by ELISA.

Discussion

We here tested whether the serum value of *I*-CaD can serve as a serum marker for glioma and the results indicate that patients with biopsy-proven gliomas have significantly increased *I*-CaD serum levels as compared to the control group. For a cut-off score of 45, sensitivity of 91% and specificity of 82% was achieved. The serum *I*-CaD level was zero in only 7% of the glioma patients, as opposed to 59% in patients with other intracranial tumors; 72% in patients with neurological disease without tumors; and 53% in the group of healthy people. *I*-CaD was detectable in 44 out of 107 (41%) of serum samples of patients with non-glial intracranial tumors and in this group only 22/107 (21%) of values were over the index value of 45. The mean serum *I*-CaD value in the group of patients with neurological disease without tumor was 5.5 with a median of 0, and of the sera of the healthy people 13.9 and 0, respectively. Therefore, *I*-CaD is a good candidate serum marker for glioma. We now have planned to investigate the contribution of serum *I*-CaD in making the diagnosis of glioma in prospective studies. For instance, the neuroradiological presentation of a solitary metastasis may be indistinguishable of that of glioma. The median value of serum *I*-CaD of the 14 patients with metastases included in the present study was only 15 with a mean value of 48.8, while that of glioma was 120 with a mean of 129. Therefore, measuring the serum *I*-CaD level may well become a valuable addition for differentiating gliomas from metastases in patients with ambiguous neuroradiology.

The source of *I*-CaD in the serum of glioma patients is from the tumor vasculature, possibly by shedding or secreting of this protein into the blood stream, or from circulating endothelial precursor cells (EPCs) released from the bone marrow which contribute to neoplastic vasculogenesis. Further, there is a scavenging mechanism for balancing the titer of cytoskeletal proteins in serum (16). However, once a protein exceeds the protective scavenging capacity, its level in serum will rise. An explanation for the high *I*-CaD serum levels in patients with gliomas is that these tumors are among the highest vascularized neoplasms in man, in which all different modalities of neoplastic vascularization, in which *I*-CaD may play its specific role, is encountered

(17). In the serum of some patients with non-glial tumors, such as carcinomas of different types, we also found a relatively high *l*-CaD expression. It may very well be that these tumors were more richly vascularized as compared to others of the same kind – the abnormal *l*-CaD expression is found in a large variety of cancers. Nevertheless, the serum levels of the majority of the patients with these tumors appeared to be low.

The presence of microvascular proliferation in a biopsy specimen of diffuse glioma prompts to make the histopathological diagnosis of anaplastic glioma. Since *l*-CaD is specifically present in the neoplastic microvasculature, one would expect a higher *l*-CaD level in the serum of patients with high-grade (anaplastic) gliomas. This difference, however, was not found. There may be various reasons for this discrepancy. The neovascularization of low-grade gliomas may be far more extensive than noticed by microscopical investigation. The neovascularization is not only brought about by branching and sprouting of pre-existent blood vessels, but also by infiltration of individual angiogenic endothelial cells (ECs) (18). This extensive process of early neovascularization may be underestimated by visual inspection of biopsy specimens because there is no multilayering of the endothelial cells yet, and the individual angiogenic ECs are only detectable after immunostaining for endothelial markers. Further, in the later and final stages of neovascularization many of the neoplastic blood vessels undergo prominent sclerosis, and the expression of various cytoskeletal proteins as *l*-CaD in these vessels tapers of significantly (14).

In summary, the study renders clinical support for the value of *l*-CaD in the prediction of glioma existence, and allows for the indirect assessment of neo-angiogenic activity of gliomas. Whether the *l*-CaD serum value will prove itself as a marker which will be applied in clinical practice, remains to be established in prospective studies.

References

1. Bauman GS, Ino Y, Ueki K, et al. Allelic loss of chromosome 1p and radiotherapy plus chemotherapy in patients with oligodendrogliomas. Int J Radiat Oncol Biol Phys 2000; 48:825-30.

2. Mukasa A, Ueki K, Matsumoto S, et al. Distinction in gene expression profiles of oligodendrogliomas with and without allelic loss of 1p. Oncogene 2002; 21:3961-8.

3. Peles E, Lidar Z, Simon AJ, Grossman R, Nass D,Ram Z. Angiogenic factors in the cerebrospinal fluid of patients with astrocytic brain tumors. Neurosurgery 2004; 55:562-8.

4. Sampath P, Weaver CE, Sungarian A, Cortez S, Alderson L,Stopa EG. Cerebrospinal fluid (vascular endothelial growth factor) and serologic (recoverin) tumor markers for malignant glioma. Cancer Control 2004; 11:174-80.

5. Tanwar MK, Gilbert MR,Holland EC. Gene expression microarray analysis reveals YKL-40 to be a potential serum marker for malignant character in human glioma**.** Cancer Res 2002; 62:4364-8.

6. Hayashi K, Yano H, Hashida T, et al. Genomic structure of the human caldesmon gene. Proc Natl Acad Sci U S A 1992; 89:12122-6.

7. Huber PA. Caldesmon. Int J Biochem Cell Biol 1997; 29:1047-51.

8. Bryan J. Caldesmon: fragments, sequence, and domain mapping. Ann N Y Acad Sci 1990; 599:100-10.

9. Hegmann TE, Schulte DL, Lin JL,Lin JJ. Inhibition of intracellular granule movement by microinjection of monoclonal antibodies against caldesmon. Cell Motil Cytoskeleton 1991; 20:109-20.

10. McManus MJ, Lingle WL, Salisbury JL,Maihle NJ. A transformation-associated complex involving tyrosine kinase signal adapter proteins and caldesmon links v-erbB signaling to actin stress fiber disassembly. Proc Natl Acad Sci U S A 1997; 94:11351-6.

11. Yamakita Y, Yamashiro S,Matsumura F. Characterization of mitotically phosphorylated caldesmon. J Biol Chem 1992; 267:12022-9.

12. Zheng PP, Luider TM, Pieters R, et al. Identification of tumor-related proteins by proteomic analysis of cerebrospinal fluid from patients with primary brain tumors. J Neuropathol Exp Neurol 2003; 62:855-62.

13. Zheng PP, Sieuwerts AM, Luider TM, van der Weiden M, Sillevis-Smitt PA,Kros JM. Differential expression of splicing variants of the human caldesmon gene (CALD1) in glioma neovascularization versus normal brain microvasculature. Am J Pathol 2004; 164:2217-28.

14. Zheng PP, M van der Weiden, Kros J.M. Differential expression of Hela-type caldesmon in tumour neovascularization: a new marker of angiogenic endothelial cells. J Pathol 2005; 205:in press.

15. Amagai M, Komai A, Hashimoto T, et al. Usefulness of enzyme-linked immunosorbent assay using recombinant desmogleins 1 and 3 for serodiagnosis of pemphigus. Br J Dermatol 1999; 140:351-7.

16. Erukhimov JA, Tang ZL, Johnson BA, et al. Actin-containing sera from patients with adult respiratory distress syndrome are toxic to sheep pulmonary endothelial cells. Am J Respir Crit Care Med 2000; 162:288-94.

17. Eberhard A, Kahlert S, Goede V, Hemmerlein B, Plate KH,Augustin HG. Heterogeneity of angiogenesis and blood vessel maturation in human tumors: implications for antiangiogenic tumor therapies. Cancer Res 2000; 60:1388-93.

18. Goldbrunner RH, Bernstein JJ, Plate KH, Vince GH, Roosen K,Tonn JC. Vascularization of human glioma spheroids implanted into rat cortex is conferred by two distinct mechanisms. J Neurosci Res 1999; 55:486-95.

Chapter 7

Summary and Concluding Remarks

Despite advances in neuroimaging, microsurgical techniques, radiotherapy and chemotherapy, the prognosis of patients with gliomas, in particular malignant gliomas, remains poor. Therefore, the selection of areas of research with the best chances to make contributions to improve outcomes for these patients, is crucial. Searching targets for tumor vessel-directed therapy would be most crucial for the benefit of glioma patients. Investigations focused on the identification of markers for improving or refining the diagnostic procedure, or predicting biological behavior, or monitoring tumor progression or regression as response to therapy, are important also. Advances in immunology, genetics, and immunohistochemistry have led to the discovery of various potential tumor markers. However, none of the putative markers identified so far has made it to the stage of being clinically applied. In this thesis we made an attempt to identify proteins which might be useful to improve making the diagnosis, or serve as target for tumor-directed therapy.

In Chapter 2 of this thesis we report on our search for tumor-associated -, or better, tumor-specifc, proteins in body fluids of patients suffering from glial tumors. These proteins were sought by the application of proteomic-based techniques. To this aim, we initially applied the classic technique of 2-dimensional electrophoresis to CSF samples of glioma patients in order to produce specific protein expression profiles of gliomas. We used CSF instead of serum as substrate, because the protein content of CSF is much lower as compared to that of serum. High concentrations of serum proteins as albumin disturb the analysis of the 2-DE fingerprints and also may frustrate the results of mass spectrometry by MALDI. Proteins have variable physical properties and differ in their ability to reach the CSF. Further, there may be various passive or active mechanisms by which proteins appear in the CSF. The reason why certain proteins reach the CSF more easily than others may well be found in the physical properties of the molecules like mass weight, molecular charge and state of post-translational modification (e.g., phosphorylation, glycosylation), and molecular degradation. The finding of caldesmon spots in the 2-DE gels of the glioma patients was robust and reproducible. N-myc was also found in the CSF of patients with gliomas, but was also observed in CSF of 2 patients with medulloblastomas. Our focus on gliomas prompted us to further investigate the expression of caldesmon isoforms. Apart from caldesmon and N-myc, many more tumor-associated proteins may be present in body fluids of glioma patients, but concentrations may vary considerably. Coomassie-staining of 2-DE gels allows subsequent MALDI-TOF analysis of the targetted spots, while silver staining, though more sensitive, hampers subsequent analysis by MALDI-MS. Advanced techniques of analyzing protein spots and protein mixtures have become available, including methods of differential fluorescent labeling of protein mixtures of different samples to be used for 2-DE fingerprinting. In addition to MALDI-TOF, mass spectrometry analysis using sophisticated techniques as Q-TOF or FT-MS have become available, and advances in bio-informatics enable to increase sensitivity and specificity of findings. Therefore, the screening of tumor-associated proteins by proteomic-based techniques is rapidly evolving.

The analysis of glioma tissue slides by immunohistochemistry for *l*-CaD pointed to the specific expression of this protein in blood vessels. The expression was seen both in normal brain vessels and glioma vasculature, but appeared to be much stronger in hyperplastic and/or proliferated glioma vessels. The findings suggested that *l*-CaD might be up-regulated in glioma vasculature. Therefore, in Chapter 3 we report on our investigations regarding the possible mechanism for the altered expression, and quantified the expression of *l*-CaD in glioma tissue samples versus normal intracranial tissues. Abnormally expressed splice variants were specifically found in the microvasculature of glioma samples, while not in the microvasculature of normal, non-neoplastic brain. It appeared that abnormal splicing of exons 1, 1+4 and 1'+4 of the *CALD1* gene is exclusively found in the neoplastic blood vessels. The protein products are of the low-molecular caldesmon class (viz., Hela type *l*-CaD I and II and WI-38 *l*-CaD I). Semi-quantitative immunoblotting of *l*-CaD confirmed the up-regulation of this protein in the glioma samples as compared to the situation in normal control tissues. The results of correlating these findings with our observations at the mRNA level were indicative of the notion that the up-

regulation of *l*-CaD in the glioma microvasculature mainly results from this abnormal splicing of the *CALD1* gene. The strong expression of caldesmon is, therefore, due to the abnormal expression of isoforms of *l*-CaD, and enhanced expression of the proteins.

In the Chapter 4 the Hela *l*-CaD expression in glioma blood vessels was further detailed. Against the background of the current view on the stages of neoplastic angiogenesis, that in gliomas in particular, abnormal expression of Hela *l*-CaD in gliomas was studied. By using a specific anti-Hela *l*-CaD antibody, specific expression in glioma microvasculature, not in the blood vessels of normal brain tissue, was confirmed. What is more, Hela *l*-CaD expression was predominantly seen in the early phase of neovascularization, viz., in the individual infiltrating endothelial cells (Ecs), in the endothelial precursor/progenitor cells (EPCs) and in the non-canalized endothelial cell chains (NCECCs). In addition to all this, immunopositive endothelial cells in newly formed sprouts of bloodvessels were observed. Therefore, the expression takes place in the early phase of neo-angiogenesis. Almost no expression of Hela *l*-CaD was seen in the late phase of neo-angiogenesis, which is characterized by intussusceptive vascular growth and fibrosis and hyalinization of vessel walls.

In Chapter 3 we already observed that over-expression of *l*-CaD was correlated with a decrease in expression of the tight-junction-related protein occludin and ZO-1. To further substantiate the functional significance of the Hela *l*-CaD expression in the ECs, focal adhesion (FA) and F-actin structures of endothelial cells in gliomas were compared with those in motile cells of cell cultures described in the literature. The redistribution of the FA protein vinculin and remodeling of F-actin was observed in the Hela *l*-CaD^{+} ECs by using confocal microscopy. The confocal technique enables to visualize the intracellular site of particular substances like proteins. The findings supported the idea that the expression of Hela *l*-CaD is associated with the activation of motility of the ECs. The hypothesis that the Hela *l*-CaD -positive cells are motile and spread through the diffusely infiltrating gliomas well into the infiltrative edges and normal cerebral tissue was supported by the finding that in these cells focal adhesions are broken down and at the same time motile or unstable adhesions, or podosomes, are being formed. This observation was also made by using confocal microscopy to triple-immunostained sections. Future studies should address several questions raised by these observations. Where do the individual, CD31- and CD43-positive cells come from? Do they represent bone-marrow-derived cells, or alternatively, are they tumor cells that transform into blood vessel forming elements? Do these cells represent stem cells invading glial tumors from sites where they have been quiescent so far?

Since gliomas are among the best vascularized tumors in man, displaying signs of extensive neo-angiogenesis, they make an ideal subject for investigations in neoangiogenesis. In order to answer the question whether the selective presence of Hela *l*-CaD is specific for glial neoplasms, or alternatively, also takes place in other tumors, the expression was sought in a variety of human cancers. In Chapter 5 we have shown results of immunostaining cancers of lung, breast, colon, stomac, liver, kidney, thyroid, endometrium, prostate, bladder and ovary. ECs and NCECCs are variably present in these tumors and the expression of Hela *l*-CaD showed considerable variation between the different tumor types. Also in these non-glial tumors, the Hela *l*-CaD-positive ECs displayed features of motile cells. Interestingly, in some tumor types as breast cancers and thyroid cancers, orthotopic expression of Hela *l*-CaD was noticed in the tumor cells and also in the epithelial cells of non-neoplastic parenchymal cells. Such orthotopic expression would invalidate Hela *l*-CaD as tumor (neoangiogenesis-) specific target for diagnosis and therapy in these cancers. In the gliomas however, the expression was never found in normal glia and her coverings (Chapter 3).

Finally, we examined the feasibility of using the serum *l*-CaD level as indicator for the presence of glioma. To this aim, the levels of *l*-CaD were examined in 57 blood samples of glioma patients and compared with a total of 173 blood samples of patients with other, non-glial CNS tumors, patients with neurological diseases but no tumors, and a group of healthy individuals. Statistically significant elevation of the *l*-CaD level was observed in the sera of the glioma patients as compared to the other groups. The high sensitivity of 91% is perhaps less important than the specificity of 84%. The findings warrant prospective studies to evaluate the contribution of the serum *l*-CaD level in clinical practice: making the diagnosis in situations of inconclusive radiology, or, perhaps more importantly, monitoring glioma progress or response to therapy.

Summary in Dutch (samenvatting in de Nederlandse taal)

Ondanks grote vooruitgang in neuroradiologische beeldvorming, neurochirurgische technieken, radiotherapeutische methodieken en de recente successen met chemotherapeutische behandeling van gliale tumoren, blijft de prognose van patienten met dergelijke tumoren, in het bijzonder de maligne gliomen, slecht. Daarom is het uitkiezen van onderzoeksvraagstellingen die relevantie hebben voor de kliniek van de patienten met gliomen, essentieel. Onderzoekonderwerpen die als doel hebben het ontdekken van tumor-gerelateerde factoren die diagnostiek verbeteren, beter voorspellen hoe het klinisch gedrag van de tumor zal zijn, of een goede maat zijn voor de reactie van de tumor op therapie, zijn derhalve favoriet. Er werden reeds verschillende van zulke tumor merkers ontdekt, maar geen van deze bleken tot dusver geschikt om in de klinische praktijk te worden toegepast.

In Hoofdstuk 2 van dit proefschrift worden de experimenten beschreven om tumor-gerelateerde (of beter: tumor-specifieke) tumormerkers in hersenvloeistof van patienten met gliomen op te sporen. De eiwitten werden gezocht met behulp van 2-dimensionale electrophorese. Voor deze experimenten gebruikten we liquor cerebrospinalis omdat deze lichaamsvloeistof minder storende eiwitconcentraties bevat dan bijvoorbeeld in patientenserum aanwezig is. Hoge concentraties serum eiwitten als bijvoorbeeld albumine kunnen de eiwit spectra analyse met behulp van 2-dimensionale electrophorese vertroebelen en ook massaspectrometrie ter identificatie van de eiwitten, verstoren. Eiwitten hebben onderling verschillende fysische eigenschappen en dringen niet alle in dezelfde mate door tot in de liquor: factoren als post-translationele veranderingen (fosforylering en transaminering), massa en lading van de moleculen spelen daarbij een rol. Bovendien bestaan verschillende passieve en actieve transportmechanismen waarop eiwitten in de liquor kunnen belanden. De caldesmon eiwit spots in de gelen van de liquor van de glioom patienten waren specifiek en reproduceerbaar. Een ander eiwit, het N-myc, werd behalve in de liquor van de glioom patienten ook in liquoren van patienten met medulloblastomen gezien. Aankleuren van de 2-dimensionale gelen met Coomassie belemmert daaropvolgende analyse met behulp van MALDI niet, in tegenstelling tot aankleuring met zilveroplossingen, waarmee echter wel hogere sensitiviteit van detectie wordt bereikt. Inmiddels zijn verbeteringen in de techniek van 2-dimensionele electrophorese aangebracht, zoals het differentieel labelen van de te analyseren eiwitmengsels. Ook hebben de methoden en technieken van de massa spectrometrie zich snel geëvolueerd. Behalve MALDI zijn ook Q-tof en FT-MS voor massa spectrometrie beschikbaar gekomen. Niet in de laatste plaats, enorme vooruitgang in de bio-informatica heeft gezorgd voor steeds toenemende specificiteit en sensitiviteit van de bevindingen. Het screenen voor biomarkers in weefsels en lichaamsvloeistoffen voor identificatie van tumor-geassocieerde eiwitten is zich snel aan het ontwikkelen.

Langs immunohistochemische weg konden we aantonen dat de expressie van het caldesmon eiwit in gliomen beperkt was tot de tumorvasculatuur. Ofschoon ook de vaten van normaal hersenweefsel positief aankleurden voor caldesmon, bleek de expressie steeds veel sterker in de tumorvaten te zijn, mogelijk door versterking (upregulation) van de gen expressie. In hoofdstuk 3 van dit proefschrift werd de verhoogde expressie gekwantificeerd en werd naar de oorzaak ervan nagegaan. Het bleek middels RT-PCR experimenten, waarbij de expressie van de verschillende splice-varianten van het caldesmon gen (*CALD1*) werd nagegaan, dat in de glioomvaten abnormale splicing van het caldesmon gen plaats vindt, die niet in de normale hersenvaten wordt gevonden. Het bleek dat exclusive expressie van de exonen 1, 1+4 en 1'+4 van het *CALD1* gen optreedt in de tumorvaten. De eiwitproducten van deze alternatieve splicing behoren alle tot de laag-moleculaire klasse van het caldesmon, namelijk het Hela type *l*-CaD I en II, en WI-38 type *l*-CaD I. Tevens werd middels semiquantitatieve immunblotting experimenten aangetoond dat deze eiwitvarianten verhoogd, tot zo'n 3.5 maal, tot expressie komen.

In hoofdstuk 4 werd de expressie van Hela *l*-CaD in de bloedvaten van gliale tumoren middels een specifiek anti-Hela *l*-CaD antilichaam verder gedetailleerd. Er worden verschillende vormen en stadia van angioneogenese onderscheiden, en de expressie van Hela *l*-CaD tegen die achtergrond bestudeerd. Het bleek dat de expressie vooral in vroege stadia van angioneogenese in de gliomen wordt gezien. De individueel infiltrerende endotheliale cellen en celclusters, en ook endotheliale voorlopercellen, toonden alle sterke expressie van Hela *l*-CaD. Er werd ook

expressie in endotheelcellen in nieuwe spruiten van pre-existente vaten gevonden. In late fasen van angioneogenese, gerepresenteerd door vaten met zich opsplitsende wanden, en fibrosering en hyalinisering van de wand, werd nauwelijks of geen expressie meer aangetroffen. In hoofdstuk 3 werd al waargenomen dat overexpressie van *l*-CaD was gecorreleerd met afname van de expressie van de eiwitten occludine en ZO-1, die deel uitmaken van tight junctions tussen de endotheelcellen. Daarmee is een verband gelegd tussen de functionele status van de cellen en de aberrante expressie van caldesmon. Om de functionele betekenis van de abnormale expressie van caldesmon in de individueel infiltrerende endothliale cellen vast te stellen, werden filamenten in deze cellen, die betrokken zijn bij cel-cel interacties, middels confocale microscopie bestudeerd. Daarbij werden veranderingen vergeleken met eigenschappen van cellen met verhoogde motiliteit, zoal beschreven in celkweken in de literatuur. In de Hela *l*-CaD-positieve endotheliale cellen werd redistributie van het eiwit vinculine, en werden veranderingen van het F-actine, een filament-gebonden eiwit, vastgesteld. De bevindingen zijn sterk suggestief voor een verband tussen de abnormale expresie van *l*-CaD enerzijds, en de vorming van zogenaamde podosomen, anderszijds. Podosomen worden beschouwd als tijdelijke adhesies tussen cellen die een sterke motiliteit tonen. Het bleek dat een redistributie van verschillende eiwitten optreedt, en conformatie van op podosomen gelijkende structuren voorkomt in de individuele cellen die zowel in de gliale tumoren, als in de infiltratieranden van de tumoren, worden gezien. Deze cellen zijn sterk positief voor het Hela *l*-CaD-specifieke antilichaam. Met behulp van confocale microscopie verricht op cellen die voor verschillende eiwitten simultaan werden gekleurd, werden aanwijzingen verzameld die erop duiden dat focale adhesies ontbonden worden en in plaats daarvan op podosomen gelijkende structuren verschijnen. De cellen waarbij dit optreedt behoeven in toekomstig onderzoek aandacht. Waar komen deze CD31, CD34-positieve cellen vandaan? Zijn ze afkomstig uit het beenmerg? Wat is hun relatie met de stamcellen die inmiddels in gliomen zijn geidentificeerd en naar de tumoren toe migreren? Of zijn het tumorcellen die zich in neoplastische endotheelcellen hebben getransformeerd?

Omdat gliomen zo rijk gevasculariseerd zijn, en alle typen en fasen van neoplastisch angiogenese in de gliale tumoren aanwezig zijn, vormen ze een ideaal substraat voor de bestudering van neoangiogenese. Om de vraag te beantwoorden, of de abnormale expressie van het laag-moleculaire caldsmon beperkt is tot de vasculatuur van gliale tumoren, of ook in bloedvaten van andere tumoren voorkomt, werd in hoofdstuk 5 de expressie van caldesmon in een grote groep niet-gliale tumoren bestudeerd. Tumoren van long, borst, colon, maag, lever, nier, schildlier, endometrium, prostaat, blaas en ovarium werden aan immunohistochemische kleuringen voor het Hela-type *l*-CaD onderworpen. De individueel infiltrerende endotheelcellen en endotheliale celclusters werden in sterk wisselende mate in deze tumoren gevonden. De expressie van Hela *l*-CaD bleek ook sterk per tumortype te varieren. Net als bij de gliomen werden met behulp van confocale microscopie ook de eigenschappen van sterk mobiele cellen gevonden in de Hela *l*-Cad-positieve endotheliale cellen. In tegenstelling tot de situatie bij de gliomen echter, werden in enkele borst- en schilkliertumoren ook niet-endotheliale, *l*-CaD-positieve tumorcellen, en ook niet-neoplastische epitheliale cellen, geidentificeerd. De betekenis daarvan blijft vooralsnog onduidelijk. De consequentie van deze bevinding is dat het ontwikkelen van op abnormale expressie van caldesmon-gerichte anti-angiogenetisch therapie, bij zulke tumoren uitgesloten is.

In het laatste hoofdstuk van dit proefschrift werd weer teruggegrepen naar de allereerste bevinding, namelijk de specifieke aanwezigheid van caldesmon in de liquor cerebrospinalis van patienten met een gliale tumor. Onderzocht werd of een verhoogde caldesmonspiegel ook in het serum aanwezig is, waarmee een eerste stap in de richting van het ontwikkelen van caldesmon als specifieke tumor merkerstof gezet is. De serum-caldesmon spiegel werd gemeten in een groep van 230 mensen, die bestond uit 57 patienten met een glioom, en 107 patienten met niet-gliale CZS tumoren, 36 patienten met neurologisch aandoeningen zonder tumor, en 30 gezonde mensen. De caldesmon serumspiegel van de glioompatienten bleek significant hoger te liggen in vergelijking tot die van de andere groepen (specificiteit 84%; sensitiviteit 91%). Deze bevindingen wijzen op de noodzaak van een nieuwe studie waarbij het serum caldesmon moet worden gemeten in situaties van patienten met een intracraniele tumor, maar bij wie de radiologie niet eenduidig voor een glioom is. Tevens is het vervolgen van de caldesmon serumspiegel van

patienten na behandeling, bij vervolgen van de tumor en het monitoren van de ziekte, aangewezen, om de waarde van het serum caldesmon voor de klinische praktijk te toetsen.

Curriculum Vitae and Publications

Name: Ping-Pin Zheng

Nationality: Chinese

Academic Degrees: **MD**: Medical College of Southeast University, PR of China

M.Phil: Dept. of Anatomical and Cellular Pathology, Chinese University of Hong Kong, PR of China

Medical Profession: Pathologist

Fellowship: Department of Pathology, Kyoto Prefectural University, Japan

PhD resulting in this thesis: February 7, 2001 – February 16, 2005

Publications

Zheng PP, van der Weiden M, Kros JM. Differential expression of Hela-type caldesmon in tumor neovascularization: a new marker of angiogenic endothelial cells. J Pathol 2005; 205, in press.

Gudinaviciene I, Pranys D, **Zheng PP**, Kros JM. 10-Month-old baby-boy with a large pineal tumor. Brain Pathology, 2005, in press.

Zheng PP, Sieuwerts AM, Luider TM, van der Weiden M, Sillevis-Smitt PA, Kros JM. Differential expression of splicing variants of the human caldesmon gene (CALD1) in glioma neovascularization versus normal brain microvasculature. Am J Pathol. 2004 Jun;164(6):2217-28.

Zheng PP, Luider TM, Pieters, R, Avezaat CJJ, van den Bent MJ, Sillevis Smitt PAE, and Kros JM. Identification of tumor-related proteins by proteomic analysis of cerebrospinal fluid from patients with primary brain tumors. J Neuropathol & Exp Neurol 62:855-862, 2003.

Zheng PP, Kros JM, Sillevis-Smitt PAE, Luider TM. Proteomics in primary brain tumors. Front Biosci. D451-463, 2003.

Kros JM, **Zheng PP**, Dinjens WN, Alers JC: Genetic aberrations in gliomatosis cerebri support monoclonal tumorigenesis. J Neuropathol Exp Neurol 9:806-814, 2002.

Kros JM, Bagdi EK, **Zheng PP**, Hop WC, Driesse MJ, Krenacs L, Dinjens WN. Analysis of immunoglobulin H gene rearrangement by polymerase chain reaction in primary central nervous system lymphoma. J Neurosurg 6:1390-1396, 2002.

Kros JM, **Zheng PP**, Wolbers J, van den Bent JM. “Oligodendroglial tumors”. In: Textbook of Neuro-Oncology. Part 2: Tumor-specific principles. Ed. Mitchel Berger & Michael Prados.

Tong, C.Y., PP. **Zheng,** J.C. Pang, W.S. Poon, A.R. Chang, and H.K. Ng. Identification of novel regions of allelic loss in ependymomas by high-resolution allelotyping with 384 microsatellite markers. J Neurosurg 1:9-14, 2001.

Zheng, PP., J.C. Pang, A.B. Hui, and H.K. Ng. Comparative genomic hybridization detects losses of chromosomes 22 and 16 as the most common recurrent genetic alterations in primary ependymomas. Cancer Genet Cytogenet 1:18-25, 2000.

Xu YG, **Zheng PP**. Gallstone spilt granulomas caused by laparoscopic cholecystectomy. Chinese Medical Journal (English Edition), 111:92-93,1998.

Zheng PP, Lu XP, Zheng K. Ewing's sarcoma of the maxilla. Chinese Medical Journal (English Edition) 111:377-378, 1998.

Zheng K, **Zheng PP**. Hemophilic pseudotumor involving maxilla and tibia. Chinese Medical Journal (English Edition) 110:233-235, 1997.

Zheng PP, Xu YG. Leiomyomatosis peritonealis disseminata: two case reports. Chinese Medical Journal (English Edition) 109:334-336, 1996.

Li ZG, **Zheng PP**, Huang ZG, You SQ. Experimental observation of effects induced by plasticizers to mouse teeth. Ningbo Medicine 8: 255-257, 1996. (Article in Chinese)

Xu YG, **Zheng PP**. Gonorrhea peritonitis – a retrospective clinico-pathological overview. Emergency Medicine 5:81-83, 1996. (Article in Chinese)

Zheng PP, Xu YG. Diagnosis and treatment by using gastroscope. An evaluation of the clinico-pathological value. Ningbo Medicine 4:6-7, 1992. (Article in Chinese)

Zheng PP. Diagnostic application of fine-needle aspiration (FNA) of malignant lesions of lymph nodes – a report on 60 cases. Journal of Clinical Cancer 7:181-182, 1992. (Article in Chinese)

Zheng PP, Zheng K. Osteosarcomas arising on the surfaces of long bones. New Medicine 22:434-435, 1991. (Article in Chinese)

Zheng PP, Yang JS, Chu Q. Clinico-pathological analysis of pulmonary fungi infection – Report on 29 cases. Journal of Clinical and Experimental Pathology 7:118-124, 1991. (Article in Chinese)

Zheng PP, Jia Y. Markers of basal membrane: implications for diagnostic application to tumors. Zhejiang Medicine 4:34-35, 1991. (Article in Chinese)

Zheng PP, Jia Y. Merkel cell carcinoma of skin. Journal of Cancer (Zhejiang). 48:43-45, 1989. (Article in Chinese)

Zheng PP, Zhou LS. Fine-needle aspiration (FNA): The cytological value of diagnosis for breast diseases – a report on 54 cases. Journal of Cancer (Zhejiang) 1:14-16, 1989. (Article in Chinese)

Acknowledgments

My deepest appreciation to Prof. dr. J.W. Oosterhuis and dr. J.M. Kros, who offered me the unique opportunity as PhD candidate to work at the Department of Pathology, Erasmus Medical Center. Specially, I am extremely grateful to dr. Max Kros, who actually supervised the whole project for the thesis, and gave me innumerable advices, support and energetic help. I maximally enjoyed scientific freedom which he allowed me. Words are insufficient to express my thankfulness to him.

I am profoundly thankful to dr. Theo Luider, who very kindly and generously invested time and energy to train me for the 2D PAGE and MALDI-TOF-MS. These techniques resulted in the identification of the interesting protein *l*-CaD and other tumor-related proteins. The results gave the foundation for my further studies. He also very kindly arranged the office computer, printer and other stuffs, and ordered all the reagents what I asked.

I am particularly indebted to Prof. dr. Peter Sillevis Smitt, who spent his valuable time for reviewing the articles in this thesis.

I would like to greatly thank Mr. Marcel van der Weiden (immunostaining), Ms. Anieta Sieuwerts (RT-PCR), Dr. Wim C. Hop (statistical analysis), Dr. Adriaan Houtsmuller and Mr. Alex Nigg (confocal laser microscope) for their technical assistance.

I would like to extend my special appreciation to each colleague who has worked, or is working, in the Neuro-Oncology Laboratory for his/her cooperation and assistance during my staying. Specifically I give thanks to Dr. Mathilde Kouwenhoven and Ms. Esther Hulsenboom for their willingness to act as my paranimfen.

Also I would like to give thanks to all those JNI colleagues who helped me with a large variety of things during my staying.

Finally, I would like to convey my deepest appreciation to my parents and my brother for their unlimited support, encouragement and understanding in all aspects.